University of São Paulo
Luiz de Queiroz College of Agriculture

Assessing tropical forest degradation and restoration through lidar remote sensing

Danilo Roberti Alves de Almeida

Thesis presented to obtain the degree of Doctor in Science. Area: Forest Resources. Option in: Silviculture and Forest Management

Piracicaba
2018

Danilo Roberti Alves de Almeida
Forestry Engineer

Assessing tropical forest degradation and restoration through lidar remote sensing

versão revisada de acordo com a resolução CoPGr 6018 de 2011

Advisor:
Prof. Dr. **PEDRO HENRIQUE SANTIN BRANCALION**

Thesis presented to obtain the degree of Doctor in Science. Area: Forest Resources. Option in: Silviculture and Forest Management

Piracicaba
2018

Dados Internacionais de Catalogação na Publicação
DIVISÃO DE BIBLIOTECA – DIBD/ESALQ/USP

Almeida, Danilo Roberti Alves de

Assessing tropical forest degradation and restoration through lidar remote sensing / Danilo Roberti Alves de Almeida. - - versão revisada de acordo com a resolução CoPGr 6018 de 2011. - - Piracicaba, 2018.

139 p.

Tese (Doutorado) - - USP / Escola Superior de Agricultura “Luiz de Queiroz”.

1. Fragmentação florestal 2. Diversidade 3. Biomassa 4. Drone I. Título

I dedicate my doctoral thesis to my family:
my father Marcos, my mother Cláudia,
and my brothers Paulo and Vitor.

ACKNOWLEDGEMENTS

First of all I thank my family for all love, support and understanding of the my need to live far from them to carry out my studies and researches. My dad Marcos for all his love and for being an example of person and researcher, always encouraging me on my researches. My mum for her infinite love and affection, and for always praying for me on my way. To my dear older brothers Paulo and Vitor for the companionship, support and love.

My girlfriend Marina for understanding, support, love, and especially patience for my anxiety during the sleepless nights working on the thesis. Her help in the last weeks of the thesis was essential for me to finish everything on time and do not get crazy, hehe.

I thank my friends who are always with me, the “Camaradas” of São Paulo, Manaus, Minas Gerais, East lansing (Jamokes) and the whole world. Especially those who lived close to me in these four years of doctorate: Daniel Papa, Diego Silva and Luisa Gurjão. To Matheus Capelari, who was a great friend, brother, “Camarada” during my internship in the United States. My friends from Rep. Strunzo, in particular, Terçado, Toindo, Bixiga, Aborto, Filhão, Faiado, Favorável, Salvo, DD2, Cilada Tortinha, Dona Nice and Alcione. It was essential to live with you at the Mansion!

To my adviser, friend and counselor Pedro Brancalion. I could not have a better advisor. To my friend and advisor in the United States Scott Stark. It was amazing the time I spent in East Lansing. To my friend and co-adviser Juliana Schietti. To friends and researchers who helped me a lot on thesis elaboration: Eric Gorgens, Eben Broadbent, Nino Amazonas, Ricardo Cesar, Paula Meli, Robin Chazdon, José Luis, Diogo Rosa, Bruce Nelson, Ruben Valbuena, Carlos Silva, Marina Duarte and Alex Mendes.

To my friend, LASTROP secretary and “salvadora” Andreia Moreno. To my friend, secretary of the forest, counselor and promoter of the best forest parties Giovana Oliveira.

I am grateful for the support of CAPES, who granted my PhD scholarship in the first year, and FAPESP (#2016/05219-9 and #2017/03867-6), which granted the doctoral scholarship for the remained years and intership in United States.

“Os cientistas as vezes parecem crianças jogando bola: achando que aquele jogo é a coisa mais importante do mundo, brigando para ver quem tem a bola mais colorida e quem faz mais gols. Contudo, não percebem que aquilo é apenas uma brincadeira quando comparada à realidade maior ao qual estão inseridos.”

“Scientists sometimes look like children playing soccer: believing that game is the most important thing in the world, fighting to see who has the most colorful ball, and who makes more goals. However, they do not realize that this is just a joke when compared to the larger reality which they are inserted.”

Danilo R. A. de Almeida

SUMÁRIO

RESUMO **7**

ABSTRACT **8**

1. INTRODUCTION **9**

REFERENCES 12

2. OPTIMIZING THE REMOTE DETECTION OF TROPICAL RAINFOREST STRUCTURE WITH AIRBORNE LIDAR: LEAF AREA PROFILE SENSITIVITY TO PULSE DENSITY AND SPATIAL SAMPLING **15**

ABSTRACT **15**

2.1. INTRODUCTION 15
2.2. MATERIAL AND METHODS 18
2.3. RESULTS 23
2.4. DISCUSSION 26
2.5. SUPPLEMENTARY MATERIAL 33
REFERENCES 34

3. PERSISTENT EFFECTS OF FRAGMENTATION ON TROPICAL RAINFOREST CANOPY STRUCTURE AFTER 20 YEARS OF ISOLATION USING LIDAR **39**

ABSTRACT **39**

3.1. INTRODUCTION 39
3.2. MATERIAL AND METHODS 42
3.3. RESULTS 47
3.4. DISCUSSION 54
3.5. CONCLUSION 59
3.6. SUPPLEMENTARY MATERIAL 60
REFERENCES 78

4. THE EFFECTIVENESS OF LIDAR REMOTE SENSING FOR MONITORING FOREST COVER ATTRIBUTES IN FOREST AND LANDSCAPE RESTORATION **85**

ABSTRACT **85**

4.1. INTRODUCTION 85
4.2. MATERIAL AND METHODS 87
4.3. RESULTS 94
4.4. DISCUSSION 99
4.5. CONCLUSION 104
4.6. SUPPLEMENTARY MATERIAL 104
REFERENCES 109

5. MONITORING THE STRUCTURE OF FOREST RESTORATION PLANTATIONS WITH A DRONE-LIDAR SYSTEM **117**

ABSTRACT **117**

5.1. INTRODUCTION 117
5.2. MATERIAL AND METHODS 120
5.3. RESULTS 124
5.4. DISCUSSION AND CONCLUSION 127
5.5. SUPPLEMENTARY MATERIAL 131
REFERENCES 133

6. FINAL CONSIDERATIONS **137**

RESUMO

Avaliação da degradação e restauração de florestas tropicais através de sensoriamento remoto lidar

O presente estudo investiga novas fronteiras do conhecimento da aplicação da tecnologia de sensoriamento remoto lidar à avaliação da degradação e restauração de florestas tropicais. A tese está estruturada na forma de um capítulo de introdução, quatro capítulos técnicos, que exploraram aspectos técnicos e científicos da aplicação da tecnologia lidar à avaliação da degradação de florestas na Amazônia e restauração de florestas na Mata Atlântica, e de um capítulo final com considerações gerais e uma síntese dos principais resultados científicos obtidos nesta tese. O capítulo 2, utilizando dados lidar aeroembarcados em avião, analisou uma questão técnica, sobre a influência da densidade de pulsos da nuvem lidar e da resolução de amostragem para a modelagem do perfil de densidade de áerea foliar em florestas tropicais (DAF). O perfil de DAF é a decomposição do índice de área foliar (IAF) ao longo do perfil vertical do dossel e pode ser utilizado para responder diversas questões ecológicas. Os resultados da capítulo 2 trouxeram importantes *insights* para a correta modelagem dos perfis de DAF. O capítulo 3, utilizando dados lidar em plataformas aeroembarcados e terrestre portátil, no Projeto Dinâmica Biologica de Fragmentos Florestais (PDBFF), demonstrou de maneira inédita o efeito da fragmentação florestal sobre a alteração da estrutura do dossel (derivados de dados lidar) e suas relações com a mudança da comunidade arbórea. Neste capítulo os resultados demonstraram que a tecnologia lidar tem enorme potencial para monitorar o impacto da fragmentação florestal para grandes áreas e em fina escala. O capítulo 4, utilizando dados de diversas tipologias florestais em restauração no bioma Mata Atlântica, a partir de um sistema lidar terrestre portátil, demonstrou a capacidade dos atributos estruturais do dossel em distinguir diferentes tipologias florestais, estimar diversidade e biomassa de madeira acima do solo. Contudo, os resultados não foram muito positivos para estimativa da diversidade da comunidade arbórea (riqueza, indice de Shannon e composição de espécies). Finalmente, o capitulo 5 demonstrou a capacidade de um sistema inovador lidar aeroembarcado em uma plataforma drone (também conhecida como VANT - veículo aéreo não tripulado) para monitorar plantios de restauração florestal. O lidar está revolucionando a maneira de mensurarmos as paisagens florestais, podendo ser uma ferramenta imprecindível para o sucesso dos projetos de restauração florestal em larga escala, tendo o potencial de auxiliar desde o planejamento ao monitoramento e fiscalização dos projetos florestais. Nesta tese, demonstramos diversas aplicações do sensoriamento remoto lidar ao contexto da restauração florestal, e estabelecemos bases metodológicas para que outros estudos expandam o uso desta tecnologia para tomada de decisão na conservação, manejo e restauração de florestas tropicias.

Palavras-chave: Fragmentação florestal; Diversidade; Biomassa; Drone; PDBFF; Efeito de borda; Monitoramento florestal; Plantios de restauração; Estrutura florestal; Densidade de área foliar

ABSTRACT

Assessing tropical forest degradation and restoration through lidar remote sensing

The present study investigates new frontiers of lidar technology knowledge assessessing of tropical forest degradation and restoration. The thesis is structured with an introductory chapter, four technical chapters, which explored technical and scientific aspects of the application of lidar technology to the evaluation of forest degradation in the Amazon and restoration of forests in the Atlantic Forest, and a final chapter with considerations and a summary of the main scientific results obtained in this thesis. The results of chapter 2 provided important insights for the correct modeling of leaf area density (LAD) proflies profiles usind airborne lidar. LAD profile is the decomposition of the leaf area index (LAI) along the vertical canopy profile and can be used to answer many ecological questions. The results of chapter 2 provided important insights for the correct modeling of LAD profiles. Chapter 3, using lidar data on aerial and portable ground platforms, in the Biological Dynamics of Forest Fragments Project (BDFFP), demonstrated in an unprecedented way the effect of forest fragmentation in the canopy structure (lidar-derived) and their relationships with the change of the tree community. In this chapter, the results showed that the lidar technology has enormous potential to monitor the impact of forest fragmentation in a high precision scale for large areas. Chapter 4, using data from several forest typologies in the Atlantic Forest biome restoration collect by a portable ground lidar system, demonstrated the potential of canopy structural attributes to distinguish different forest typologies and to estimate above ground woody dry biomass. However, the results were not positive for estimating tree community diversity (richness, Shannon index and species composition). Finally, chapter 5 demonstrated the potential of a novel lidar system on a drone platform (also known as UAV – unmanned aerial vehicle) to monitor forest restoration plantations. Lidar is revolutionizing the way we measure forest landscapes and can be an indispensable tool for the success of forest restoration projects, having the potential to support on planning, monitoring and inspection of forest restoration landscapes. In this thesis, we demonstrate several applications of remote sensing to address the context of forest restoration, and we established methodological bases for other studies to expand the use of this technology for decision making in tropical forest conservation, management and restoration.

Keywords: Forest fragmentation; Diversity; Biomass; Drone; BDFFP; Edge effect; Forest monitoring; Mixed plantations; Forest structure; Leaf area density

1. INTRODUCTION

Forests and other natural ecosystems are important for ecosystem services that are imperative for human life, such as provision of food and regulating of climate and hydrological cycles (Chazdon, 2008; FAO, 2016). Our billions people, modern consumption society has generated several damages to the environment, resulting in vast degraded areas (Achard et al., 2002; Lamb et al., 2005). Approximately one third of the global land surface was already transformed by agriculture. On the other hand, we are living an unprecedented opportunity moment in forest restoration and conservation. The Bonn Challenge (2018) (WRI, 2018) plan to restore over 350 million hectares worldwide by 2030, which has been materialized in Latin America by the 20x20 Initiative, with the aim to restore 53.2 million hectares by 2020 (Chazdon et al., 2017). On a national scale, the Brazilian National Plan for the Recovery of Native Vegetation (PLANAVEG), aims to restore 12 million hectares of native vegetation in the next 20 years. At the biome scale, the Atlantic Forest Restoration Pact seeks to restore 15 million hectares of degraded lands in the Atlantic Forest biome by 2050, and thereby increase the current forest cover of the biome from 17% to at least 30% (Melo et al., 2013). These pledges have placed forests as the centerpiece in an integrated landscape management framework known as Forest Landscape Restoration (FLR). FLR has emerged to recover ecological functionality of deforested lands, by deliberately managing landscapes to generate multiple outputs in a sustainable manner 'with the least trade-off costs and where possible synergies are maximized, supporting both social and ecological objectives' (Sabogal et al., 2015). FLR strategies include many forest cover types (Aronson et al., 2017; Laestadius et al., 2015), that satisfy different stakeholders' preferences, ecological objectives and site requirements (Stanturf et al., 2014).

To achieve ambitious goals of forest conservation and restoration, it is necessary the development of novel methodological approaches that are cost-effective for monitoring structure and physiological attributes associated with ecological functions at broad scales (Chazdon et al., 2017; Holl, 2017). Some imaging satellite remote sensing systems, such as Landsat, have the capacity to roughly estimate forest classes at large scales (Souza et al., 2013). But their signal saturates in areas with high vegetation density (Jensen et al., 2011; Turner et al., 1999), and is resolved at too

coarse a spatial scale, severely limiting their applicability to monitor restoration and the recovery of forest functions.

Over the past few years, novel remote sensing technologies such as lidar (light detection and ranging) have emerged as alternatives to monitoring forest structure and associated functions at broader spatial scales and in ecosystems with high vegetation density, as tropical forests. Lidar has the potential penetrate in forest canopy producing three-dimensional forest models (Lefsky et al., 2002). Lidar raw data is a three-dimensional cloud of thousands (or millions) of points with information on the geographic position (x-longitude, y-latitude) and altitude (z) of each point (Figure 1.1).

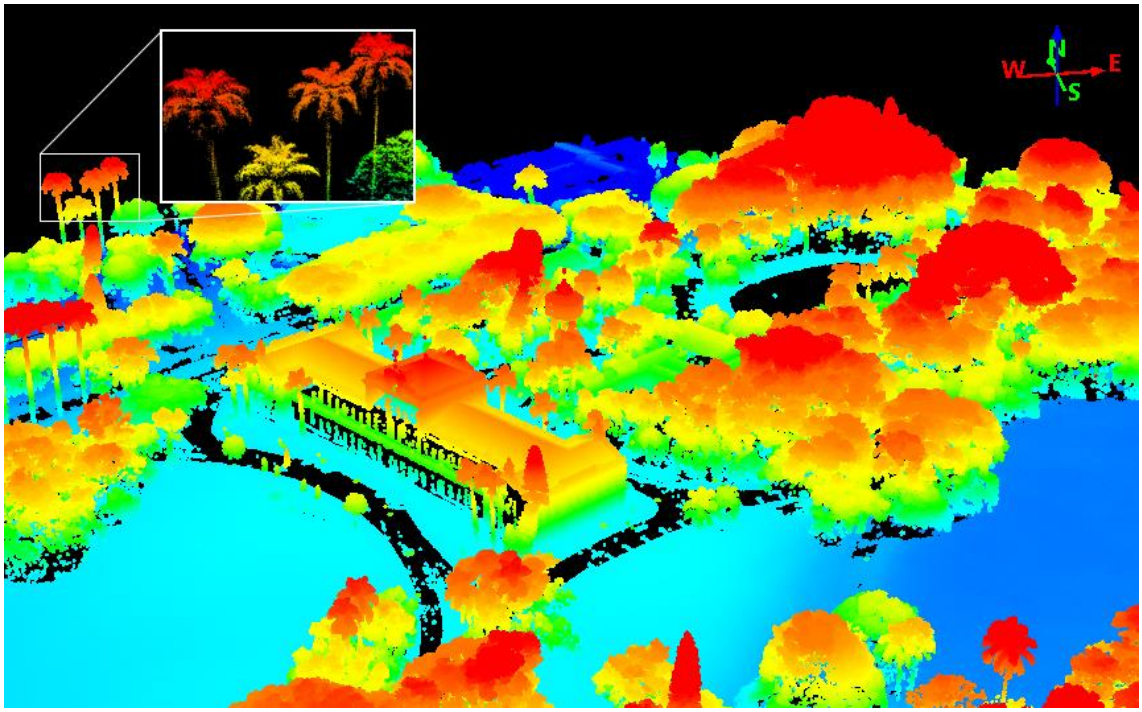

Figure 1. Example of a 3D lidar point cloud at the ESALQ campus (Escola Superior "Luiz de Queiroz", University of São Paulo, Piracicaba, SP)

The points from the lidar point cloud correspond to the position of the target (e.g. leaves, branches, ground) hit by a laser at the near infrared spectrum (~900 nm), which has high reflection by the vegetation. From the time between the emission and reception of the laser pulse it is possible to calculate the exact position of the objects. Each laser pulse can have more than one return, depending of the lidar sensor used (Lefsky et al., 2002).

Lidar is commonly used on ground or aerial platforms. There are fixed or mobile ground platforms (Parker et al., 2004; van Leeuwen and Nieuwenhuis, 2010). Aerial platforms can be airplanes or UAV (unmanned aerial vehicles) (Longo et al., 2016; Sankey et al., 2017). The increasing popularization UAVs is giving autonomy for remote sensing data collection and new systems with UAV-borne lidar for forest measurement have been created (Sankey et al., 2017; GatorEye, 2018). For airborne systems, flight altitude and speed during the collection data will influence important parameters of lidar data. Some parameters such as pulses emission angle and density of returns can influence the modelling of forest structural parameters.

Lidar has been used in forestry science since the 1990s, mainly in temperate forests (Dubayah, 2000; van Leeuwen and Nieuwenhuis, 2010). Between 2000-2015, 17 reviews of lidar applied in forests were published (White et al., 2016). Many studies use statistical parameters of lidar Z values (such as median, 90th percentile, kurtosis, among others) to generate predictive models of the field variables (e.g. above ground biomass) (Longo et al., 2016). One of the main uses of airborne lidar is measure vegetation height, technically known as canopy height model (CHM). The CHM is a determined resolution raster where Z values are the height at the top canopy. CHM is obtained by the difference between the digital surface model (DSM) (canopy surface altitude in relation to sea level) and the digital terrain model (DTM) (altitude of the ground in relation to sea level). The DTM is obtained from algorithms that classify returns that reached the ground (Meng et al., 2010), and the DSM can be easily obtained (after the spurious return filter) by the maximum values of Z values for a given resolution grid. Therefore, by the difference between DSM and DTM, it is possible to have a standard model of vegetation height, without the influence of the terrain altitude. From the CHM, other structural canopy parameters can be calculated for a given area or forest plot, such as the average of the top canopy, the canopy rugosity (horizontal top canopy heterogeneity) and the gap fraction (Hunter et al., 2015; Longo et al., 2016; Palminteri et al., 2012).

Some studies have used the lidar cloud to modelling structural parameters such as lead area density (LAD, $m^2\ m^{-3}$) and leaf area index (LAI, $m^2\ m^{-2}$) (Stark et al., 2012, 2015; Almeida et al., 2016). LAI is a widely used variable in ecology in aspects such as diversity, light environment, water interception, dynamics and seasonality (Bréda, 2003; Tymen et al., 2017). However, the modeling of LAD and LAI with lidar data is still quite recent and yet needs to be better understood and improved. It is still

not known as lidar data quality parameters (such as the pulse density) and the sampling resolution for LAD modeling can affect LAD estimates.

The use of lidar data in tropical forests is relatively recent and many questions still need to be answered. To the best of our knowledge, no work has used airborne lidar to date to measure the effect of forest fragmentation on tropical forests. Few papers have been published using lidar for tropical forest restoration, and none using UAV-lidar systems.

The objective of this thesis is to fill some knowledge gaps about lidar remote sensing applied in conservation and restoration of tropical forests. This study counts with four independent, but integrated, chapters in format of scientific article (chapters 2, 3, 4 and 5). In Chapter 2 a technical question was investigated, about the effect of lidar returns density and the sampling resolution on LAD estimates in a site in Central Amazon using airborne lidar data. In chapter 3, ecological questions about the effect of forest fragmentation (in a site in the Central Amazon) on the structural parameters of the canopy were investigated using airborne and portable ground lidar systems. In chapter 4, we analyzed the potential of the structural parameters of the canopy for the distinction of forest cover types, estimation of aboveground biomass and diversity using a portable ground lidar in sites in Atlantic Forest Biome. Finally, in chapter 5 an innovative UAV-borne lidar system was used to monitor an experimental forest restoration plantation in the Atlantic Forest Biome.

References

Achard, F., Eva, H.D., Stibig, H.J., Mayaux, P., Gallego, J., Richards, T., Malingreau, J.P., 2002. Determination of deforestation rates of the world's humid tropical forests. Science (80-.). doi:10.1126/science.1070656

Aronson, J., Blignaut, J.N., Aronson, T.B., 2017. Conceptual Frameworks and References for Landscape-scale Restoration: Reflecting Back and Looking Forward ,. Ann. Missouri Bot. Gard. 102, 188–200. doi:10.3417/2017003

Bonn challenge 2018. Link: http://www.bonnchallenge.org/. Acceded in 21/10/2018

Bréda, N.J.J., 2003. Ground-based measurements of leaf area index: A review of methods, instruments and current controversies. J. Exp. Bot. 54, 2403–2417. doi:10.1093/jxb/erg263

Chazdon, R.L., 2008. Beyond deforestation: Restoring forests and ecosystem services on degraded lands. Science (80-.). doi:10.1126/science.1155365

Chazdon, R.L., Brancalion, P.H.S., Lamb, D., Laestadius, L., Calmon, M., Kumar, C., 2017. A Policy-Driven Knowledge Agenda for Global Forest and Landscape Restoration. Conserv. Lett. 10, 125–132. doi:10.1111/conl.12220

Dubayah, 2000. Lidar Remote Sensing for Forestry Applications. J. For. doi:10.1093/jof/98.6.44

FAO 2016. State of the world's forests 2016: forests and agriculture: land-use challenges and opportunities

GatorEye 2018. http://www.speclab.org/gatoreye.html. Acceded in 21/10/2018

Holl, K.D., 2017. Restoring tropical forests from the bottom up. Science (80-.). doi:10.1126/science.aam5432

Hunter, M.O., Keller, M., Morton, D., Cook, B., Lefsky, M., Ducey, M., Saleska, S., De Oliveira, R.C., Schietti, J., Zang, R., 2015. Structural dynamics of tropical moist forest gaps. PLoS One. doi:10.1371/journal.pone.0132144

Jensen, J.L.R., Humes, K.S., Hudak, A.T., Vierling, L.A., Delmelle, E., 2011. Evaluation of the MODIS LAI product using independent lidar-derived LAI: A case study in mixed conifer forest. Remote Sens. Environ. 115, 3625–3639. doi:10.1016/j.rse.2011.08.023

Laestadius, L., Buckingham, K., Maginnis, S., Saint-Laurent, C., 2015. Back to Bonn and beyond: A history of forest landscape restoration and an outlook for the future. Unasylva 245, 11–18.

Lamb, D., Erskine, P.D., Parrotta, J.A., 2005. Restoration of degraded tropical forest landscapes. Science (80-.). doi:10.1126/science.1111773

Lefsky, M.A., Cohen, W.B., Parker, G.G., Harding, D.J., 2002. Lidar remote sensing for ecosystem studies. Bioscience 52, 19–30. doi:10.1641/0006-3568(2002)052[0019:LRSFES]2.0.CO;2

Longo, M., Keller, M., dos-Santos, M.N., Leitold, V., Pinagé, E.R., Baccini, A., Saatchi, S., Nogueira, E.M., Batistella, M., Morton, D.C., 2016. Aboveground biomass variability across intact and degraded forests in the Brazilian Amazon. Global Biogeochem. Cycles 30, 1639–1660. doi:10.1002/2016GB005465

Melo, F.P.L., Pinto, S.R.R., Brancalion, P.H.S., Castro, P.S., Rodrigues, R.R., Aronson, J., Tabarelli, M., 2013. Priority setting for scaling-up tropical forest restoration projects: Early lessons from the Atlantic forest restoration pact. Environ. Sci. Policy. doi:10.1016/j.envsci.2013.07.013

Meng, X., Currit, N., Zhao, K., 2010. Ground filtering algorithms for airborne LiDAR data: A review of critical issues. Remote Sens. doi:10.3390/rs2030833

Palminteri, S., Powell, G.V.N., Asner, G.P., Peres, C.A., 2012. LiDAR measurements of canopy structure predict spatial distribution of a tropical mature forest primate.

Remote Sens. Environ. doi:10.1016/j.rse.2012.08.014

Parker, G.G., Harding, D.J., Berger, M.L., 2004. A portable LIDAR system for rapid determination of forest canopy structure. J. Appl. Ecol. 41, 755–767. doi:10.1111/j.0021-8901.2004.00925.x

PLANAVEG http://www.mma.gov.br/florestas/pol%C3%ADtica-nacional-de recupera%C3%A7%C3%A3o-da-vegeta%C3%A7%C3%A3o-nativa. Acceded in 04/07/2018

Sabogal, C., Besacier, C., McGuire, D., 2015. Forest and landscape restoration: concepts, approaches and challenges for implementation. Unasylva 66, 3.

Sankey, T., Donager, J., McVay, J., Sankey, J.B., 2017. UAV lidar and hyperspectral fusion for forest monitoring in the southwestern USA. Remote Sens. Environ. doi:10.1016/j.rse.2017.04.007

Souza, C.M., Siqueira, J. V., Sales, M.H., Fonseca, A. V., Ribeiro, J.G., Numata, I., Cochrane, M.A., Barber, C.P., Roberts, D.A., Barlow, J., 2013. Ten-year landsat classification of deforestation and forest degradation in the brazilian amazon. Remote Sens. doi:10.3390/rs5115493

Stanturf, J.A., Palik, B.J., Dumroese, R.K., 2014. Contemporary forest restoration: A review emphasizing function. For. Ecol. Manage. doi:10.1016/j.foreco.2014.07.029

Turner, D.P., Cohen, W.B., Kennedy, R.E., Fassnacht, K.S., Briggs, J.M., 1999. Relationships between leaf area index and Landsat TM spectral vegetation indices across three temperate zone sites. Remote Sens. Environ. 70, 52–68. doi:10.1016/S0034-4257(99)00057-7

Tymen, B., Vincent, G., Courtois, E.A., Heurtebize, J., Dauzat, J., Marechaux, I., Chave, J., 2017. Quantifying micro-environmental variation in tropical rainforest understory at landscape scale by combining airborne LiDAR scanning and a sensor network. Ann. For. Sci. 74. doi:10.1007/s13595-017-0628-z

van Leeuwen, M., Nieuwenhuis, M., 2010. Retrieval of forest structural parameters using LiDAR remote sensing. Eur. J. For. Res. doi:10.1007/s10342-010-0381-4

White, J.C., Coops, N.C., Wulder, M.A., Vastaranta, M., Hilker, T., Tompalski, P., 2016. Remote Sensing Technologies for Enhancing Forest Inventories: A Review. Can. J. Remote Sens. doi:10.1080/07038992.2016.1207484

WRI, 2018. Initiative 20x20. World Resources Institute. http://www.wri.org/our-work/project/initiative-20x20/about-initiative-20x20#project-tabs. Acceded in 21/10/2018.

2. OPTIMIZING THE REMOTE DETECTION OF TROPICAL RAINFOREST STRUCTURE WITH AIRBORNE LIDAR: LEAF AREA PROFILE SENSITIVITY TO PULSE DENSITY AND SPATIAL SAMPLING

ABSTRACT

Airborne Laser Scanning (ALS) has been considered as a primary source to model forest canopy structure and function through the indicators leaf area index (LAI) and vertical canopy profiles of leaf area density (LAD). However, little is known about the effects of the laser pulse density and the grain size (horizontal binning resolution) of the laser point cloud on the estimation of LAD profiles and their associated LAIs. Our objective was to determine optimal values for reliable and stable estimates of LAD profiles from ALS data obtained over a dense tropical forest. Profiles were compared using three methods: destructive field sampling, Portable Canopy profiling Lidar (PCL) and ALS. Stable LAD profiles from ALS, concordant with the other two analytical methods, were obtained when grain size was less than 10 m and pulse density was high (>15 pulses m^{-2}). Lower pulse densities also provided stable and reliable LAD profiles when using an appropriate adjustment (coefficient K). We also discuss how LAD profiles might be corrected throughout the landscape when using ALS surveys of lower density, by calibrating with LAI measurements in the field or from PCL. Appropriate choices of grain size, pulse density and K provide reliable estimates of LAD and associated tree plot demography and biomass in dense forest ecosystems.

Keywords: LAI; LAD; Leaf area index; Canopy; Beer-Lambert law

2.1. INTRODUCTION

Measuring the density and distribution of leaves in forest canopies is key to understanding ecological and microclimate processes that drive forest function (Putz, 1983; Breda et al., 2008; Tymen et al., 2017; Stark et al., 2012, 2015; Atkins et al., 2018). The spatial structure of leaf area influences light transmittance and absorbance, biodiversity conservation, carbon fluxes, ecophysiology, leaf phenology, disturbances, and water and climate interactions (Breda et al., 2008). Advances in laser remote sensing have transformed the way forest canopies are measured, allowing detailed inference about canopy spatial structure with increasing application to leaf area estimation *per se*. Airborne Laser Scanning (ALS)—i.e., scanning lidar (Light Detection and Ranging)—has been used to model the leaf environment, obtaining attributes such as Leaf Area Index (LAI) and its decomposition into Leaf Area Density (LAD) distribution within the vertical canopy profile (Stark et al., 2012). While lidar has proven its reliability and accuracy for canopy height and aboveground biomass estimation at different spatial scales (Asner & Mascaro, 2014; Longo et al.,

2016), previous studies have also detected considerable laser acquisition parameter (e.g., pulse density) and processing method (e.g., binning resolution) effects (Roussel et al., 2017; Silva et al., 2017). Yet, to date, little is known about the effects of these factors on the estimation of leaf area, and LAD profiles specifically (Shao et al., 2019). Thus, the stability and robustness of estimates of leaf area attributes from lidar require further investigation.

LAI represents the area of leaves per unit of ground area (m^2 m^{-2}). In the field, LAI can be estimated indirectly by raising a pole through the canopy, counting how many times the pole touches a leaf along the vertical profile (Wilson, 1958). The frequency of leaves in units along the vertical profile yields the LAD distribution, expressed as leaf area at each height interval per volume of canopy (m^2 m^{-3}). LAD values are, thus, the partial volumetric components of LAI. Measuring LAD and LAI by destructively harvesting and scanning leaf area in a fixed footprint may be the most accurate approach for LAD profile quantification, but it is very difficult and laborious, especially in dense tropical forests (McWilliam et al., 1993; Clark et al., 2008). Non-destructive indirect techniques, such as vegetation indices from orbital sensors, canopy gap area assessed through hemispherical photographs, and light intensity attenuation from paired above/below canopy light sensors, are commonly employed to estimate LAI. However, all three techniques have critical limitations. Vegetation indices are saturated in dense forests where LAI generally exceeds 4.0 (Turner et al., 1999; Jensen et al., 2011). The use of hemispherical photographs should be restricted to narrow time windows near dawn and dusk. Light sensors require a large open area or tower for an above-canopy measurement of light intensity close to each simultaneous understory measurement (Olivas et al., 2013). The signal of light sensors also becomes saturated in dense forests (Martens et al., 1993). Alternatively, lidar systems are active sensors potentially free of these limitations—if they can effectively penetrate the full canopy depth. Indeed, lidar-derived estimates have revealed ecologically relevant differences in LAD profiles for different dense rainforest types, including those with LAI above 5.0 (Stark et al., 2012; 2015; Almeida et al., 2016).

The MacArthur-Horn equation is commonly used for estimating LAI and LAD from discrete return lidar data (MacArthur & Horn, 1969; Parker et al., 2004; Sumida et al., 2009; Stark et al., 2012; 2015; Almeida et al., 2016; Tynem et al., 2017; Shao et al., 2019). This model follows the principle of the Beer-Lambert Law, which

estimates the concentration of an absorbing compound mixed in a transparent liquid, according to the fraction of incident light that is transmitted (Swinehart, 1962). In the MacArthur-Horn equation the concentration of the substance is replaced by the density of vegetation within a unit of canopy volume (voxel). Here, the incident light intensity is the number of lidar pulses entering that voxel and attenuation of transmittance is caused by the presence of leaves obstructing some of those pulses, which are then detected by the lidar sensor (Parker et al., 2004). Key assumptions of the MacArthur-Horn equation as applied to LAD estimates are that leaves are distributed randomly in voxels, that they do not transmit pulses, and that pulses are parallel and emitted vertically. For estimating leaf area instead of plant area (which includes non-leaf surface areas) with this method, an additional assumption is that leaf area is a constant fraction of the plant surface area that determines lidar pulse transmission so that a constant can scale profiles to LAD.

From a nadir view of airborne lidar, taller leafy crowns partially occlude lower ones, influencing the retrieval of information from underneath the topmost parts of the canopy. For this reason, the quality of LAD profile estimation might be highly influenced by the lidar pulse density, with higher pulse numbers better sampling the upper extent of the canopy. The other factor that influences the apparent lidar pulse density when sampling LAD profiles is the horizontal binning resolution (grain size). Here, there is an inherent relationship between lidar pulse density and the horizontal grain size (Adnan et al, 2017); the larger the grain size, the more pulses within a voxel and in the profile sample generally. While higher sampling is desirable, increasing grain size may mask effects of low lidar pulse densities leading to poor sampling low in the canopy (e.g., in the understory). Furthermore, leaf area is clumped at multiple spatial scales, and clumping influences the estimation of leaf area by optical transmission methods, including the MacArthur-Horn method (Weiss et al., 2004). Thus, there is a clear need to assess the accuracy and the scale dependency of LAD profile estimation as a function of lidar pulse density and grain size. However, no previous studies have been devoted to evaluating how lidar pulse density and the grain size employed affect estimates of LAD and LAI in tropical forests.

To address these dependencies in ALS-based LAD profile estimation, a comparison approach is needed. Comparison possibilities include other very high-density lidar-based approaches, and destructive surveys. Recent studies have

estimated the LAD profiles using a very high pulse density system, known as Portable Canopy profiling Lidar (PCL) which operates from the ground by emitting pulses skyward through the canopy (Parker et al., 2004; Almeida et al., 2016; Hardiman 2011; 2013). The vegetation profiles obtained by PCL can be used to validate vegetation profiles derived from lower pulse density airborne systems (Stark et al., 2012). Where PCL measurements overlap with independent measurements of LAI the system can be calibrated to estimate leaf area (not plant area), and where destructive sampling exists, a more complete validation is possible (Stark et al., 2012).

Our objective in this study was to determine the optimal parameters for reliably estimating LAD profiles from ALS data in dense tropical forests. We assess LAD profile stability and accuracy associated with changes in (i) laser pulse density and (ii) grain size (voxel horizontal binning resolution). The ALS-derived LAD profiles were compared to those from destructive field sampling (from McWilliam et al., 1993) and from the PCL.

2.2. Material and methods

Lidar data were collected at the Ducke Forest Reserve (Figure 1), located 26 km north-west of Manaus (02º55'S, 59º59'W at the Reserve headquarters). The reserve covers 10,000 ha of dense upland (*terra firme*) tropical forest, having a mean LAI of 5.7 ± 0.5 (SD), 790 trees ha^{-1} (DBH > 10 cm), approximately 300 Mg ha^{-1} of aboveground biomass (McWilliam et al., 1993; Biot et al., 1998), 2% of the canopy was open to a height lower than 15 meters, and around 1,170 tree species, with greater dominance of the families Fabaceae, Burseraceae, Lecythidaceae and Sapotaceae (Ribeiro, 1999). The Köppen climate type is Af, in which the mean annual temperature is circa 26ºC, the mean annual rainfall ranges between 2400 and 2700 mm, and there is a less rainy season typically in August and September, with less than 100 mm rainfall per month (Marques-Filho et al., 1981). The ALS data covered 12.5% of the total area of the Reserve, in three strips (Figure 1). Elevation above sea level of the area covered by ALS scanning varies from 30 to 90 m. Mean canopy height is 27 m, with the tallest trees reaching up to 55 m (as measured in the canopy height model derived from ALS).

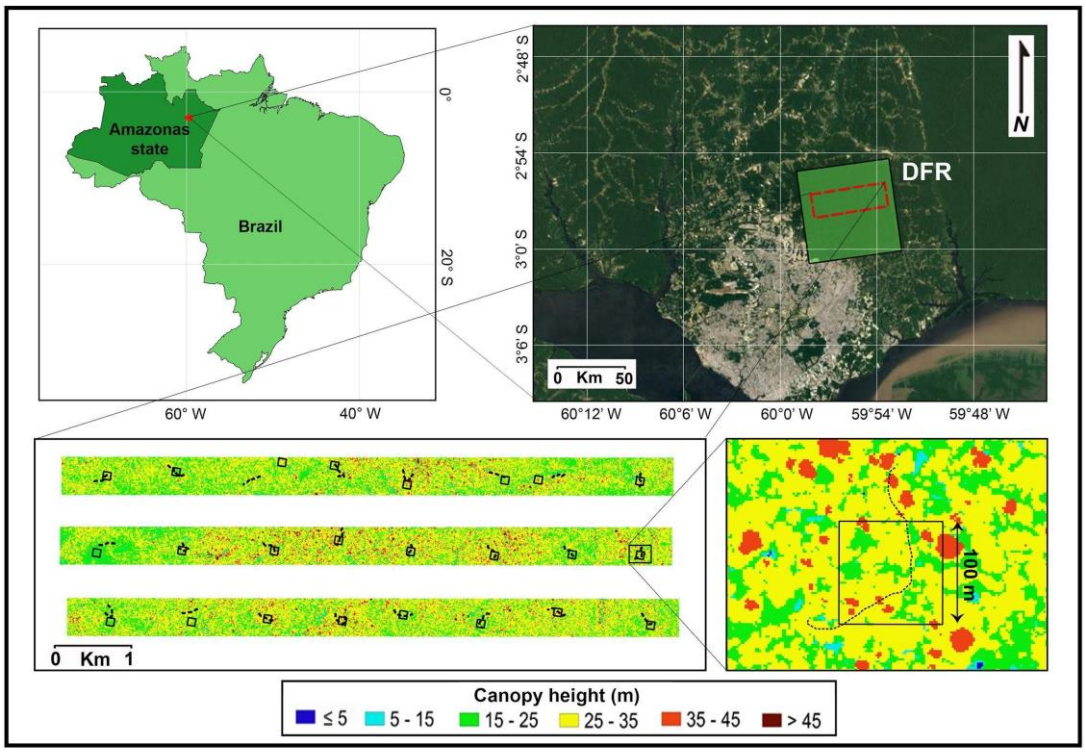

Figure 1. Location of the Ducke Forest Reserve (DFR) and study sampling design. Bottom-left panel shows the airborne ALS strips and the 1-ha ALS plots within (black squares). Bottom-right panel shows one ALS plot and the 250m long upward-looking PCL transect (dashed black line) crossing the plot.

ALS data were collected in June 2008 using a Leica ALS50 system (Heerbrugg, Switzerland) on board a Navajo EMB 820C (Embraer Ltd., Brazil), operated at pulse rate of 100 KHz, maximum 5° off-nadir view angle, ground beam diameter of 12 cm (a.k.a. Lidar footprint), mean flight altitude of 816 m above the ground level (overlap of 27%), and a Novatel OEMv4 GNSS receiver. Lidar data were georeferenced in the Universal Transverse Mercator (UTM) 20S coordinate system using the WGS84 datum. The acquired ALS point cloud has a mean density of 42 pulses m^{-2} (considering only the first returns). This high density was crucial for the data thinning objectives of this paper.

Ground returns were identified using all returns (of which 77% were first returns), using the Kraus and Pfeifer (1998) algorithm implemented in FUSION/LDV (McGaughey, 2016), using the command “GroundFilter” with a window size of 8 × 8 m and the default values for all other parameters. This produced a cloud of ground-returns with a mean density of 0.9 returns m^{-2}. The bare ground elevation was interpolated to 2 m horizontal resolution by simple kriging implemented in R environment (R Core Team, 2017) with lidR package (Roussel & Auty, 2017). This ground elevation was subtracted from the elevation of each ALS return to obtain its

aboveground height, and all analyses we conducted on these ground elevation-corrected data (aka normalized cloud).

The next step was to subsample pulse returns to create Lidar samples with different rarified pulse return densities for analysis based on this high-pulse-density data set. Considering just first return pulses at a 1 m horizontal resolution (finest grain size considered), we randomly thinned pulse densities to 30, 25, 20, 15, 10, 5 and 2 pulse returns m^{-2} (Figure 2). Whenever a cell's true pulse density was lower than the target rarified density, all the available pulses were used. The first-return point cloud was then binned into voxels (canopy volume units) and the number of first returns within each voxel was calculated for LAD estimation (next paragraph). We analyzed voxels at seven grain sizes: 1, 2, 5, 10, 25, 50 and 100 m. The vertical resolution (Dz in meters) was fixed at 1 m (Figure 3) to maximize potential to recover forest structural information (Stark et al., 2015). ALS data were analyzed for 24 one-hectare field plots of 100 m x 100 m. Each plot was traversed by an associated 250 m long upward-looking ground PCL transect (See Stark et al. 2012 for additional description).

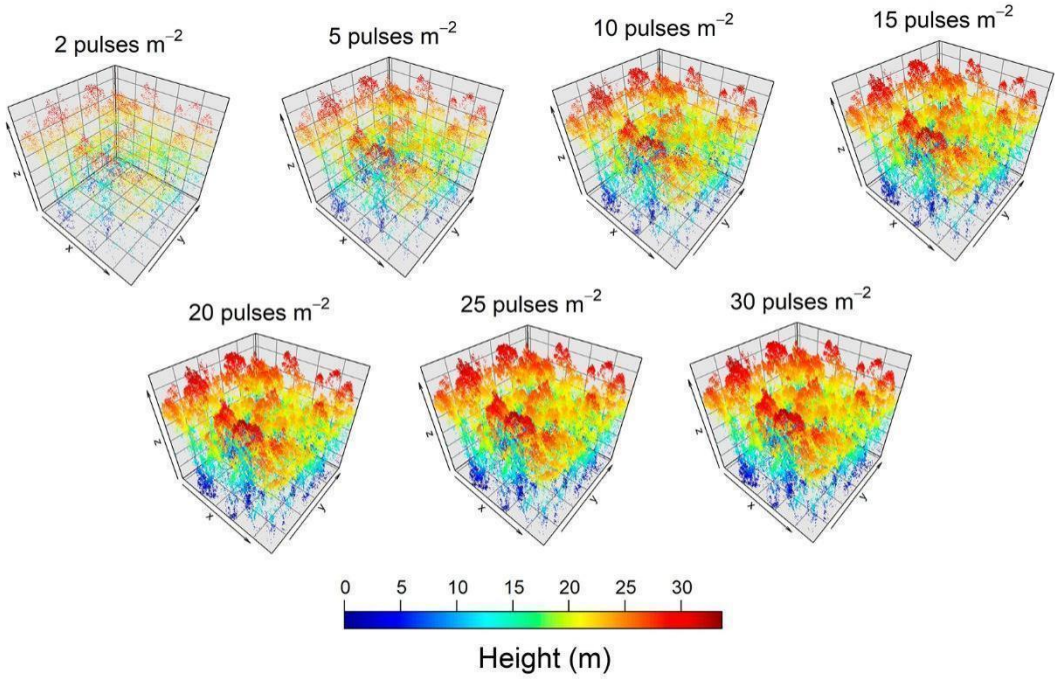

Figure 2. Example of pulse density reduction in a 1-ha ALS plot.

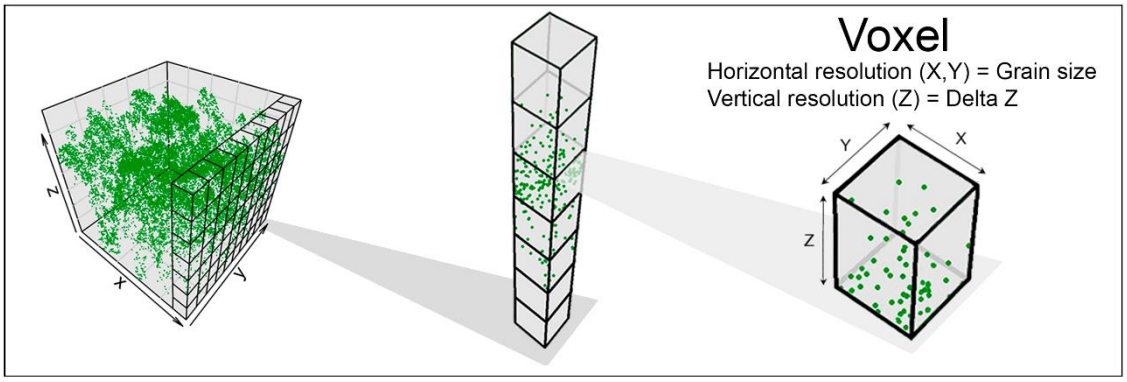

Figure 3. Voxel resolution and point cloud binning process for a square field plot clipped from the ALS data.

For each combination of voxel size and pulse return density, we calculated the number of pulses that entered a voxel *i* (*pulses.in*$_i$) and the number of pulses that passed through that voxel (*pulses.out*). Our assumption is that each lidar pulse is vertically incident. This means that we can track the passages and reflections of pulses within voxel columns to calculate the estimated pulses entering the tops of voxels and the pulses leaving the bottoms of voxels. All entering pulses that were not detected as returns from a voxel were assumed to pass through and enter the next voxel in a column. The MacArthur-Horn equation (equation 1) was applied for each voxel to compute its Leaf Area Density (*LAD*$_i$) (Figure 4).

$$LAD_i = \ln(pulses.in_i / pulses.out_i) \times \frac{1}{Dz} \times \frac{1}{K} \quad (1)$$

The *K* coefficient performs an inverse linear calibration of LAD to a known LAI. It can be assumed constant if certain factors remain fixed (e.g., lidar beam width, pulse intensity, pulse wavelength, distribution of leaf blade angles, degree of clustering of leaves, contribution of non-leaf area to returns). While the choice of *K* coefficient changes the LAD values, and consequently the derived LAI estimate, the relative LAD proportions found along the vertical strata are unaffected by *K*. We fixed *K* = 1, so we calculated an “effective LAD” and “effective LAI”. For convenience, these are hereafter referred to as simply LAD and LAI. The *K* coefficient effect is addressed in detail in the discussion section.

Occluded voxels—those where *pulses.out* = 0, or *pulses.in* = 0—were assigned as no-data (NA). After applying the MacArthur-Horn equation to all voxels, the mean LAD for each one-meter vertical stratum across a one-hectare field plot was obtained. Note that NA voxels are not considered when calculating the mean LAD of a stratum; in effect the horizontal area is renormalized to discount these

areas with NA-values, which have not been sampled by lidar pulses. The mean LAI for the entire plot was simply the sum of the mean LADs from each stratum (Figure 4).

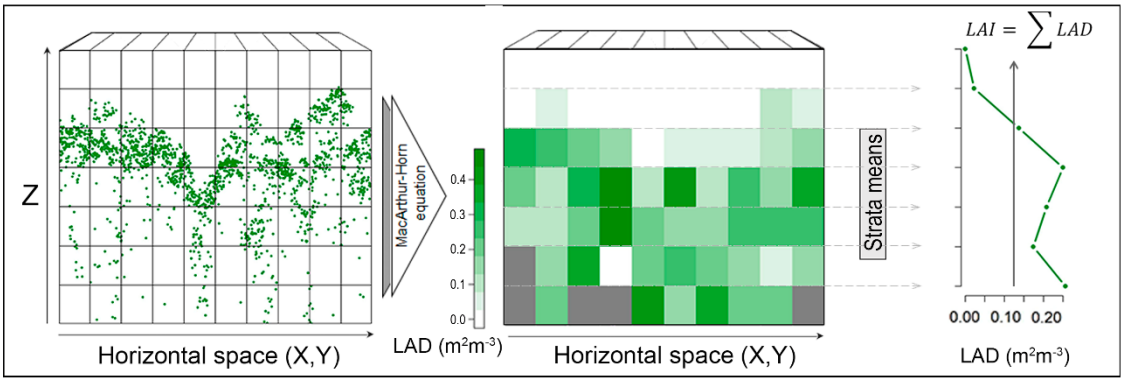

Figure 4. LAD profile and LAI calculation. Gray voxels indicate no data captured (coded as NA voxels). This NA value is important so that occluded forest voxels are not counted as zeros when obtaining mean LAD of a transect at each height interval above the ground.

The PCL data were collected in April 2009 using last returns from an upward-looking Riegl model LD90-3100VHS-FLP (Horn, Austria), along the 24 transects of 250 m in length. These transects overlap the 1-ha ALS plots. The locations of the ALS plots were limited to areas with high return density so that the point clouds could be thinned to target densities. As a result, ALS plots do not always coincide with the ground lidar transects. However, care was taken to ensure that the corresponding conditions were as close as possible, particularly the hillslope compartment (elevation).

The PCL instrument operates at a pulse rate of 1 KHz. Since the lidar surveys a vertical profile of the canopy and the data is acquired along a transect, the PCL produces a 2-D point cloud (height above ground x along-track distance). The instrument is attached to a gimbal to maintain vertical upward aim. A small 12v battery and a water-resistant computer complete the system (Almeida et al., 2016). The operator walks at a constant pace, using an electronic metronome and field markers spaced every two meters. Walking at a speed of half a meter per second, the PCL emits a total of 2,000 pulses per meter along the transect. For vertical and horizontal resolutions, the PCL-based LAD profiles used Dz = 1 m and Dx = 2 m, respectively (Almeida et al., 2016; Stark et al., 2012). The LAD strata estimated from both ALS and ground lidar were limited to pulse returns above one meter from the ground. This avoids ground-return interference in the ALS data and is also imposed by the ground lidar sensor height.

To investigate the effects of pulse density and grain size on the ALS LAD profile estimation, we obtained LAD at each 1m height interval averaged over the 24 plots. We first examined the change of the mean LAD profile (average of 24 plots) in absolute values (m^2 m^{-3}; K = 1) with varied grain size and pulse density. We then compared, also as a function of grain size and pulse density, the behaviors of (i) the 24-plot mean ALS profile of relative LAD (LAD as % of LAI, which cancels K); (ii) the 24-transect mean profile of ground lidar-derived relative LAD; and (iii) a mean profile of directly measured relative LAD, collected from four mature old growth forest plots of 100-m^2 close to the Ducke Forest Reserve (see McWilliam et al., 1993). Utilizing McWilliam et al., (1993) for comparison we assume that the average forest structure is stable through time (see also Stark et al., 2012), and indeed this forest with low turnover has not been implicated in any major disturbance processes (Ribeiro et al., 1999). Finally, we investigated the stability of the ranking (by Spearman rank correlations) of the 24 plots by their LAI value (using K = 1), as a function of different grain sizes and pulse densities.

2.3. Results

Vegetation profiles expressed as absolute LAD (m^2 m^{-3}) tended to stabilize when grain size reached 10 m independent of pulse density or when pulse density reached 15 pulses m^{-2}, regardless of grain size (Figure 5). Within each of the smaller grain sizes (1, 2 and 5 m), vegetation density increased logarithmically with pulse density, until saturating at 15 pulses m^{-2}. As grain size increased from 1 m to 10 m, understory LAD increased greatly and LAD in the upper canopy decreased slightly, shifting the overall shape of the profile.

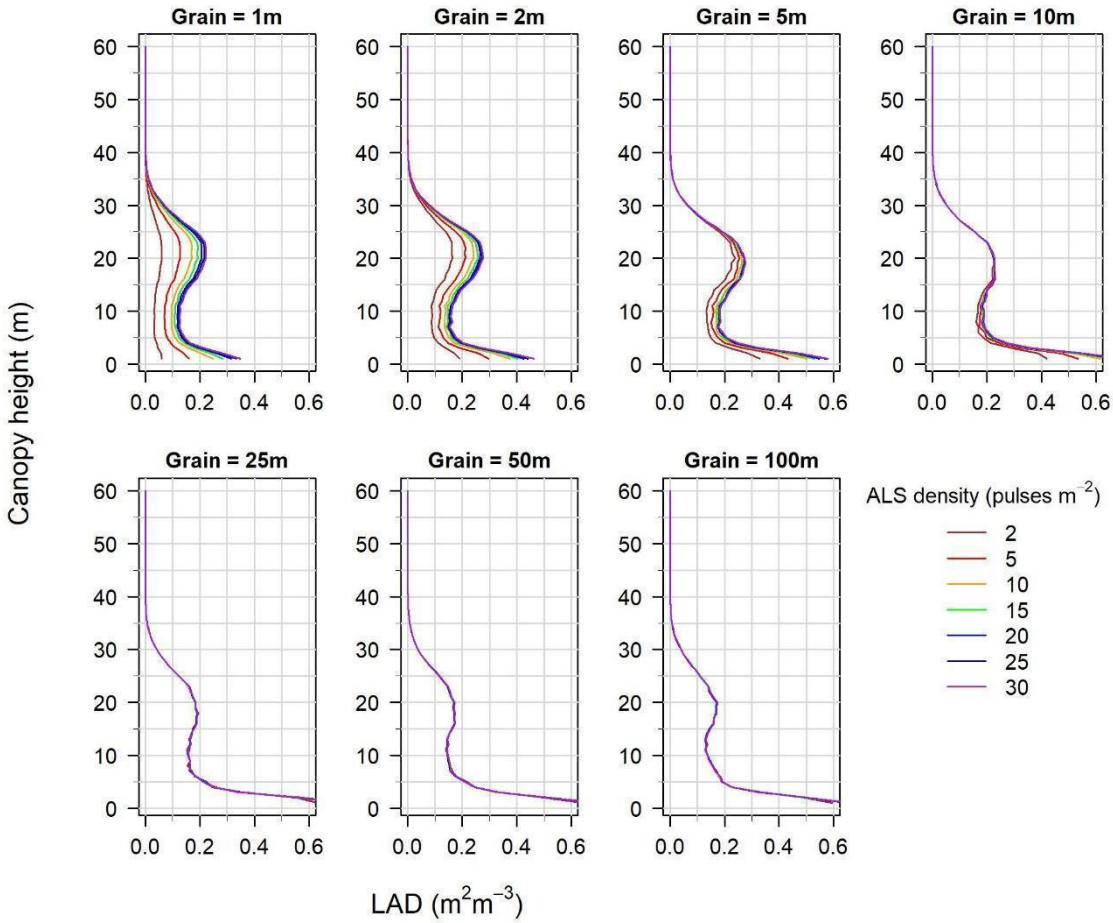

Figure 5. Changes in the 24-plots mean ALS profile of LAD (in absolute values; m^2 m^{-3}) as a function of grain size (panels) and pulse density (profile colors).

The 24-plot mean profile of relative LAD was unaffected by pulse density (Figure 6). Increasing grain size had the same effect of shifting the profile observed in the profile with absolute LAD values, with the upper canopy decreasing and lower canopy increasing in density. Stability at large grain size did not lead to improved accuracy—increasing the grain size also increased the difference between the ALS profile and the profiles derived from field measurements and ground lidar.

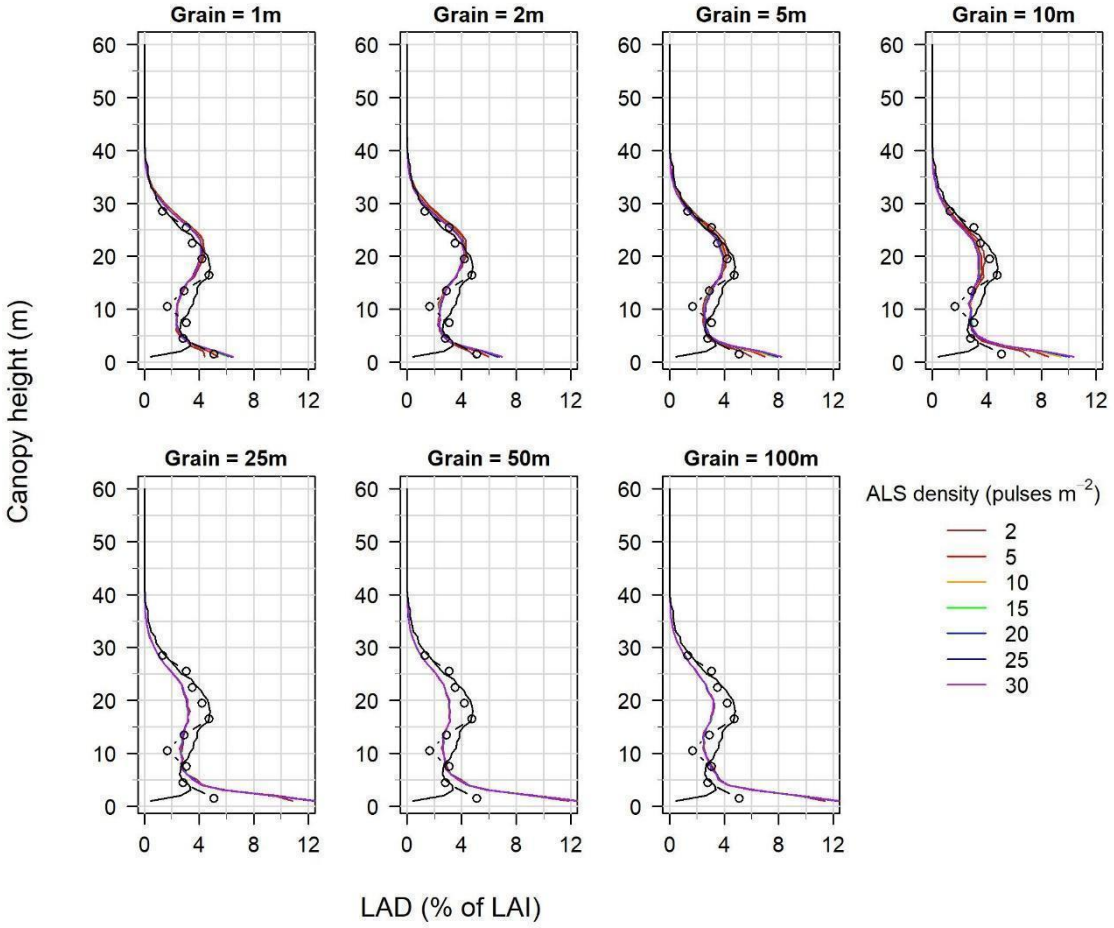

Figure 6. Behavior of the 24-plot mean LAD profile in relative values (% of LAI), as a function of grain size (panels). For ALS, different pulse densities are shown as different colored profile lines, but these overlap to a high degree. The black line is the 24-plot mean relative LAD from the PCL at a fixed, high pulse density (2,000 pulses m^{-1}) and at different grain sizes (panels). Open circles show the four-plot mean relative LAD profile of destructively measured field data with a fixed grain size of $100m^2$ and no pulse density.

Ranking of the 24 plots by their LAI values was completely stable with respect to pulse density. Spearman Rank Correlation was 1.0 across all seven classes of pulse density. This was true at all seven grain sizes (Figure 7). Ranking of plots by their LAI was affected somewhat by different grain sizes: Rank Correlation was 0.83 across all seven classes of grain size, when evaluated separately for each pulse density class and then averaged (Figure 8). However, if considering only the four smaller grain sizes in Figure 8 (1m, 2m, 5m and 10m), ranking of plots by their LAI was very stable as a function of grain size, with Rank Correlation = 0.95.

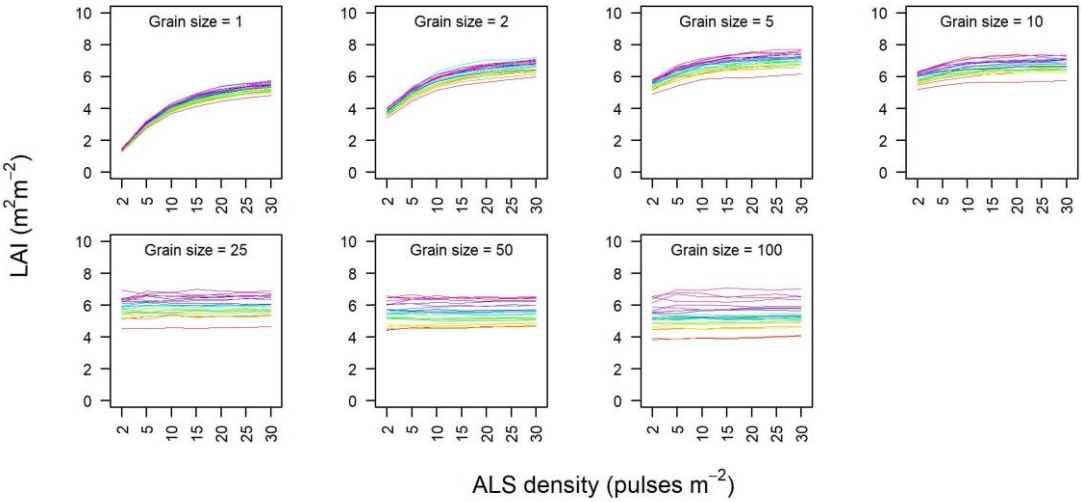

Figure 7. Leaf Area Indices (LAIs) from ALS, one for each of the 24 1-ha plots, as a function of seven classes of pulse density (x-axis) at each grain size. Colored lines identify plots. Consistent ordering of colors along each x-axis in the panels indicates stable ranking of plot LAIs, irrespective of pulse density.

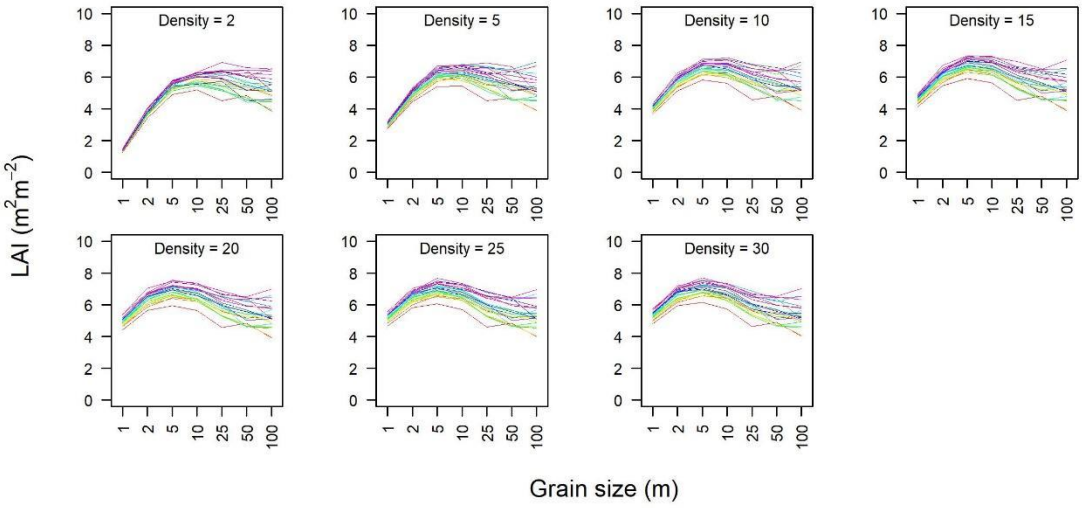

Figure 8. Leaf Area Indices (LAIs) from ALS, one for each of the 24 1-ha plots, as a function of seven classes of grain size (x-axis) at each pulse density. Colored lines identify plots. Consistent ordering of colors along each x-axis in the panels indicates stable ranking of plot LAIs, irrespective of grain size.

2.4. Discussion

2.4.1. Grain size and pulse density effects on LAD and LAI

To the best of our knowledge, this is the first study to assess the impacts of ALS pulse density and voxel resolution on the estimation of LAD profiles and LAI, using the MacArthur-Horn equation (Beer-Lambert Law) applied to small-footprint lidar (ALS) in a tropical forest. In general, the LAD and LAI estimates tended to

stabilize with increasing grain size and increasing ALS pulse density. At small grain sizes of 1m, 2m, and 5m, absolute LAD profiles became stable at respective pulse densities of 15, 15, and 10 pulses m^{-2}. At grain sizes of 10m or larger, pulse density can be as low as 2 pulses m^{-2} and still provide a LAD profile very similar to those obtained at higher pulse density (Figure 5).

The 'sweet spot' in the trade-off between pulse density and grain size hinges on accuracy. Smaller ALS grain sizes (< 10 m) showed better agreement with the vegetation profiles from destructive field measurements and from PCL ground lidar (Figure 6). This is particularly evident when comparing ALS results to those obtained by field measurements in the portion of the vegetation profile below ~4 m height. Grain sizes ≥ 10 m will overestimate vegetation in this portion of the profile, particularly when pulse density is high. Thus, for lower density lidar surveys, a grain size of 10 m may be effective, and may mitigate some of the unwanted artificial shift in vertical LAD distributions observed at larger spatial scales. Increasing grain size that could approximate length scales of branches or whole trees—primary elements of leaf architectural support—might be expected to create strong leaf clumping and thus violate the MacArthur-Horn assumption of random leaf distribution. This could help explain the increasing LAD profile errors that we observed with increasing grain size.

Shao et al. (2019) assessed the LAD estimation from multitemporal ALS data and developed a correction method to enhance inter comparability over multiple laser sensors. According to them, pulse return density had little appreciable bias impact above 20 returns m^{-2} using a grain size of 2m for plots with 0.25 ha.

Our results show that a very consistent LAI ranking of different sites can be obtained independent of pulse density. While relative LAD values are effective for assessing potential scale dependencies in the shape of LAD profiles, relative LAD information alone is limited to compare sites, since LAI differences are also critical to study canopy structure and function. Less expensive low-density ALS contracts may be able to provide consistent discrimination of site density and distribution of leaves. We caution, however, that the lower accuracy particularly of LAD profile estimation at coarse grain size or low pulse densities may be unacceptable for some applications, particularly models and methods that rely on the fine scale vertical and horizontal heterogeneity of canopy structure to make ecological inferences. Examples include the estimation of forest stock or demographic structure (Stark et al., 2015) or light

interception and absorption (if the methods of Atkins et al., 2018 were applied to ALS data). For these applications our results suggest that pulse densities of 20 pulses m^{-2} or greater and grain sizes between 2 and 5 meters, which maximize accuracy and stability, should be utilized.

Our results agree with classic 'optical probe' based investigations of leaf area estimation. Aber et al. (1978), using the MacArthur-Horn equation and point-quadrat sampling (Wilson 1958, 1965), also found a positive relation between LAI estimates and sample size, analogous to our Figure 7. Aber et al. (1978) showed that, despite a sample size effect impacting absolute LAD values and LAI, the fraction of LAI in each vertical stratum was fairly constant over different sample sizes. In apparent agreement, we found that for small grain sizes, the vegetation profile shapes are stable with respect to pulse density if LAD is expressed in relative units (% of LAI), while absolute LAD profiles converged to a stable shape (and LAI) only with high pulse density (≥ 15 pulses m^{-2}) (Figures 5 and 6).

2.4.2. Tackling with occluded voxels

At small grain sizes, the number of occluded voxels (no-data voxels) increases and one must take care to avoid their influence on mean plot-wide LAD profile shape and mean plot-wide LAI (or transect mean LAI, in the case of ground lidar). No-data voxels do not affect the mean LAD obtained across all voxels at the same aboveground height across a plot. Plot-scale mean LAI obtained from the sum of these stratum means will be a proper estimate (Stark et al., 2012, 2015; Almeida et al., 2016). But if one sums the LAD values in each voxel column to obtain the LAI at each horizontal grid footprint in the forest, each of these sums will be affected by the number of no-data voxels in their respective columns. A mean plot-wide LAI from these column LAIs will be incorrect. Such a column-level LAI mapping must consider columns with any no-data voxels to have no LAI data as well. Kükenbrink et al (2017) in a Swiss deciduous forest, with a pulse density of 11 pulses m^{-2} and grain size of 1 m, found at least 25% of the forest canopy volume remains occluded in the ALS data. Here we found a similar result, with 29, 23, 10 and 3% occluded when grain size is, respectively, 1-, 2-, 5- and 10-m and pulse density is fixed at 10 pulses m^{-2}. In this sense, larger grain sizes effectively mask areas that are occluded in the canopy that fall within voxels with varied pulse sampling. And the spatial structure of occluded

areas may create apparent leaf area clumping that influences leaf area estimation. Our expectation is that the same grain sizes that produce maximal correspondence with PCL and destructive LAD profile data also optimize LAI estimation accuracy for comparisons.

We assume that LAD of visible voxel at any given height provide an unbiased estimate of the LAD of occluded voxels at that height. Where there are many gaps with well illuminated low canopy, the LAD of these lower visible voxels may be higher than the LAD of occluded understory voxels at the same height. Occluded voxels are more likely to fall in low light environments where LAD is also low because with the down-facing ALS occluded increases with depth and leaf area above. Nonetheless, forests with a lot of gaps should have a high mode of LAD in the lower mid-canopy and this is what we observe in gap-rich forests whether using up-facing PCL or down-facing ALS, which suggest that no significant bias is present since this environment-driven occlusion effectis not expected from an up-facing system (Stark et al., 2012).

2.4.3. Calibrating the K coefficient

In the absence of a known calibration LAI from a reference site, some authors have used K = 1 (Sumida et al., 2009, Almeida et al., 2016). However, for accurate values of absolute LAI, particularly at low pulse densities for which lower portions of the canopy will have many no-data voxels, the coefficient K should be adjusted to calibrate estimated LAI to a correct, independently measured LAI (equation 2). An alternative is then to calibrate K with a given lidar system at a reference LAI site, then estimate LAI with that same system for another site with unknown LAI, under the assumption that leaf properties such as clumping and leaf angles that could affect K-calibration are constant (see Weiss et al., 2004). Calibrated K is obtained as the ratio between the mean LAI derived from lidar (K = 1; $LAI_{k=1}$) and the correct mean LAI of the reference site (LAI_{Site}):

$$K = \frac{LAI_{K=1}}{LAI_{Site}} \quad (2)$$

Figure 9 shows the appropriate K values for maintaining agreement between ALS-derived LAI and a field-measured mean LAI of 5.7 (the latter from McWilliams et al., 1993). Calibrated K is clearly sensitive to both grain size and pulse density. It

tends to stabilize as pulse density increases but remains sensitive to grain size even at high pulse densities. The robustness of the *K*-curves in Figure 9 is still unknown. Different forest types with different specie composition, leaf orientation and leaf clumping may produce varied relations between grain size, pulse density and K coefficient. Probably forest types with lower LAI present better results with lower pulse densities, since obstruction is also reduced.

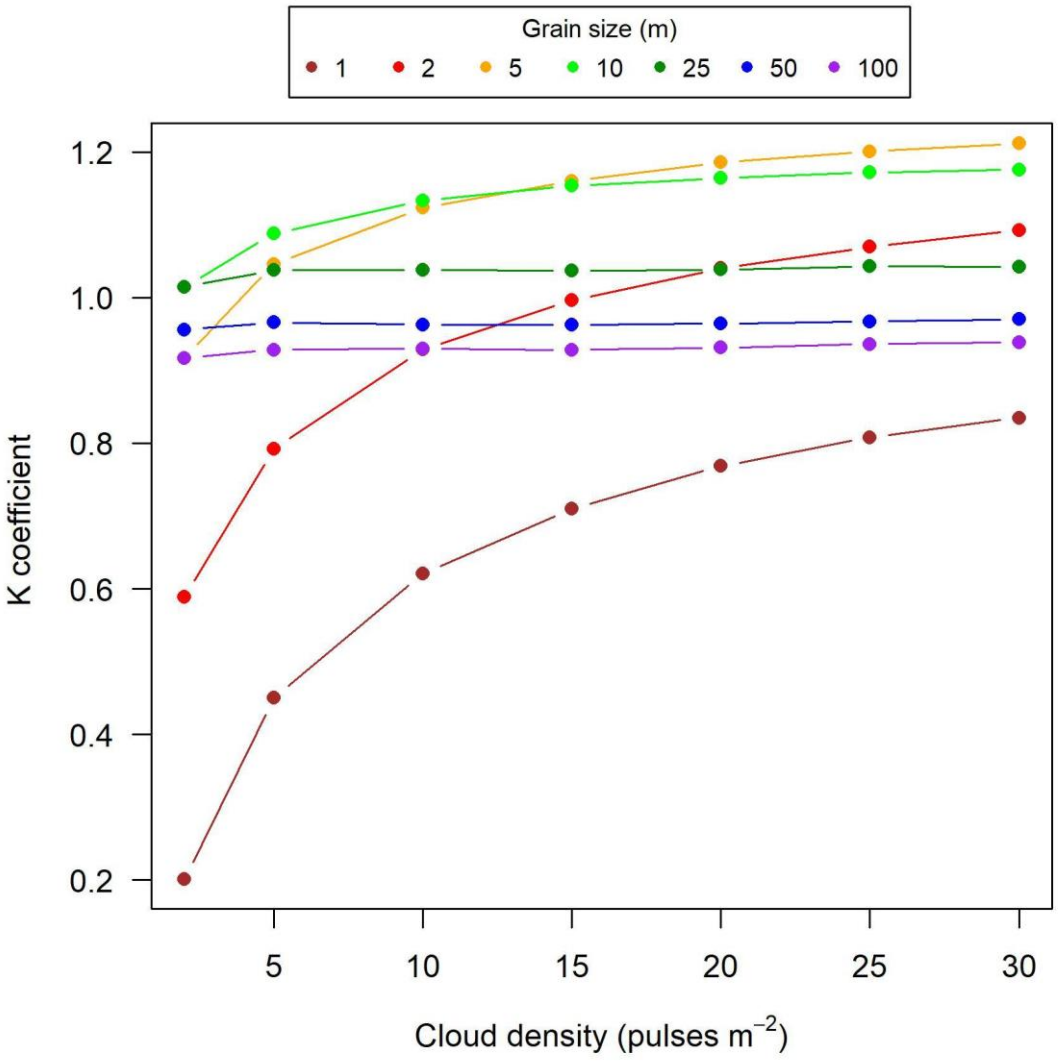

Figure 9. Appropriate values for *K* coefficient to maintain a constant LAI from MacArthur-Horn equation, as function of pulse density (x-axis) and grain size (line colors). Constant *K* here has a value of 5.7, derived from direct destructive measurement (McWilliams et al., 1993).

2.4.4. Limitations of this study

We found a discrepancy between PCL and ALS profiles at 1-4 m (low-canopy) height, which should not be considered when evaluating ALS accuracy (Figure 6).

This is attributable to removing some of the understory, mainly palm fronds, to allow passage of the ground lidar operator at a constant walking speed. Although the ALS LAD profiles (using grain size of 1 and 2 m) at the lowest portion of the canopy are very similar to those from field destructive samples, and the Ducke site is characterized by dense understory vegetation (particularly palms; Ribeiro et al., 1999), it is possible that this increase of LAD at low-canopy height is an effect of the ground estimation errors (ie., real ground returns not classified as ground points). The lowest pulse penetration and highest error is expected in the understory with ALS data, and future work should take care to exclude low positions from analysis (or explore corrections) when appropriate. We also note that ground estimation errors will increase as sampling density decreases over ALS collections, particularly in heterogeneous terrain (Leitold et al., 2014), a factor that was not considered in our analysis since ground surfaces were estimated prior to pulse rarefactions.

We used four profiles of field collected LAD from small patches of dense forest as our “gold standard”. However, the true mean profile of LAD across a larger landscape will include forest gaps. These should affect the shape of the mean profile of LAD, increasing LAD in the lower half of the profile.

Many other factors (e.g., instrument type, beam divergence, scan angle, and flight altitude) could influence relationships between grain size, pulses density and the estimation of LAD profiles. For example, our study used a maximum of 5° off-nadir scan angle; higher scan angles may introduce biases in LAD profiles since one of the key assumptions of the MacArthur-Horn equation is that pulses are parallel and emitted vertically. Additionally, higher flight altitude would increase ground footprint size, which could decrease penetration rates and increase exclusion problems, all else fixed (Goodwin et al., 2006).

In practice, low pulse densities shown in our study to be sufficient for obtaining LAD profiles may be associated with high altitude flights and wide scan angle collections, to maximize coverage at low cost. The effects of wide angles (e.g., +/- 30 degrees), and the larger pulse footprints expected from greater beam divergences, on estimates of LAD profiles still require study. To improve comparability with our study LAD profiles could be extracted from only near vertical angles found closer to the flight track, where the MacArthur-Horn equation assumption of vertical pulse transmission is better satisfied.

2.4.5. Conclusions and implications for future research

For accurate and stable estimation of LAD profiles and of LAI from ALS data in tropical rainforests, we recommend voxels with small grain size (< 10 meters) only when pulse density is greater than 15 pulses m^{-2}. For pulse densities less than 15 pulses m^{-2} we recommend a 10 meters grain size. We also highlight the importance of using a calibrated *K* coefficient in the MacArthur-Horn equation, particularly so when using small grain size (1-5 meters) with low pulse densities. For stable ranking/discrimination of sites by their LAI values using fixed *K*, pulse density had no effect, and grain size had almost no effect for dimensions ≤ 10m.

However, it is important to highlight that our results were obtained with a specific ALS instrument, forest type and survey configuration. Thus, we have isolated pulse density effects per se. More field collected reference plots in different forest types (with different LAI values), and lidar data sets that include repeated collections with survey parameters systematically varied to explore not just pulse density but also scan angle, pulse footprint, and other factors' effects, are recommended to improve understanding of LAD and LAI estimation from lidar. Shao et al. 2019 found that flight parameters with different lidar sensors can effect LAD estimates and they developed a correction method to enhance inter comparability over multiple laser sensors. However, the individual effect of each parameter, such as the scan angle, still need to be better understood.

New lidar technologies, as Geiger lidar (aka, "single pulse lidar") (Abdullah et al., 2016), have the potential to generate high-density clouds from low-cost flights, which might estimate LAD with high resolutions (~ 1m). Geiger lidar allows to split the single laser pulse into multiple sub-pulses, resulting in a denser point cloud from the same or a less efficient laser source.

We examined how analysis grain (presented in Figure 5) impacts vegetation profile estimation when we included all returns, not just the 77% which are first returns (Supplementary material Figures S1 and S2). The effect is to decrease the estimated upper canopy LAD values. This may be an artifact, however, since the MacArthur-Horn approach assumes that each pulse represents an independent canopy probe, while in fact 2nd returns are effectively only possible after 1st returns (below 1st returns for airborne lidar) and so forth for 3rd and 4th returns. Thus,

additional algorithm development and validation could lead to more accurate MacArthur-Horn LAD estimation from multiple return lidar data.

LAD profiles have seen a gamut of applications in recent tropical forest studies: impact of fire and sensitivity to fire (Almeida et al., 2016); estimating tree diameter-class frequencies (Stark et al., 2015); forest type discrimination; and radiation transfer and absorption modeling (Stark et al., 2012; Tymen et al., 2017; Wu et al., 2018; Atkins et al., 2018). ALS-derived estimations of LAD profiles and of LAI provide unprecedented opportunities for estimating canopy structure and function, including modeling the leaf environments and forest demographic structure, on a broad spatial scale to address problems in forest conservation and management.

2.5. Supplementary material

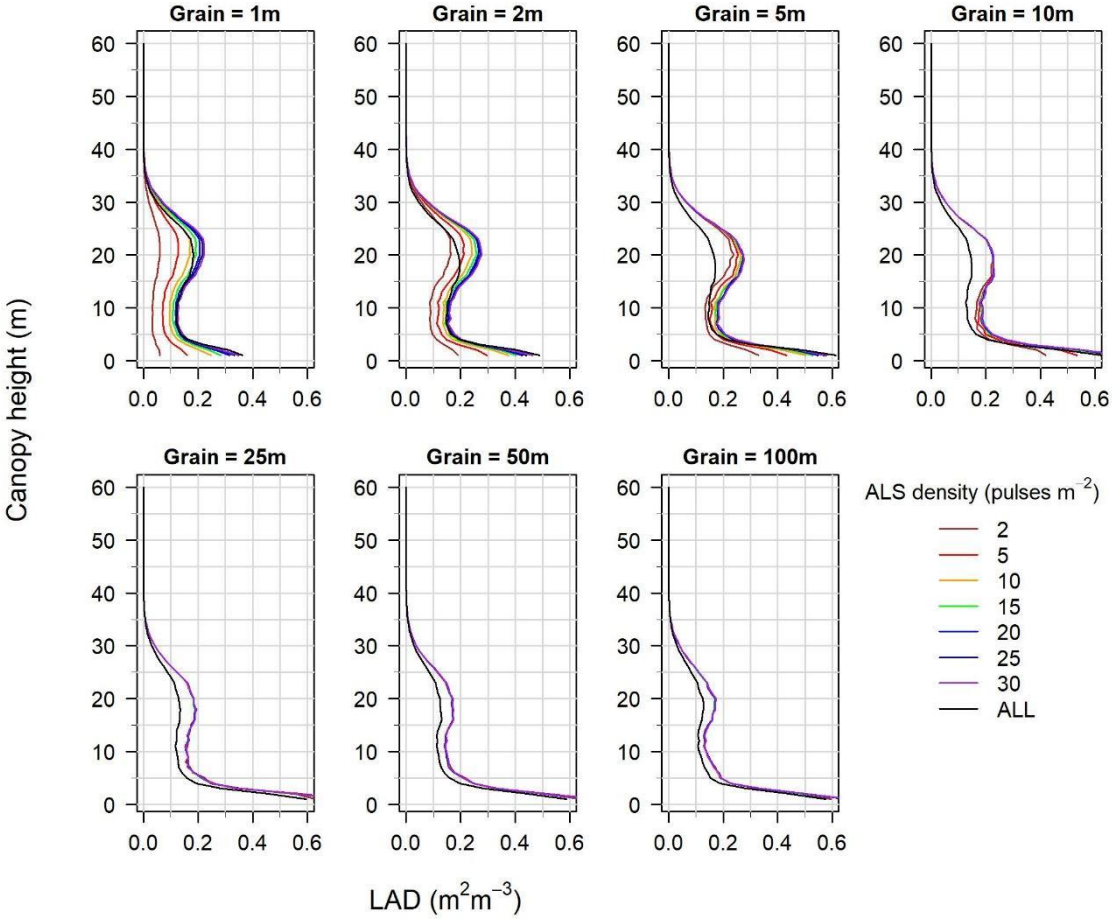

Figure S1. Changes in the 24-plot mean ALS profile of LAD (in absolute values; m^2 m^{-3}) as a function of grain size (panels) and pulse density (profile colors). In this figure we added the profile using ALL returns (including multiple returns) totaling a density of 55 returns m^{-2}.

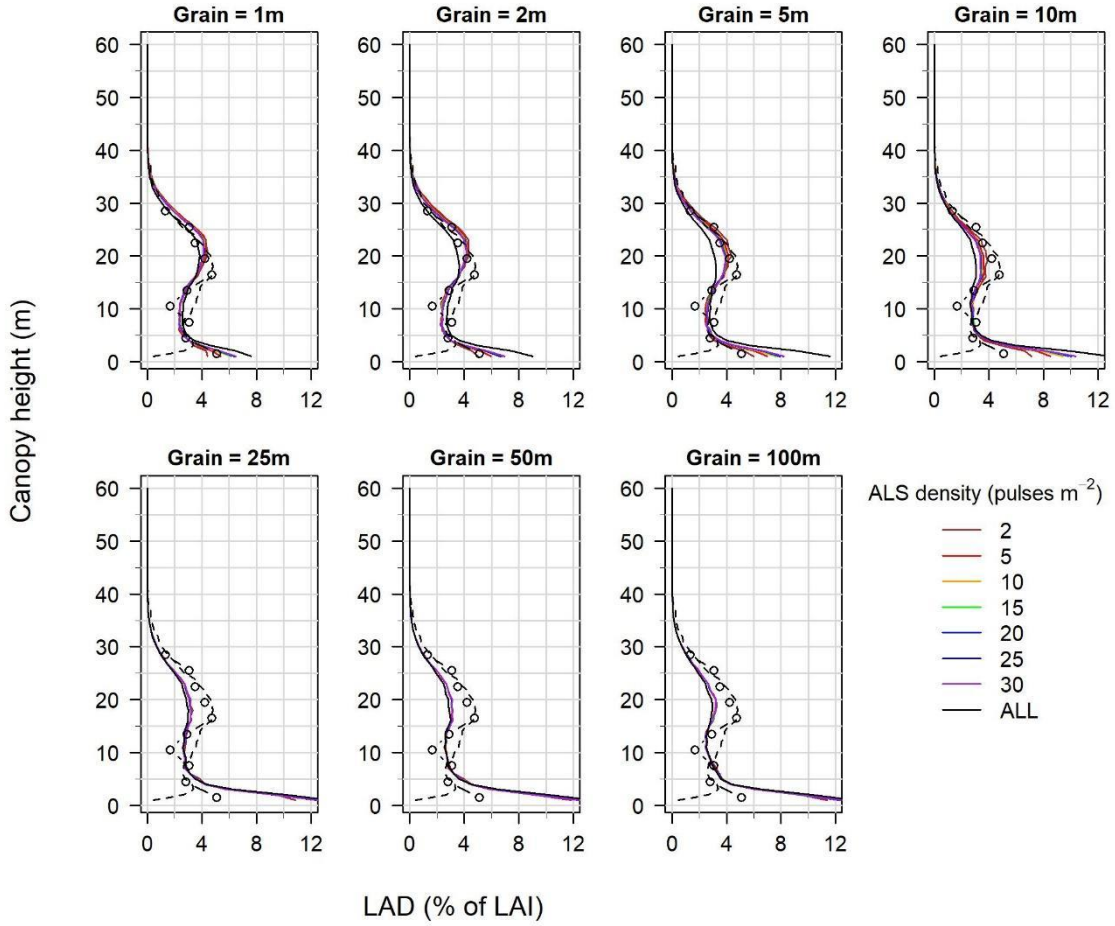

Figure S2. Behavior of the 24-plot mean LAD profile in relative values (% of LAI), as a function of grain size (panels). For ALS, different pulse densities are shown as different colored profile lines, but these overlap to a high degree. The black dashed line is the 24-plot mean relative LAD from the PCL at a fixed, high pulse density (2,000 pulses m^{-1}) and at different grain sizes (panels). Open circles show the four-plot mean relative LAD profile of destructively measured field data with a fixed grain size of 100m^2 and no pulse density. In this figure we added the profile using ALL returns (including multiple returns) totalizing a density of 55 returns m^{-2}.

References

Aber, J.D., 1979. A method for estimating foliage-height profiles in broad-leaved forests. J. Ecol. 67, 35–40. doi:10.2307/2259335

Adnan, S., Maltamo, M., Coomes, D.A., Valbuena, R., 2017. Effects of plot size, stand density, and scan density on the relationship between airborne laser scanning metrics and the Gini coefficient of tree size inequality. Can. J. For. Res. 47, 1590–1602. doi: 10.1139/cjfr-2017-0084

Almeida, D.R.A. de, Nelson, B.W., Schietti, J., Gorgens, E.B., Resende, A.F., Stark, S.C., Valbuena, R., 2016. Contrasting fire damage and fire susceptibility

between seasonally flooded forest and upland forest in the Central Amazon using portable profiling LiDAR. Remote Sens. Environ. 184, 153–160.doi:10.1016/j.rse.2016.06.017

Asner, G.P., Mascaro, J., 2014. Mapping tropical forest carbon: Calibrating plot estimates to a simple LiDAR metric. Remote Sens. Environ. 140, 614–624. doi:10.1016/j.rse.2013.09.023

Atkins, J.W., Fahey, R.T., Hardiman, B.H. and Gough, C.M., 2018. Forest canopy structural complexity and light absorption relationships at the sub-continental scale. Journal of Geophysical Research: Biogeosciences. doi:10.1002/2017JG004256

Bréda, N.J.J., 2003. Ground-based measurements of leaf area index: A review of methods, instruments and current controversies. J. Exp. Bot. 54, 2403–2417. doi:10.1093/jxb/erg263

Clark, D.B., Olivas, P.C., Oberbauer, S.F., Clark, D.A., Ryan, M.G., 2008. First direct landscape-scale measurement of tropical rain forest Leaf Area Index, a key driver of global primary productivity. Ecol. Lett. 11, 163–172. doi:10.1111/j.1461-0248.2007.01134.x

Goodwin, N.R., Coops, N.C., Culvenor, D.S., 2006. Assessment of forest structure with airborne LiDAR and the effects of platform altitude. Remote Sens. Environ. doi:10.1016/j.rse.2006.03.003

Hardiman, B.S., Bohrer, G., Gough, C.M., Vogel, C.S., Curtis, P.S., 2011. The role of canopy structural complexity in wood net primary production of a maturing northern deciduous forest. Ecology 92, 1818–1827. doi:10.1890/10-2192.1

Hardiman, B.S., Gough, C.M., Halperin, A., Hofmeister, K.L., Nave, L.E., Bohrer, G., Curtis, P.S., 2013. Maintaining high rates of carbon storage in old forests: A mechanism linking canopy structure to forest function. For. Ecol. Manage. doi:10.1016/j.foreco.2013.02.031

Jensen, J.L.R., Humes, K.S., Hudak, A.T., Vierling, L.A., Delmelle, E., 2011. Evaluation of the MODIS LAI product using independent lidar-derived LAI: A case study in mixed conifer forest. Remote Sens. Environ. 115, 3625–3639. doi:10.1016/j.rse.2011.08.023

Kraus, K., Pfeifer, N., 1998. Determination of terrain models in wooded areas with airborne laser scanner data. ISPRS J. Photogramm. Remote Sens. 53, 193–203. doi:10.1016/S0924-2716(98)00009-4

Kükenbrink, D., Schneider, F.D., Leiterer, R., Schaepman, M.E., Morsdorf, F., 2017. Quantification of hidden canopy volume of airborne laser scanning data using a voxel traversal algorithm. Remote Sens. Environ. doi:10.1016/j.rse.2016.10.023

Leitold, V., Michael Keller, Douglas C Morton, Bruce D Cook, Yosio E Shimabukuro, 2014. Airborne lidar-based estimates of tropical forest structure in complex terrain: Opportunities and trade-offs for REDD+. Carbon Balance Manag. 10. doi:10.1186/s13021-015-0013-x

Longo, M., Keller, M., dos-Santos, M.N., Leitold, V., Pinagé, E.R., Baccini, A., Saatchi, S., Nogueira, E.M., Batistella, M., Morton, D.C., 2016. Aboveground biomass variability across intact and degraded forests in the Brazilian Amazon. Global Biogeochem. Cycles 30, 1639–1660. doi:10.1002/2016GB005465

MacArthur, R.H., Horn, H.S., 1969. Foliage profile by vertical measurements. Ecology 50, 802–804. doi:10.2307/1933693

Martens, S.N., Ustin, S.L., Rousseau, R.A., 1993. Estimation of tree canopy leaf area index by gap fraction analysis. For. Ecol. Manage. 61, 91–108. doi:10.1016/0378-1127(93)90192-P

McGaughey, R.J., 2016. FUSION/LDV: Software for LIDAR data analysis and visualization. US Dep. Agric. For. Serv. Pacific Northwest Res. Stn. Seattle, WA, USA 123.

McWilliam, A.-L.C., Roberts, J.M., Cabral, O.M.R., Leitao, M.V.B.R., de Costa, A.C.L., Maitelli, G.T., Zamparoni, C.A.G.P., 1993. Leaf Area Index and above-ground biomass of terra firme rain forest and adjacent clearings in Amazonia. Funct. Ecol. 7, 310. doi:10.2307/2390210

Olivas, P.C., Oberbauer, S.F., Clark, D.B., Clark, D.A., Ryan, M.G., O'Brien, J.J., Ordoñez, H., 2013. Comparison of direct and indirect methods for assessing leaf area index across a tropical rain forest landscape. Agric. For. Meteorol. 177, 110–116. doi:10.1016/j.agrformet.2013.04.010

Parker, G.G., Harding, D.J., Berger, M.L., 2004. A portable LIDAR system for rapid determination of forest canopy structure. J. Appl. Ecol. 41, 755–767. doi:10.1111/j.0021-8901.2004.00925.x

Putz, F.E., 1983. Liana biomass and leaf area of a "Tierra Firme" forest in the Rio Negro Basin, Venezuela. Biotropica 15, 185–189. doi:10.2307/2387827

R Core Team, 2017. R: A language and environment for statistical computing. R Found. Stat. Comput. Vienna, Austria. URL http//www.R-project.org/. R Foundation for Statistical Computing.

Ribeiro, J.E.L.S., Hopkins, M.J.G., Vicentini, A., Sothers, C.A., Costa, M.A.S., Brito, J.M., Souza, M.A.D., Martins, L.H.P., Lohmann, L.G., Assunção, P.A.C.L., Pereira, E.C., Silva, C.F., Mesquita, M.R., Procópio, L.C., 1999. Flora da Reserva Ducke: guia de identificação das plantas vasculares de uma floresta de terra-firme na Amazônia Central, Instituto Nacional de Pesquisas da Amazônia.

Roussel, J.R., Auty, D., 2017. lidR: Airborne LiDAR Data Manipulation and Visualization for Forestry Applications. R package version 1.3.1.

Roussel, J.R., Caspersen, J., Béland, M., Thomas, S., Achim, A., 2017. Removing bias from LiDAR-based estimates of canopy height: Accounting for the effects of pulse density and footprint size. Remote Sens. Environ. 198, 1–16. doi:10.1016/j.rse.2017.05.032

Silva, C.A., Hudak, A.T., Vierling, L.A., Klauberg, C., Garcia, M., Ferraz, A., Keller, M., Eitel, J., Saatchi, S., 2017. Impacts of airborne lidar pulse density on estimating biomass stocks and changes in a selectively logged tropical forest. Remote Sens. 9. doi:10.3390/rs9101068

Stark, S.C., Leitold, V., Wu, J.L., Hunter, M.O., de Castilho, C. V., Costa, F.R.C., McMahon, S.M., Parker, G.G., Shimabukuro, M.T., Lefsky, M.A., Keller, M., Alves, L.F., Schietti, J., Shimabukuro, Y.E., Brandão, D.O., Woodcock, T.K., Higuchi, N., de Camargo, P.B., de Oliveira, R.C., Saleska, S.R., 2012. Amazon forest carbon dynamics predicted by profiles of canopy leaf area and light environment. Ecol. Lett. 15, 1406–1414. doi:10.1111/j.1461-0248.2012.01864.x

Sumida, A., Nakai, T., Yamada, M., Ono, K., Uemura, S., Hara, T., 2009. Ground-based estimation of leaf area index and vertical distribution of leaf area density in a *Betula ermanii* forest. Silva Fenn. 43, 799–816. doi:10.14214/sf.174

Swinehart, D.F., 1962. The Beer-Lambert Law. J. Chem. Educ. 39, 333. doi:10.1021/ed039p333

Tang, H., Dubayah, R., Swatantran, A., Hofton, M., Sheldon, S., Clark, D.B., Blair, B., 2012. Retrieval of vertical LAI profiles over tropical rain forests using waveform lidar at La Selva, Costa Rica. Remote Sens. Environ. 124, 242–250. doi:10.1016/j.rse.2012.05.005

Turner, D.P., Cohen, W.B., Kennedy, R.E., Fassnacht, K.S., Briggs, J.M., 1999. Relationships between leaf area index and Landsat TM spectral vegetation indices across three temperate zone sites. Remote Sens. Environ. 70, 52–68. doi:10.1016/S0034-4257(99)00057-7

Tymen, B., Vincent, G., Courtois, E.A., Heurtebize, J., Dauzat, J., Marechaux, I., Chave, J., 2017. Quantifying micro-environmental variation in tropical rainforest understory at landscape scale by combining airborne LiDAR scanning and a sensor network. Ann. For. Sci. 74. doi:10.1007/s13595-017-0628-z

Warren W.J., 1965. Stand structure and light penetration. I. Analysis by point quadrats. J. Appl. Ecol. 2, 383–390. doi:10.2307/2401487

Weiss, M., Baret, F., Smith, G.J., Jonckheere, I., Coppin, P., 2004. Review of methods for in situ leaf area index (LAI) determination Part II. Estimation of LAI, errors and sampling. Agric. For. Meteorol. doi:10.1016/j.agrformet.2003.08.001

Wilson, J.W., 1959. Analysis of the spatial distribution of foliage by two-dimensional point-quadrats. New Phytol. 58, 92–99.

Wu, J., Kobayashi, H., Stark, S.C., Meng, R., Guan, K., Tran, N.N., Gao, S., Yang, W., Restrepo-Coupe, N., Miura, T., Oliveira, R.C., Rogers, A., Dye, D.G., Nelson, B.W., Serbin, S.P., Huete, A.R., Saleska, S.R., 2018. Biological processes dominate seasonality of remotely sensed canopy greenness in an Amazon evergreen forest. New Phytol. doi:10.1111/nph.14939

3. PERSISTENT EFFECTS OF FRAGMENTATION ON TROPICAL RAINFOREST CANOPY STRUCTURE AFTER 20 YEARS OF ISOLATION USING LIDAR

ABSTRACT

Assessing the persistent impacts of fragmentation on above ground structure of tropical forests is essential to understanding the consequences of land use change for carbon storage and other ecosystem functions. We investigated the influence of edge distance and fragment size on canopy structure, aboveground woody biomass (AGB), and AGB turnover in the Biological Dynamics of Forest Fragments Project (BDFFP) in central Amazon, Brazil, after 22+ years of fragment isolation, by combining canopy variables gathered with Portable Canopy profiling Lidar (PCL) and airborne laser scanning (ALS) surveys with long-term forest inventories. Forest height decreased by 30% at edges of large fragments (> 10ha) and interiors of small fragments (< 3ha). In larger fragments, canopy height was reduced up to 40 m from edge. Canopy organization (leaf area density profile) differed near edges: the density of understory vegetation was higher and midstory vegetation lower, consistent with increased regeneration of pioneers following post-fragmentation mortality of large trees. However, canopy openness and leaf area index remained similar to control forests throughout fragments, while canopy rugosity (canopy heterogeneity) inconsistently increased away from edges. AGB stocks and fluxes were positively related to canopy height and negatively related to rugosity. Other forest structure variables typically adopted to assess the ecological impacts of fragmentation (basal area, density of individuals, and density of pioneer trees) were also related to lidar-derived canopy surface variables. Canopy reorganization through the replacement of edge-sensitive species by disturbance-tolerant ones may have mitigated the fragmentation impacts on AGB loss observed in the first years. Lidar technology offered novel insights and observational scales for analysis of the ecological impacts of fragmentation on forest structure and function.

Keywords: Amazon; BDFFP; Edge effects; Carbon cycle; Forest degradation; Forest dynamics; Forest succession; Land use change; Leaf area density; Vegetation structure

3.1. Introduction

The effects of forest fragmentation on biodiversity, structure, and function of tropical forest remnants are an important issue in conservation biology due to its close association with land use change (Ewers et al 2011; Laurance et al., 2017). Globally, it is estimated that there are more than 50 million tropical forest fragments, comprising an area of almost 300 million hectares, with 50 million linear kilometers of edges (Brinck et al., 2017). The air near forest edges is drier and hotter, light incidence is higher, and winds are stronger (Kapos, 1989; Camargo & Kapos, 1995; Didham and Lawton, 1999). Such alterations in forest microclimate have favored the replacement of large late-successional trees by light-wooded, fast-growing pioneers (Bierregaard et al., 1992; Ferreira & Laurance 1997), and is one of the major drivers

of forest aboveground biomass (AGB) collapse near edges (Laurance et al., 1997; 2000) and net carbon emissions after fragmentation (Brinck et al., 2017). The consequences of fragmentation for tropical forest structure and function are thus critical for understanding global changes in biodiversity and climate (Laurance et al., 1998; Broadbent et al., 2008; Chaplin-Kramer et al., 2015). However, previous assessments of the ecological impacts of tropical forest fragmentation were mostly based on short-term studies evaluating forest horizontal structure through inventories, which have prevented a broader spatial scale overview of the persistent impacts and global relevance of fragmentation.

The scarce quantitative information available on the impacts of fragmentation on the canopy structure of tropical forests was gathered through time consuming, local-scale visual methods with low accuracy and precision (Camargo & Kapos, 1995; Didham & Lawton, 1999). The findings of these previous studies have mostly shown that forest fragmentation increases the frequency of gaps and reduces canopy height due to high initial mortality of large remnant trees (D'Angelo et al., 2004; Kapos, 1989; Ferreira & Laurance, 1997; Nascimento & Laurance, 2006; Laurance et al., 2006a, 1998). For instance, Camargo & Kapos (1995) found that the density of understory trees (< 5 m height) was higher, and density of midstory trees (10-30 m height) was lower, in 4-year-old fragment edges compared to forest interior and adjacent non-fragmented forests in Central Amazon, Brazil; Didham & Lawton (1999) found that these results persisted ten years after fragmentation in the same experiment. However, it is not clear yet if the AGB decline observed in the first years of fragmentation persists over time, since initial AGB loss from remnant tree mortality can gradually recover from the regeneration of new trees in the community (Laurance et al., 2017).

Technological advances in remote sensing now allow for high precision, fast, and broader scale quantitative three-dimensional characterization of forest canopy structure (Lefsky et al., 2002; Chambers et al., 2007). Lidar (light detection and ranging) provides unique quantitative information about forest canopy structure, including vertical and horizontal variation in the density of vegetation surfaces, allowing for linkage of forest structure to forest function (Lefsky et al., 2002; Tang & Dubayah 2017; Valbuena et al., 2017). The application of lidar technology to tropical forests is rapidly expanding, and has been used to estimate canopy height, openness and rugosity (canopy heterogeneity), and vegetation density profiles, which can be

linked to AGB and AGB dynamics (Simonson et al., 2014; van Leeuwen & Nieuwenhuis, 2010; Stark et al., 2012; Almeida et al., 2016; Coomes et al., 2017). The Biological Dynamics of Forest Fragments Project (BDFFP) in the Central Brazilian Amazon is one of the largest and oldest (> 20 years) controlled experiments on forest fragmentation and has contributed fundamentally to expand the understanding of the consequences of fragmentation for forest diversity, dynamics, and function (Lovejoy et al., 1984; Ewers et al., 2011; Laurance et al., 2017). The use of lidar technology to evaluate fragmentation impacts on forest AGB and canopy structure in this experiment offers the opportunity to complement previous studies performed with traditional methods and new insights about the longer-term impacts of fragmentation.

Here, we investigated the influence of edge effects and fragment size on canopy structure and its relationship with AGB and dynamics of more than 20-year-old forest fragments (with original boundaries continuously maintained) at the BDFFP. We associated canopy metrics generated from Portable Canopy profiling Lidar (PCL) surveys conducted in 2015, and Airborne Laser Scanning (ALS) surveys conducted in 2008, with forest inventory data from 2008-2009. We extend the previously reported AGB and forest dynamics results by 10 years (Laurance et al., 2006a most recently reported on a 1999 re-census). We addressed the following questions:

(1) *Is canopy height influenced by proximity to forest edges and fragment size?* We hypothesized that canopy height will increase with distance to forest edge, and that the mean canopy height of small fragments (up to 3 ha) and of the edges of larger fragments will be lower than that of the interior of larger fragments (> 10 ha) and continuous forest, as consequence of higher mortality of large remnant trees in forest edges and small fragments.

(2) *Are canopy openness and rugosity influenced by proximity to forest edges and fragment size?* We hypothesized that the canopy would be more open and have greater rugosity (i.e. higher heterogeneity) closer to forest edges, especially in smaller fragments, as a consequence of higher mortality of large remnant trees in forest edges.

(3) *Are LAI and leaf area density of different vertical strata influenced by proximity to forest edges?* We hypothesized that LAI and leaf area density (hereafter LAD) of fragment interiors would be similar to that of continuous forest but reduced near edges. LAI and LAD of low-stature understory vegetation may be higher near edges due to higher light availability but reduced in upper strata because of the mortality of large trees.

(4) *Do negative impacts of edge proximity on basal area, AGB, and density of trees persist after more than 20 years of fragmentation?* We hypothesized that negative influences of proximity to forest edge on basal area, AGB, and tree density observed primarily in the first five years following fragmentation will persist 22 years after fragmentation. Continued degradation or partial recovery are possible alternatives.

(5) *Are canopy structure variables obtained by lidar able to reveal field metrics of fragmentation impacts?* We hypothesized that the impacts of fragmentation on basal area, AGB, density of individuals, and density of pioneer trees can be predicted from lidar metrics, since these variables are likely linked with canopy structure.

3.2. Material and methods

3.2.1. Study area and forest inventories

The study area is located in Central Amazonia, 80 km North from Manaus, state of Amazonas, Brazil (2 ° 30’ S, 60 ° 00’ W) (Figure 1). Vegetation is characterized as dense, “terra-firme” (not seasonally flooded) tropical rainforest, with more than 280 tree species per hectare (De Oliveira & Mori, 1999); soils are acidic and nutrient-poor, elevation varies from 50-100 m a.s.l., and annual precipitation varies from 1,900-3,500 mm, with a dry period from June to October (climate type: Af, Köppen classification). The study area is surrounded by continuous, non-fragmented forest (> 200 km) to the north, east and west. In the 1980s, eleven fragments with three distinct size classes (~2, ~10 and 100 ha) were isolated with distances between

70-1000 meters from a continuous forest. Fragments at the “Colosso” site (Figure 1) were isolated in July and August 1980 and the surrounding remnant vegetation and debris burned. Thereafter, some of the surrounding areas were maintained as pasture, while others were abandoned to become secondary forest. Secondary forest was re-cut in 1987 and maintained as pasture thereafter. The fragments at “Dimona” site (Figure 1) were isolated in August and September 1984 and had their surrounding areas burned. The clear-cut area was maintained as pasture thereafter, and original borders have been maintained throughout the study. Fragments were not affected by logging or other disturbance factor once isolated; therefore, turnover and canopy change are purely the result of demographic and ecological processes.

Since creation, forest inventories have been carried out at five-year intervals in 69 1-ha plots distributed within the forest fragments (edges and interiors) and also in control plots in the adjacent continuous forest (“Cabo frio”, “Florestal”, “Gavião” and “Km 41” sites - Figure 1). This study used 51 plots, described in the next section. To date, plots have been inventoried 5 to 8 times. All trees with diameter at breast height (DBH) > 10cm were identified and recorded. The following variables were calculated with data from each inventory: basal area, tree density, pioneer species density, and AGB, as further described.

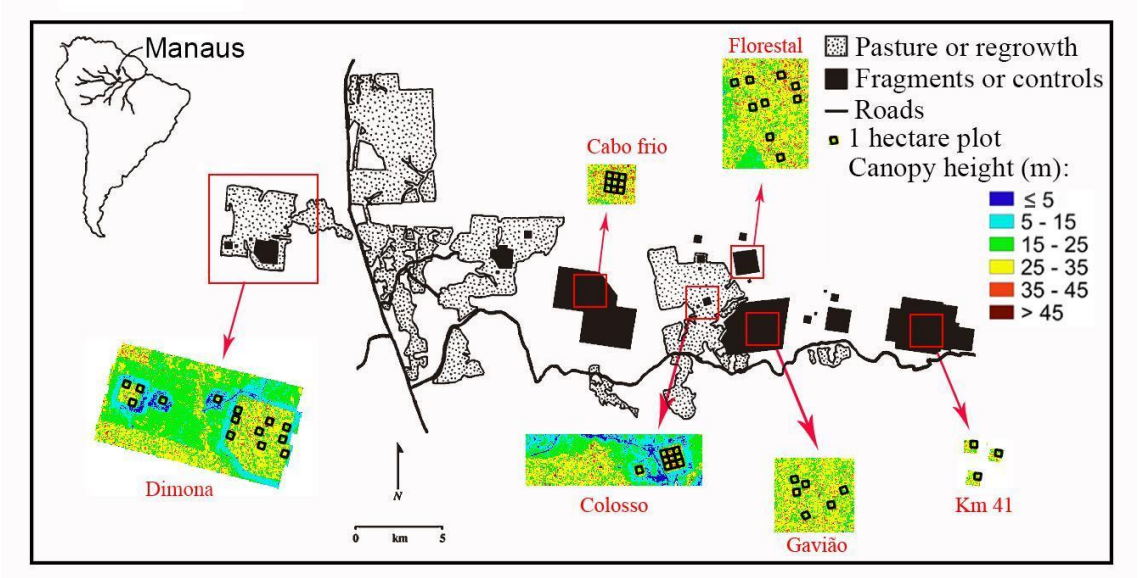

Figure 1. Location of study sites at the Biological Dynamics of Forest Fragments Project near Manaus, central Amazon, Brazil. The black polygons represent the forest fragments and controls, the dotted areas around them represent pasturelands, and the white background represents continuous forests. Colored figures show Canopy Height Model, derived by Airborne Laser Scanner, for each experimental site. The black squares within the colored figures are the 1-ha permanent inventory plots used in the study.

3.2.2. Lidar data collection

ALS data were collected in June 2008 (> 20 years after fragmentation) by a private company (Esteio company, Curitiba, PR, Brazil) using a Leica ALS50 system (Heerbrugg, Switzerland) on board a Navajo EMB 820C aircraft (Embraer company, São José dos Campos, SP, Brazil). The small footprint point cloud was acquired with return density of 12.2 pts·m^{-2} (~ 10 pulses·m^{-2}), average flight height of 725 meters, maximum scan angle of 24° and a ground footprint diameter of 11 cm. Coverage included six forest fragments (three of ~ 2-ha, two of ~ 10-ha and one of 100-ha) and four adjacent continuous forests, totaling 51 plots (three in ~ 2-ha fragments, twelve in ~ 10-ha fragments, nine in 100-ha fragments, and twenty-seven in continuous forest; Figure 1).

The profiling lidar (PCL) (Parker et al., 2004) data were collected in 18 plots during July 2015 (~30 years after fragmentation): nine plots of the 100-ha fragment (“Dimona” site) and nine plots in adjacent forest ("Forestal" site; Figure 1). In each plot, two linear transects of 100 m each were established 40 m apart. These transects were parallel to the fragment edge, and were considered independent sampling units, each with its respective distance from the edge (Figure S1). The PCL system employs a profiling range-finder type laser, model LD90-3100VHS-FLP manufactured by Riegl (Horn, Austria). The PCL accuracy is ± 25 mm and the nominal range is 200 m. The equipment records 2,000 pulses per second (Figure S2). The instrument is held in a gimbal (one meter above the ground) to maintain vertical aim (Stark et al., 2012; Almeida et al., 2016). The operator walks at a constant pace along the transect, controlling the speed (0.33 m·s^{-1}) with the aid of an electronic metronome and markers spaced every two meters.

3.2.3. Data processing

ALS and PCL lidar pulse reflection point clouds were processed to estimate canopy biophysical properties; data processing was done in R (R Core Team, 2017). The ALS cloud was divided into columns of 2 x 2 x Z m ("Z" is the highest return within the 2 x 2 horizontal grid cell). After ensuring that there was no clear outlier return elevations, the Digital Terrain Model (DTM) was created by analyzing the minimum points from each 2 x 2 cell (‘raw ground,’; Figure S3). A smooth spline

regression from *qsreg* R function by “fields” package (Nychka et al., 2015), was applied to produce the DTM (least values of fits to all horizontal ‘columns’ and ‘rows’ in the raw ground image) (Figure S4). This preferred DTM was selected based upon comparison, including visual analysis, against other alternatives (see Figure S5). The Digital Surface Model (DSM; 2-m grid cell) was generated using the maximum points of each column (Figure S6). The Canopy Height Model (CHM; 2-m grid cell), used to estimate the structural canopy attributes, was calculated by the difference between DSM and DTM (Figure S7). Three structural canopy attributes were calculated based on ALS products: (i) the average canopy height (CHM mean), (ii) rugosity (CHM standard deviation) and (iii) canopy openness (fraction of CHM cells lower than the 15-meter-high threshold) (Table 1). According to Runkle (1982), a 15-m cutoff maximizes the sensitivity of this metric to gaps spanning early through middle stages of regeneration.

ALS scenes were classified as open matrix (cleared) or forest (fragment or otherwise) via a manual edge demarcation of CHM rasters using QGIS (QGIS Development Team, 2015). Edges were clear and distinct and easy to demarcate with reference to the CHM due to the careful maintenance of the original edges with periodic manual clearing. Distance from edge was calculated from the median of all linear distances within the plot at a resolution of 2 × 2 m.

Each 100-meter PCL transect was divided into fifty 2-m columns and subdivided into 1-m intervals along the vertical profile (Figure S8a). The leaf area density (LAD) was estimated using the equation of MacArthur and Horn (1969) with the method proposed by Almeida et al., (2016) (Figure S8b). In summary, the method is based on the rates at which ranging pulses pass through (vs. are reflected) within units of canopy volume, providing a basis to estimate volumetric variation in vegetation density from optical transmission rates (MacArthur & Horn 1969; Parker et al., 2004; Stark et al., 2012). Pulses are reflected by leaves, branches, and other structural elements. The PCL approach, however, has been calibrated against independent LAI estimates, including destructive leaf area sampling, for sites in the region with the aim of effectively factoring out the influence of non-leaf area (Stark et al. 2012); thus, we estimate LAI, and LAD).

We established four vertical strata in LAD profiles: understory (1-5 m), the lower-middle (5-15 m), upper-middle (15-25 m) and upper canopy (> 25m). We

assessed potential relationships between these strata-specific total LAI values (LAI_{1-5m}, LAI_{5-15m}, LAI_{15-25m}, LAI_{25-45m}) and distance from edges with regression analysis.

We calculated AGB with tree inventory data using the equation of Chave et al. (2014): $AGB(kg)=\exp(-1.803-0.976*E+0.976*\ln(WD)+2.673*\ln(DBH)-0.0299*[\ln(DBH)]^2)$, where, E is a measure of environmental stress, WD is the wood density, and DBH is the diameter at breast height. The environmental coefficient for the study area (E = -0.127) was obtained from the *retrieve_raster* function (Chave et al., 2014) in R and the wood density for each tree, based on species, genera, or family identity, according to availability, was obtained from the "Global Wood Density Database" (Zanne et al., 2009). Wood density estimates were obtained at the species level for 57% of individuals, at genera level for 39%, at family level for 3%, and the remaining 1% of trees were assigned the average in their plot. Because pioneers tend to have lower wood densities and different allometric relations, we used the equation for pioneer species of Nelson et al (1999) to estimate biomass for pioneer trees. The pioneer trees were based on a list of 52 species classified as pioneers by Laurance et al. (2006b).

Table 1. Methods employed to gather forest structure metrics used to evaluate research questions (described in the end of Introduction) about the influence of edge distance and fragment size on forest structure in the BDFFP fragmentation experiment in central Amazon, Brazil.

Method	**Metrics**	**Questions**
Airborne Laser Scanning (ALS).	Canopy height, rugosity, and canopy openness.	(1), (2) and (5)
Portable Canopy profiling Lidar (PCL).	Leaf area density (LAD) profiles, and leaf area index (LAI) for different vertical strata.	(3)
Field inventory data.	Basal area, above ground biomass, density of trees, density of pioneer tree species.	(4) and (5)

3.2.4. Data analysis

We related canopy biophysical properties to fragmentation and forest plot variables with statistical model fitting. First, an exponential model (equation 1) related canopy height (CH) to distance from fragment edge (dist):

$$CH = \alpha + (\beta - \alpha)\, exp(\frac{-(dist)}{\gamma}) \quad (1)$$

where alpha (α) is the asymptote of the model representing the height of the vegetation in the interior of the fragment, beta (β) is the intercept of the model and represents the height of the vegetation at the edge of the fragment, and gamma (γ) is related to the rate of change of canopy height by the independent variable (distance to edge). The model was adjusted with the non-linear least squares method. Values of the alpha and beta coefficients of each forest fragment were compared to assess the potential effect of fragment size.

Structural attributes of the canopy (rugosity and canopy openness fraction) and the forest inventory variables (basal area, tree density, and AGB) were regressed against one another, as well as distance from edge, to assess potential effects and relationships. Lidar-derived canopy structural attributes were related to continuous inventory variables with Pearson's correlation and univariate least squares linear regression.

3.3. Results

Canopy height assessed through ALS was related to distance from the edge and fragment size in the six fragments (Figure 2). Coefficient values fitted for each fragment are specified in Figure 3, where α (asymptote) is the height of vegetation in meters at the fragment interior and β (intercept) at the fragment edge, while γ is related to the change rate. All model coefficients were significant at $p < 0.001$ levels. Canopy height was lower at the edges and progressively increased until asymptote of 24-41 m away from the edge. Smaller fragments (2 ha), however, appeared to have modestly, but consistently, lower canopy heights than larger fragments (maximum ~ 5 m difference; Figure 4). The canopy height in the interior of the larger fragments was similar to the mean canopy height of the continuous forest plots (28.83 ± 1.25 m; mean ± SD; Figure S9).

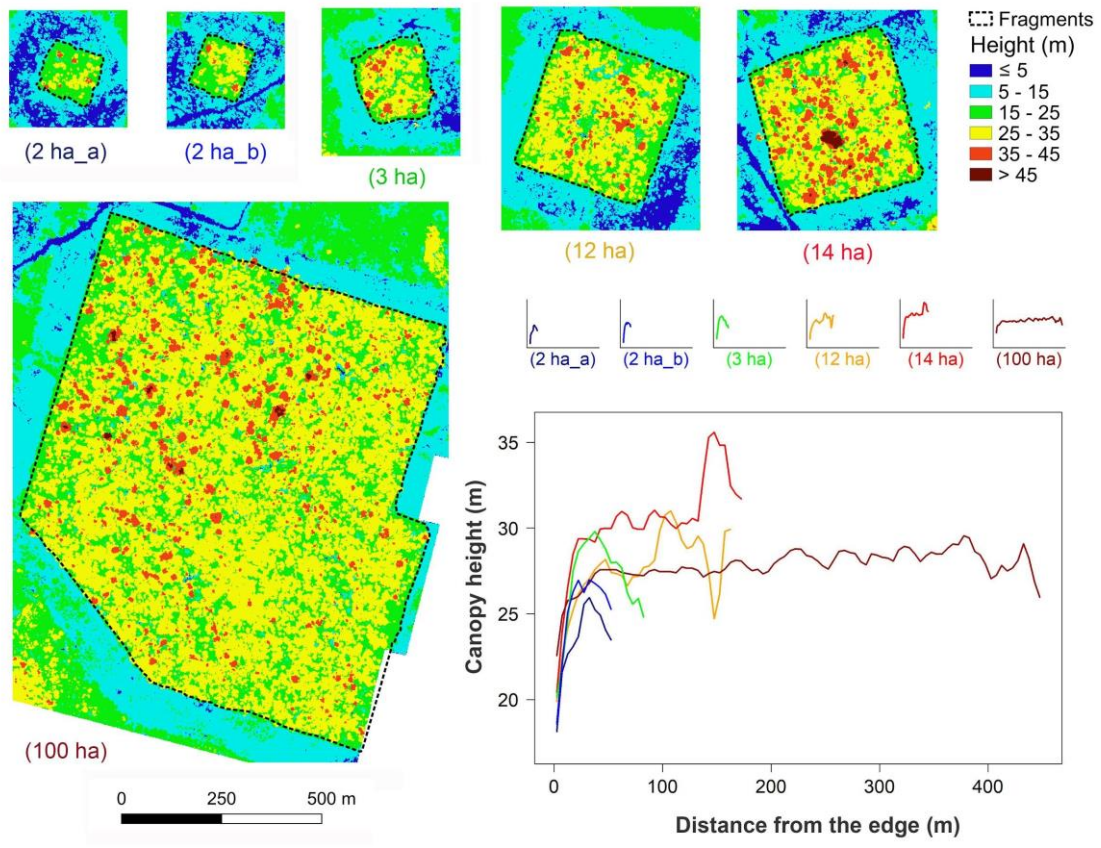

Figure 2. Canopy height, obtained by Airborne Laser Scanning, at different distances from edge in six forest fragments in central Amazon, Brazil. The colored raster images are the Canopy Height Model (CHM) of each fragment (2 x 2 m resolution). Lines in the graphs are the canopy height mean of all CHM cells in the respective distance class (5-meter intervals). The canopy openness can be observed by the blue pixels (CHM < 15m) within the fragments.

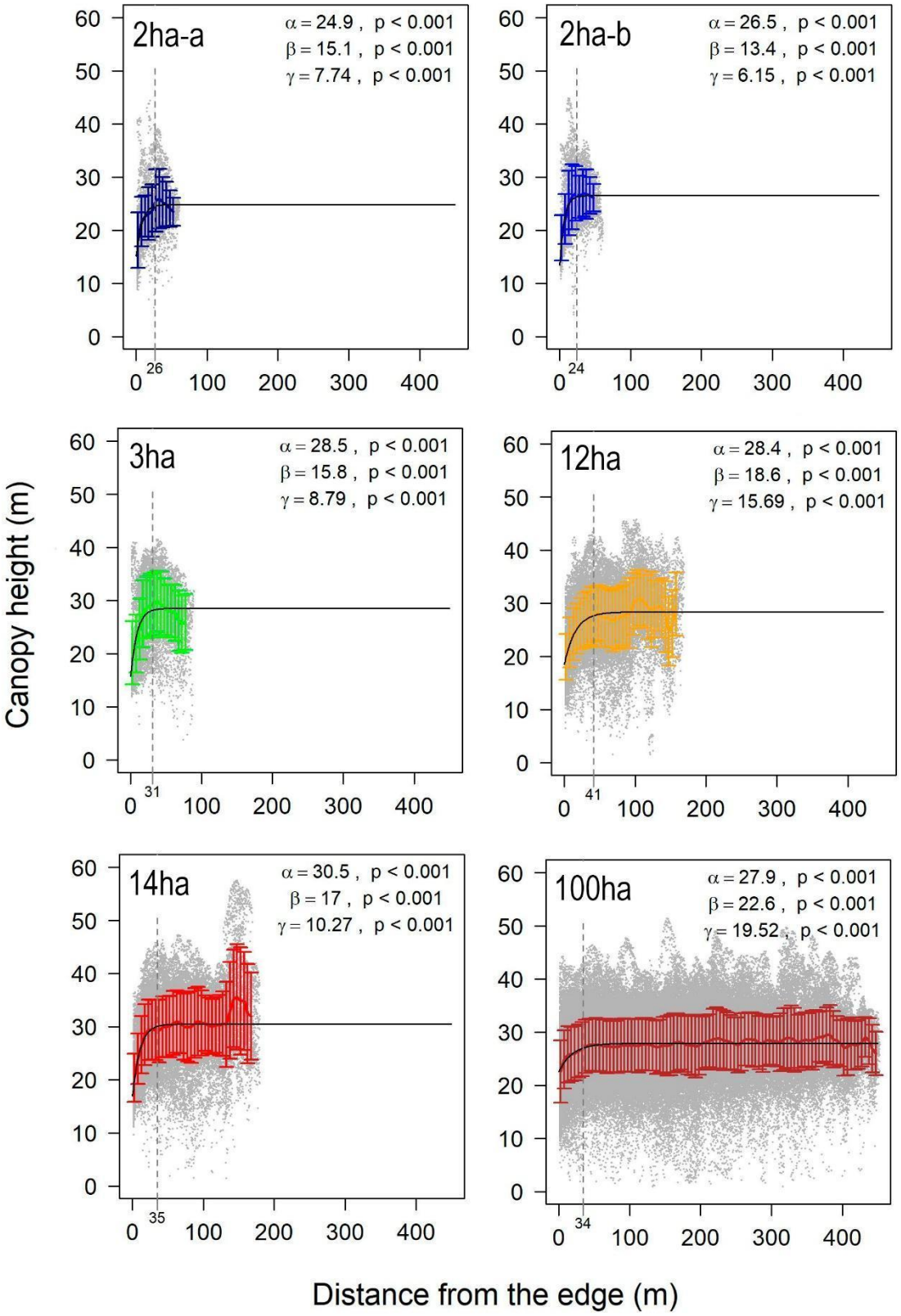

Figure 3. Canopy height, obtained by Airborne Laser Scanning, at different distances from edge in six forest fragments in central Amazon, Brazil. The gray dots are the height values of the Canopy Height Model (resolution 2 x 2 meters); the vertical dashed line indicates the distance where the rate of change in canopy height becomes less than 0.05 meters; vertical bars are the standard deviation of heights in each distance class (5-meter intervals). α is the asymptote of the model and represents the height at the fragment interior; β is the intercept of the model and represents the height of the canopy at the fragment edge, and γ determines the rate of change.

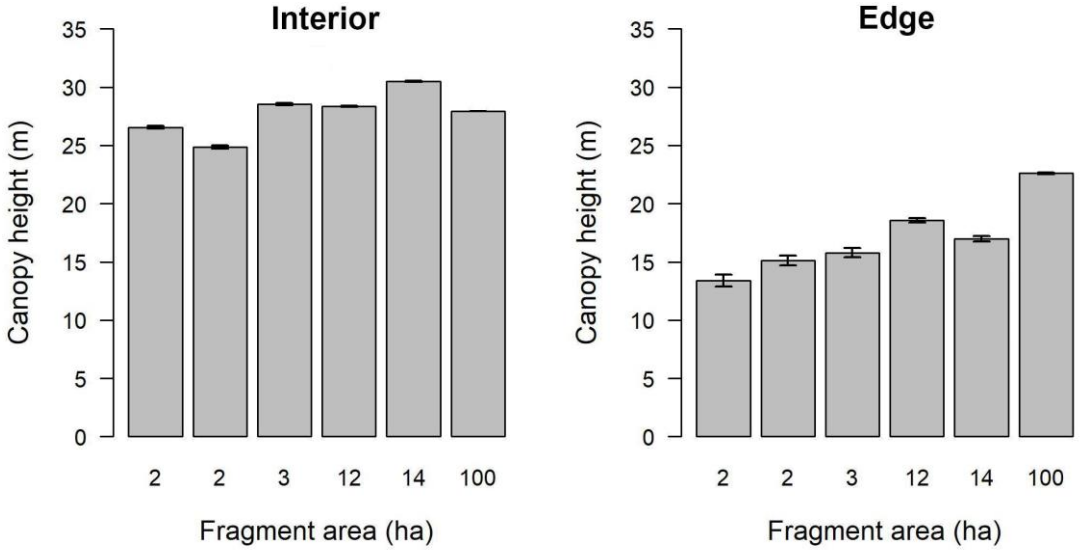

Figure 4. Comparison of the canopy height, obtained with Portable Profiling Lidar (PCL) at the interior (A) and edges (e.g., within 40 m of edges) (B) of forest fragments of different sizes, based on the fit parameters of Equation 1 (see Methods), among six forest fragments in central Amazon, Brazil. Vertical bars express the 95% confidence intervals of the estimated coefficients.

Canopy rugosity increased with increasing distance from the edge in fragments of intermediate size (12 and 14 ha, $p < 0.001$), but showed no relationship with distance from the edge in the smallest and largest fragments (Figure 5). The canopy openness fraction ($p = 0.128$; Figure 2 and Figure S10) and the total LAI (LAI_{total}; $p = 0.301$) were not related to distance from edge. However, LAD and LAI did significantly differ considering values in canopy strata, determined by height classes: the LAI of understory ($LAI_{1\text{-}5m}$) and upper ($LAI_{25\text{-}45m}$) strata increased with distance from the edge ($p = 0.025$ and $p < 0.001$, respectively), whereas LAI of the middle strata ($LAI_{5\text{-}15m}$ and $LAI_{15\text{-}25m}$) decreased ($p < 0.001$ and $p = 0.012$; Figure 6 and Figure S11).

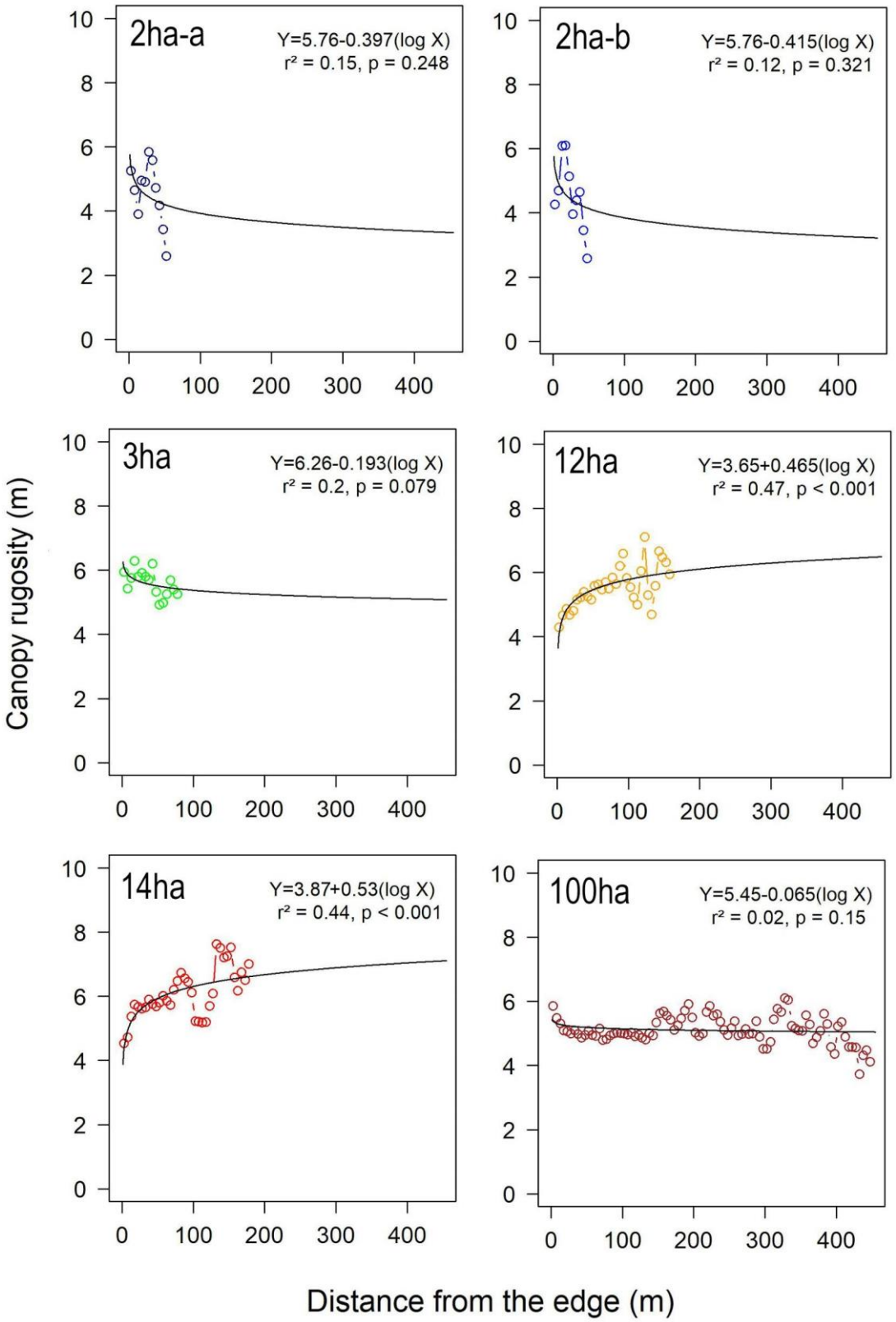

Figure 5. Relationship between canopy rugosity, measured as the standard deviation of the canopy heights obtained with Airborne Laser Scanner in each distance classes of 5 m, and distance from the edge in two forest fragments in central Amazon, Brazil. Points indicate rugosity for each distance classes while black solid lines show non-linear regression models.

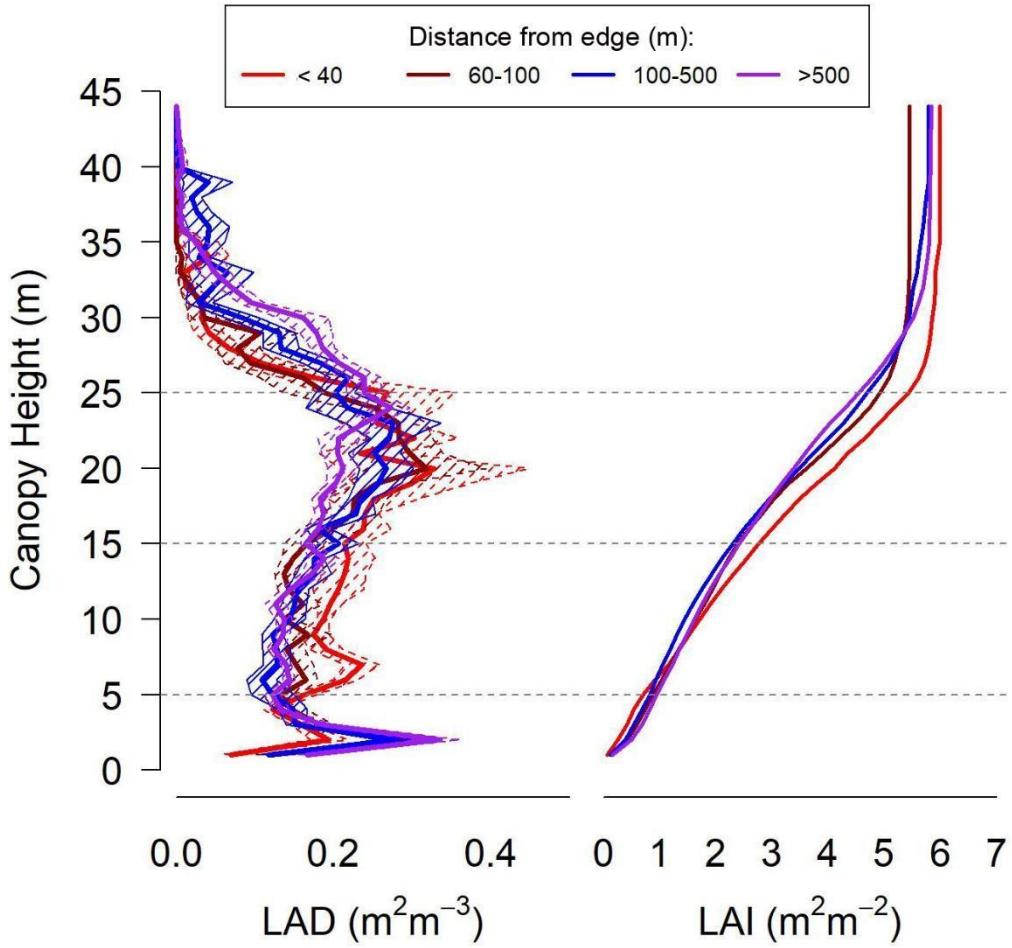

Figure 6. Vertical profiles of Leaf Area Density (LAD) (left) and accumulated Leaf Area Index (LAI) (right) obtained with a portable profiling lidar. Dashed horizontal lines represent the four vertical strata analyzed. Line colors indicate distance-from-edge classes. Hashed regions surrounding LAD vertical profiles are the mean standard error.

Basal area, AGB, and density of individuals obtained with forest inventory data were positively correlated to distance from the edges in the first five years after fragmentation ($p < 0.001$ in all three cases) (Figures 7, S13, S14 and S15). Ten years after fragmentation, positive relationships remained for basal area and AGB ($p < 0.001$ for both), but not for tree density. Twenty-two years after fragmentation, however, basal area and AGB were no longer related to distance from edge (Figures 7, S16 and S17), whereas tree density ($p = 0.005$; Figures 7 and S18) and the proportion of pioneer trees ($p = 0.001$; Figures 7, S19 and S20) increased near edges.

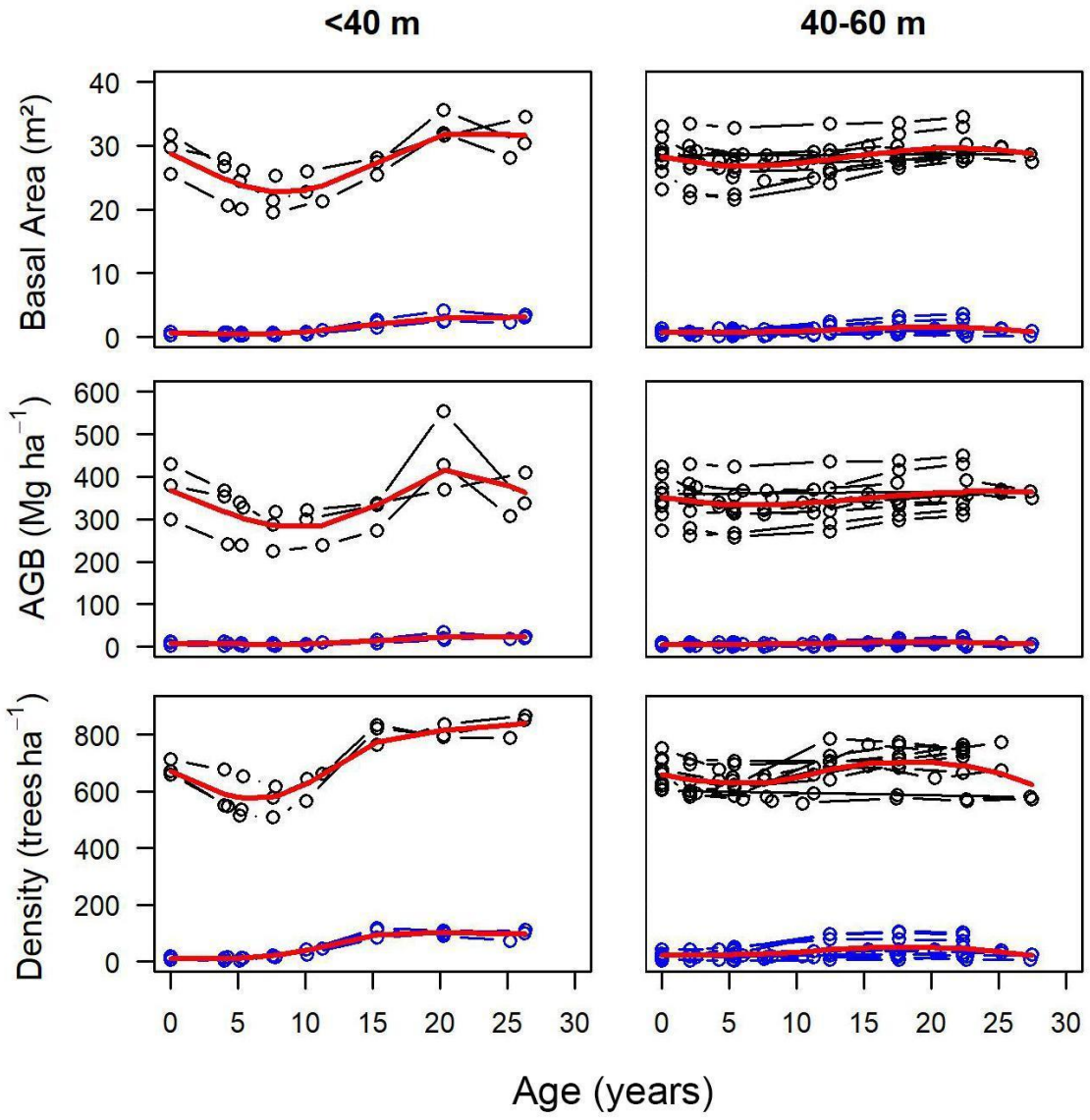

Figure 7. Mean basal area, AGB and density of trees over time (years after fragmentation), calculated with field inventory data, in two classes of distance from forest edges (<40m, left graphs; 40-60m, right graphs) of six forest fragments in central Amazon, Brazil. Black and blue circles (and lines) represent all species and pioneer species, respectively (i.e., pioneers are the lower groups); each blue and black line represents one plot. Red lines are means over all plots.

We found significant correlations between variables obtained from lidar and forest inventories (Figure 8). Canopy height was a significant predictor of AGB (r^2 = 0.35, $p < 0.001$). Rugosity was a significant predictor of change in basal area between the first and last inventories (2008; r^2 = 0.28, $p < 0.001$), as well AGB turnover (r^2 = 0.21, $p < 0.001$). Canopy height was also significantly correlated with two variables: (a) change in tree density from the pre-fragmentation state to 5 years after fragmentation (r^2 = 0.29, $p < 0.001$, positive relationship) and (b) the proportion of pioneer tree species in the last inventory (r^2 = 0.41, $p < 0.001$, negative

relationship). Both variables were correlated (negative relationship) with each other (r = -0.59, p <0.001; Table S1).

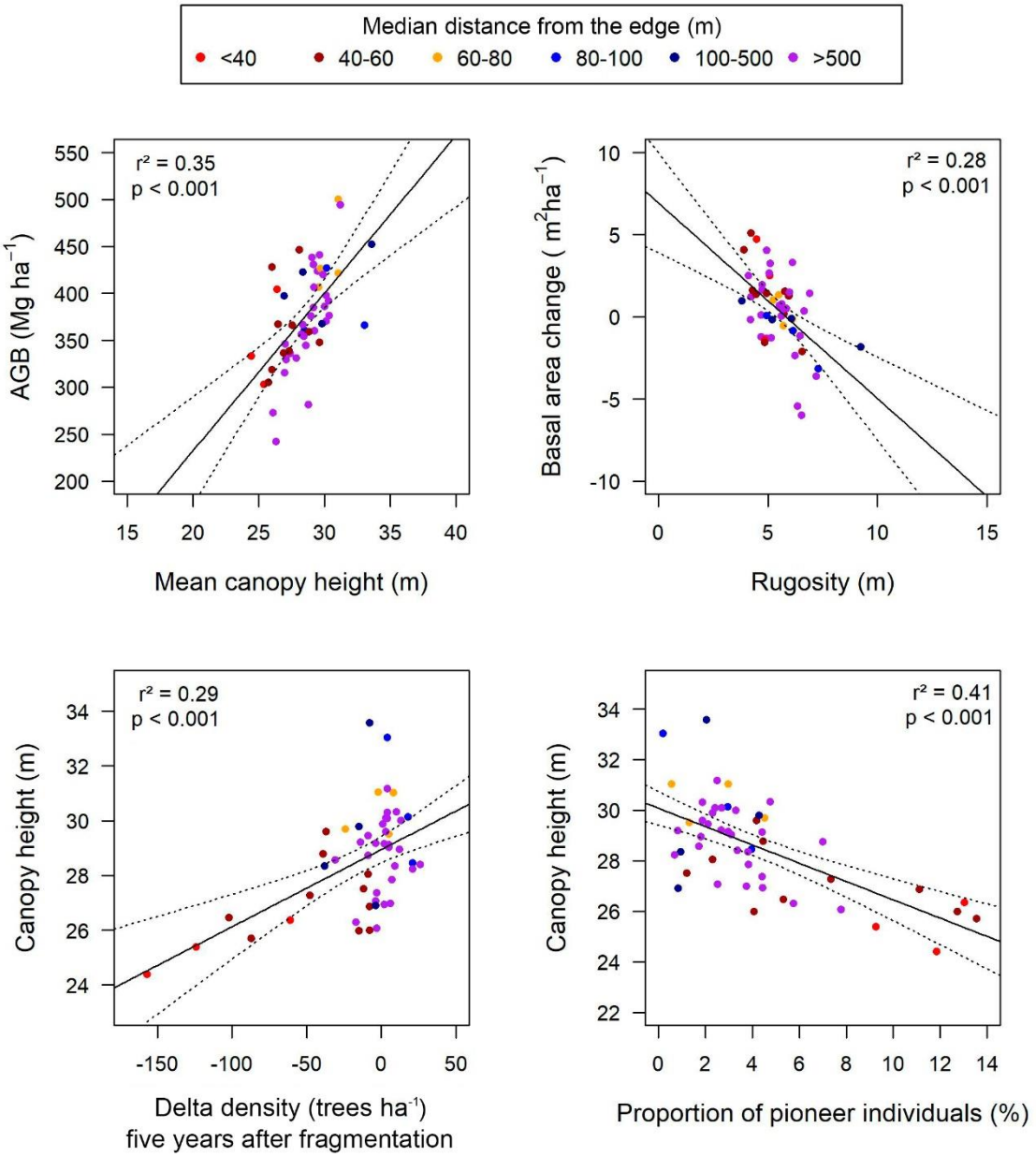

Figure 8. Relationships between canopy structural variables measured by Airborne Laser Scanner and field inventories in six forest fragments and adjacent contiguous forest in central Amazon, Brazil. The points represent the field plots and their color distance classes from the forest edges. Dashed lines are linear regression estimates.

3.4. Discussion

Fragmentation effects on forest structure and dynamics changed with time, revealing both persistent and non-persistent impacts of forest fragmentation 20+

years after fragment isolation. Overall, canopy height was persistently reduced near fragment edges and all over small remnants, whereas AGB and basal area decreased in these conditions in the first years after fragmentation but recovered pre-fragmentation values after two decades. The density of understory vegetation was higher and midstory vegetation lower. These results were attributed to the increased regeneration of pioneers following post-fragmentation mortality of large trees. Other forest structure variables typically adopted to assess the ecological impacts of fragmentation (basal area, density of individuals, and density of pioneer trees) were also related to lidar-derived canopy surface variables, thus revealing the potential of this technology for for high precision, fast, and broader scale quantitative three-dimensional characterization of forest canopy structure and associated impacts of fragmentation. In this section, we discuss in detail the impacts of fragmentation on forest structure variables, as well the integration of lidar technologies and forest inventory monitoring for their assessment.

3.4.1. Canopy height

Canopy height is negatively influenced by proximity to forest edges and fragment size. Canopy height was lower at the edges of all six studied fragments, but especially in smaller fragments (2ha), with persistent effects up to 41 m away from the edges. Canopy heights are reduced near edges most likely due to mortality of larger trees typical of the forest interiors in the first few years after fragmentation, and the enhanced regeneration of shorter trees (Figures S17-19; Bierregaard et al., 1992; Ferreira & Laurance, 1997; Laurance et al., 2006a; Laurance et al., 2000). Two interrelated processes help to explain this phenomenon. First, the higher incidence of winds along edges is more harmful to large trees (D'Angelo et al., 2004; Laurance et al., 2000), which form gaps when they fall and stimulate the regeneration of pioneer species (Ferreira & Laurance, 1997; Laurance et al., 2006a). In addition, soil desiccation, resulting from a higher incidence of dry and hot winds (Kapos, 1989), and aggravated by higher incidence of light, favors ruderal trees and climber species that may keep forest edges in an arrested successional state (Ferreira & Laurance, 1997; Laurance et al., 2006a; 2006b).

3.4.2. Canopy gaps and horizontal heterogeneity

Canopy openness and rugosity are not clearly influenced by proximity to forest edges. Considering two metrics of horizontal heterogeneity broadly related to gap and canopy surface (i.e., horizontal) heterogeneity, we found mixed, inconclusive evidence of fragmentation impacts. Contrary to our expectations, canopy openness was not related to fragmentation. This may be explained by the regeneration of trees prior to lidar assessments. The most dynamic period occurred immediately after fragmentation (0-5 years), when mortality of remnant trees increases substantially (Figure 7; Laurance et al., 1998) and indirectly promoted the vigorous regeneration of pioneer trees (5-10 years; Figure 7) and lianas (Laurance et al., 2001). Furthermore, canopy openness was low throughout the studied forests, suggesting that other metrics may reveal canopy dynamics more effectively. Rugosity did display potential impacts of fragmentation, but only in intermediate-sized fragments (10-15 ha). Since lower statured, more homogeneous vegetation may be a feature of persistent edges, associated with the dominance of pioneer trees, we expected lower rugosities near edges. Interior forest, with broader size distributions of trees typical of mature forest, on the other hand, was expected to be more rugose (Stark et al., 2012, Hardiman et al., 2011). Overall, canopy surface heterogeneity metrics did not respond clearly to edge effects, as was the case for canopy height.

3.4.3. Leaf area profiles

The vertical organization of the canopy, but not total LAI, changed with proximity to edge. Previous studies in the BDFFP found that understory vegetation at fragment edges was denser than midstory vegetation (Camargo & Kapos, 1995; Malcolm, 1994). But we find the opposite pattern, with the highest vegetation density near edges occurring in the midstory. Since these prior studies of leaf area profiles were conducted ~20 years before our profiling lidar surveys, tree growth and regeneration at edges most likely explain these contrasting results. In this case, the relatively sparse midstory near forest edges in the 1990s—as direct consequence of the documented increases in tree mortality 5+ years after fragmentation (Bierregaard et al., 1992; Ferreira & Laurance, 1997)—shifted to a denser strata due to the abundant regeneration of pioneer trees (Figure 7). The accumulation of vegetation in

the middle stratum of the canopy may reduce light penetration and consequently limit the growth of new individuals in the understory. Thus, the reorganization of canopy structure near fragment edges appears to be the result of an ongoing regeneration process, rather than a new equilibrium; however, we acknowledge the need for caution comparing PCL results to plot surveys given the 6-year time span between the plot inventories and more recent PCL surveys.

3.4.4. Resilience of field metrics of forest structure

Forest edges showed the strongest and most dynamic responses to fragmentation in this and prior studies in the BDFFP. Forest inventories monitoring forest change throughout the study, however, suggest the potential for a surprising degree of resilience of AGB stocks near forest edges. Even though edges exhibited losses in basal area, AGB, and tree density in the initial years after fragmentation, these variables were no longer different after 20+ years—except tree density, which significantly increased near edges. The only consistent difference near edges among these factors was higher variation (Figure S12 and S13). Although Nascimento & Laurance (2004) found lower average plot AGB at the edges 10 years after fragmentation, AGB stocks recovered after 5 more years (Figures 7, S13 and S16). Our results indicate that the immediate impacts of fragmentation on forest structure and function can partially recover in a few decades. Higher densities of intermediate-sized, early successional individuals may have compensated for initial AGB losses caused by higher mortality of a few large remnant trees.

3.4.5. Canopy structure and forest field metrics

Canopy structure observations reveal critical elements of AGB stock and dynamics in forest fragments. Relationships between canopy structure variables obtained from ALS and field inventories (AGB vs. mean canopy height; basal area and AGB vs. canopy rugosity) were highly significant, explaining 20-35% of variation (Figure 8), comparable to similar studies of mature tropical forest sites in the region (Stark et al., 2012). Edge distance categories did not explain additional variation in these relationships, and analyses included continuous (control) forest pots. This

suggests that whatever impacts fragmentation has on the AGB stocks, the relationships between forest structure and function did not differ from those observed in continuous forests. Fragmentation, in this case, impacts forest structure and forest function consistently, perhaps due to integral mechanisms linking these properties. The practical implication of this finding is that lidar should prove robust in monitoring fragmentation impacts through time and over heterogeneous landscapes. Jucker et al. (2017) have also found a robust model to estimate AGB for different landscapes, including fragmented forests, in tropical forests of Borneo.

The negative relationship between rugosity and basal area/AGB change is likely a result of tree mortality and associated gap dynamics. In this case, tree loss is associated with the loss of leaf area and increases canopy heterogeneity (rugosity). Gain from tree growth, on the other hand, may result from regeneration of pioneer trees in forest gaps, leading to lower heterogeneity. While both relationships were significant, the predictability of basal area change from canopy rugosity was relatively higher than AGB change. Differences in leaf area—if associated with differences in rugosity—might better reflect changes in basal area, because basal area is likely tightly associated with leaf area (see discussion and citations in Stark et al., 2015). AGB, on the other hand, is essentially the product of tree height, basal area, and wood density (WD), which is not likely related to lidar metrics. Tree wood density variation is potentially impacted by fragmentation due to increases in pioneer trees with low wood gravity (Figure S20; Laurance et al., 2006b); however, basal area and leaf area also increase with the regeneration of pioneer trees, regardless of the decline in the average wood density of the tree community.

Canopy height was also related to the proportion of pioneers—which have lighter wood and faster population dynamics, thus impacting carbon storage and turnover rates (Laurance et al., 1998; Laurance, 2002; Laurance et al., 2006a). Intriguingly, the change (in this case, ‘loss’) in density of individuals in the 5 years that followed fragmentation was a predictor of canopy height at the time of the lidar survey some 20 years later, though, seemingly, this relationship was only apparent near fragment edges. These relationships may be linked: initial tree loss (density decrease) led to high recruitment and regeneration of pioneer species (to densities higher than the initial state), which have lower stature than later successional species, and may have not achieved the pre-fragmentation height after 20 years.

3.5. Conclusion

After more than 20 years of isolation, the canopy structure and carbon cycle function of forest fragments in the BDFFP displayed persistent and non-persistent impacts, differentiating or not these forests from nearby contiguous areas, depending on the forest structure variable considered. While impacts on canopy height have been documented from forest inventory data in the BDFFP, these impacts have not previously been documented quantitatively with lidar, nor have the effects on canopy openness, rugosity, and LAI and LAD profiles been explored. Canopy height is negatively influenced by proximity to forest edges and fragment size. Canopy openness and rugosity are not clearly influenced by proximity to forest edges. The vertical organization of the canopy, but not total LAI, changes with proximity to edge. Considering just long-term BDFFP forest inventories, we also found that the previously reported initial negative effects of fragmentation on AGB stocks have been partially neutralized by ongoing forest regeneration near forest edges. In addition to AGB, other forest structure variables typically adopted to assess the ecological impacts of fragmentation (basal area, density of individuals, and density of pioneer trees) may be estimated with lidar variables. Lidar technology offered novel insights and observational scales for analysis of the ecological impacts of fragmentation on forest structure and function. This will be particularly critical in the future as Amazon land use change continues while hotter and drier conditions from climate change have the potential to exacerbate the effects of forest fragmentation by promoting fire, water stress, and other factors.

3.6. Supplementary material

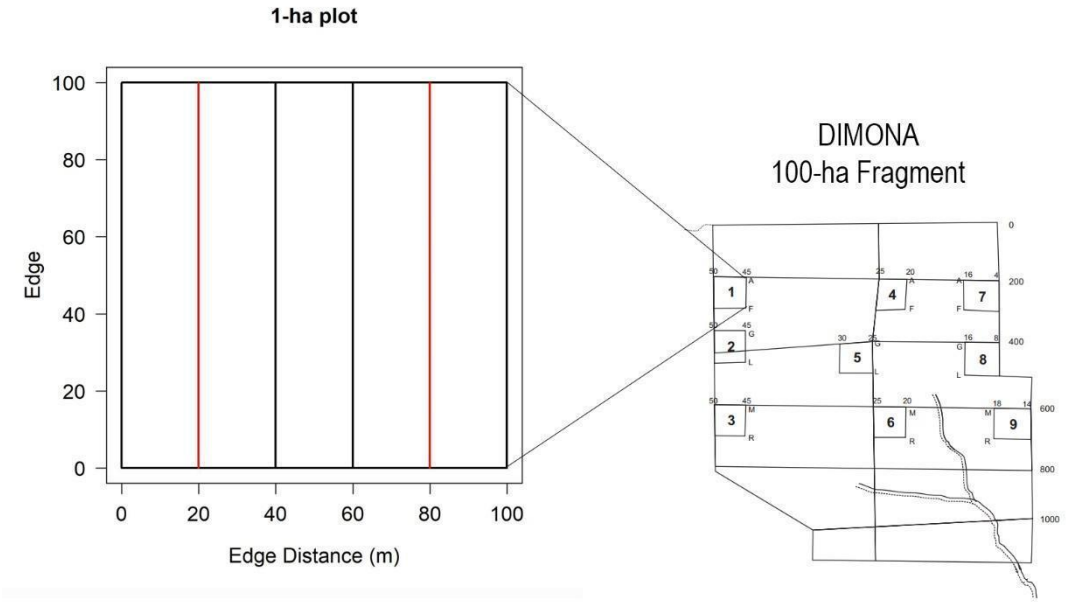

Figure S1. Left: scheme used to collect Portable Canopy profiling Lidar (PCL) data in each 1-ha plot; red lines show transects measured with the PGL, black lines show the sub-blots thresholds. Right: a sketch of the 100 hectare fragment with its nine plots. On the left is 1-ha plot.

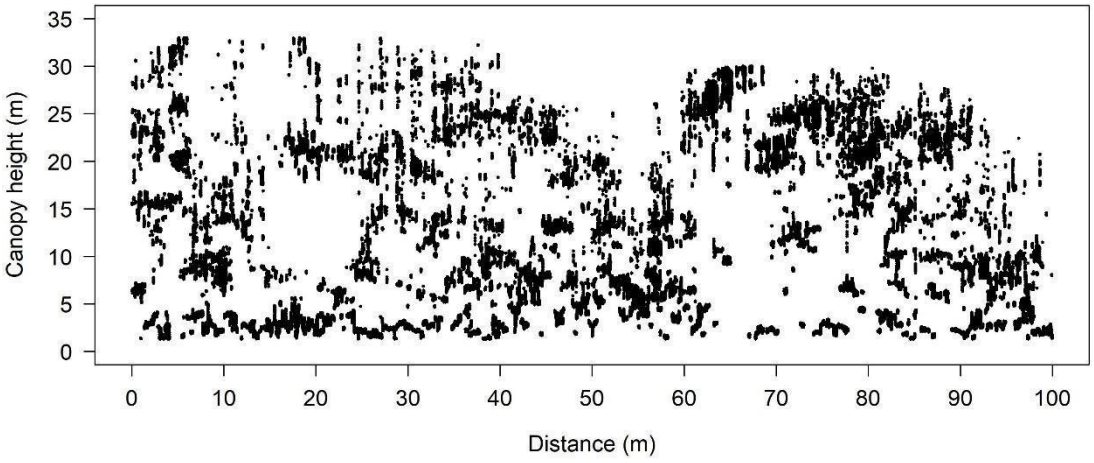

Figure S2. Example of Portable Canopy profiling Lidar (PCL) data from plot 1 of the 100-ha fragment (site "Dimona"), 80 m away from the margin of the fragment (Fig. S1).

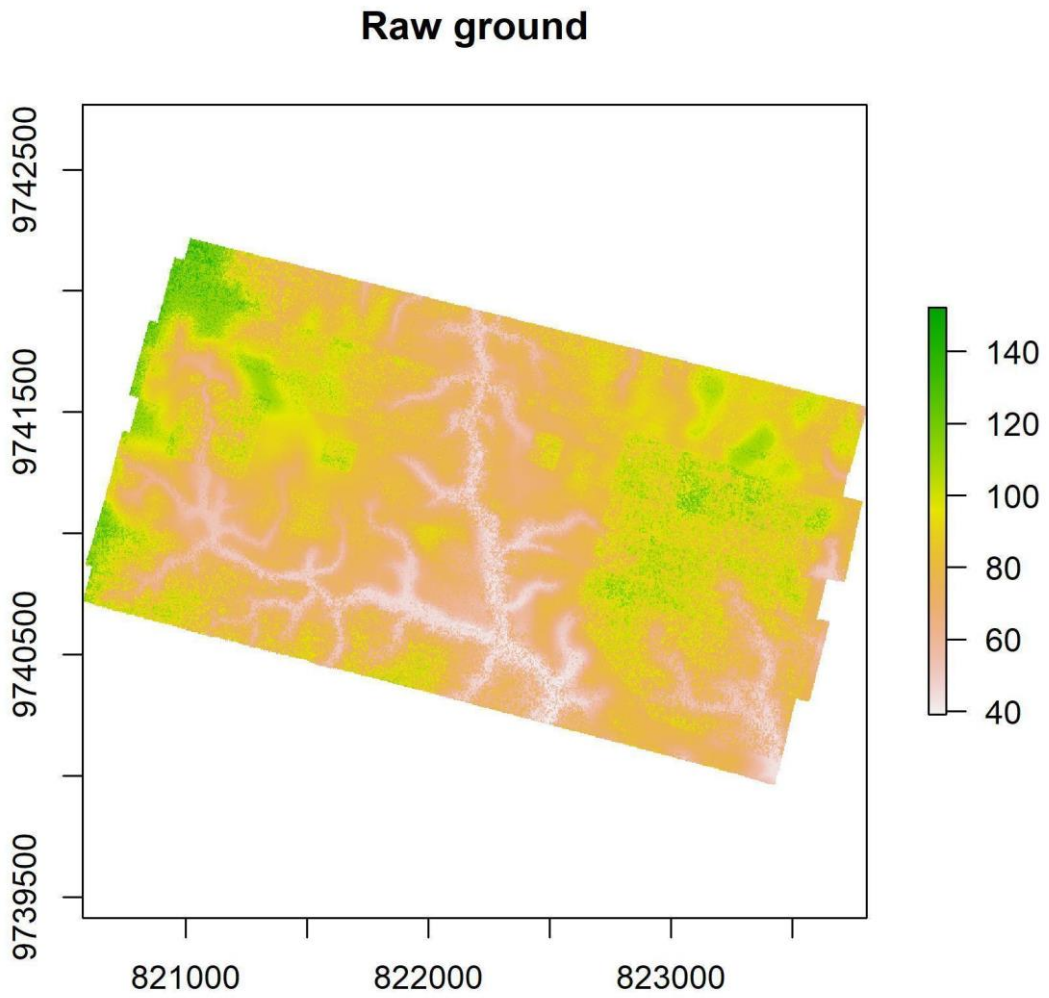

Figure S3. Raw ground of “Dimona” site. The raw ground is the minimum returns on 2x2 m grid. The axes are UTM and the colors are altitude (meters).

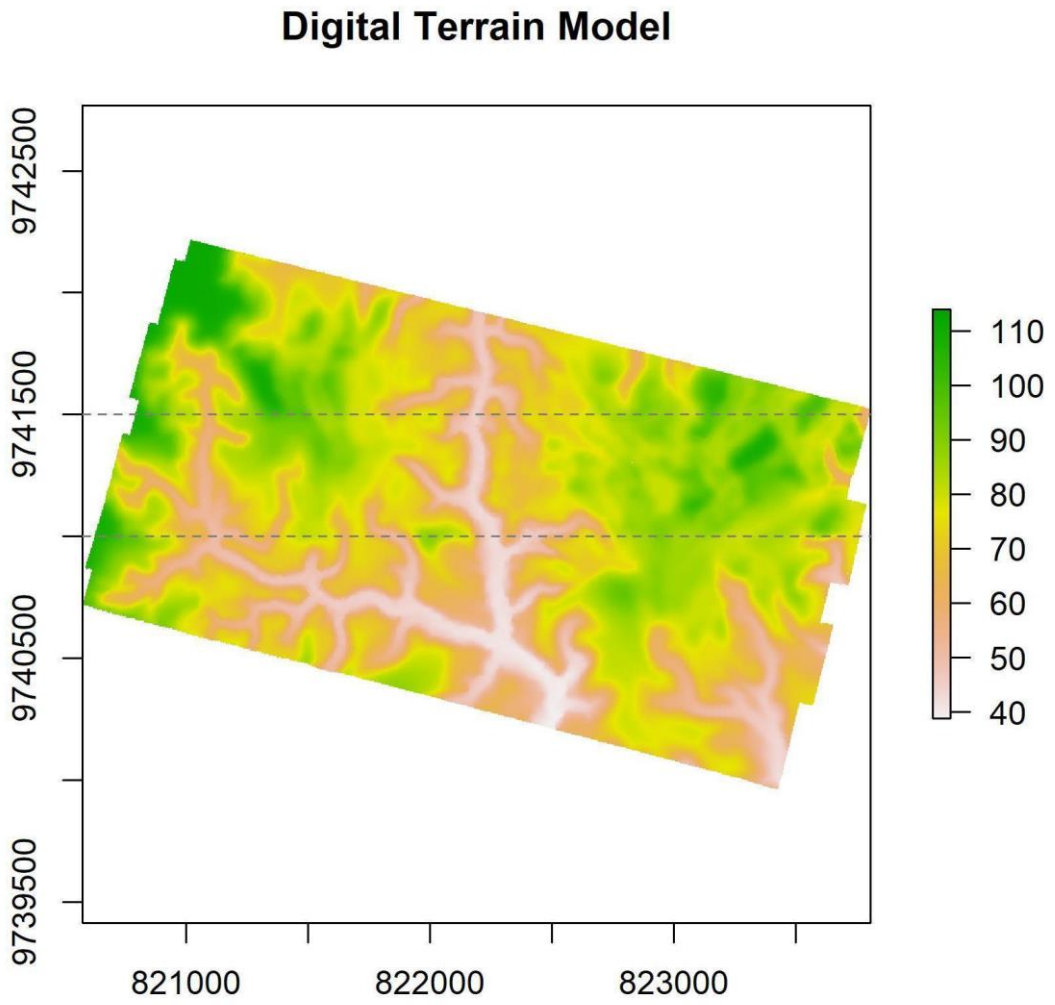

Figure S4. Digital Terrain Model (DTM; 2-m grid cell) of “Dimona” site. The two horizontal dashed lines are the latitude values for visual validation in Figure S5. The axes are UTM and the colors are altitude (meters).

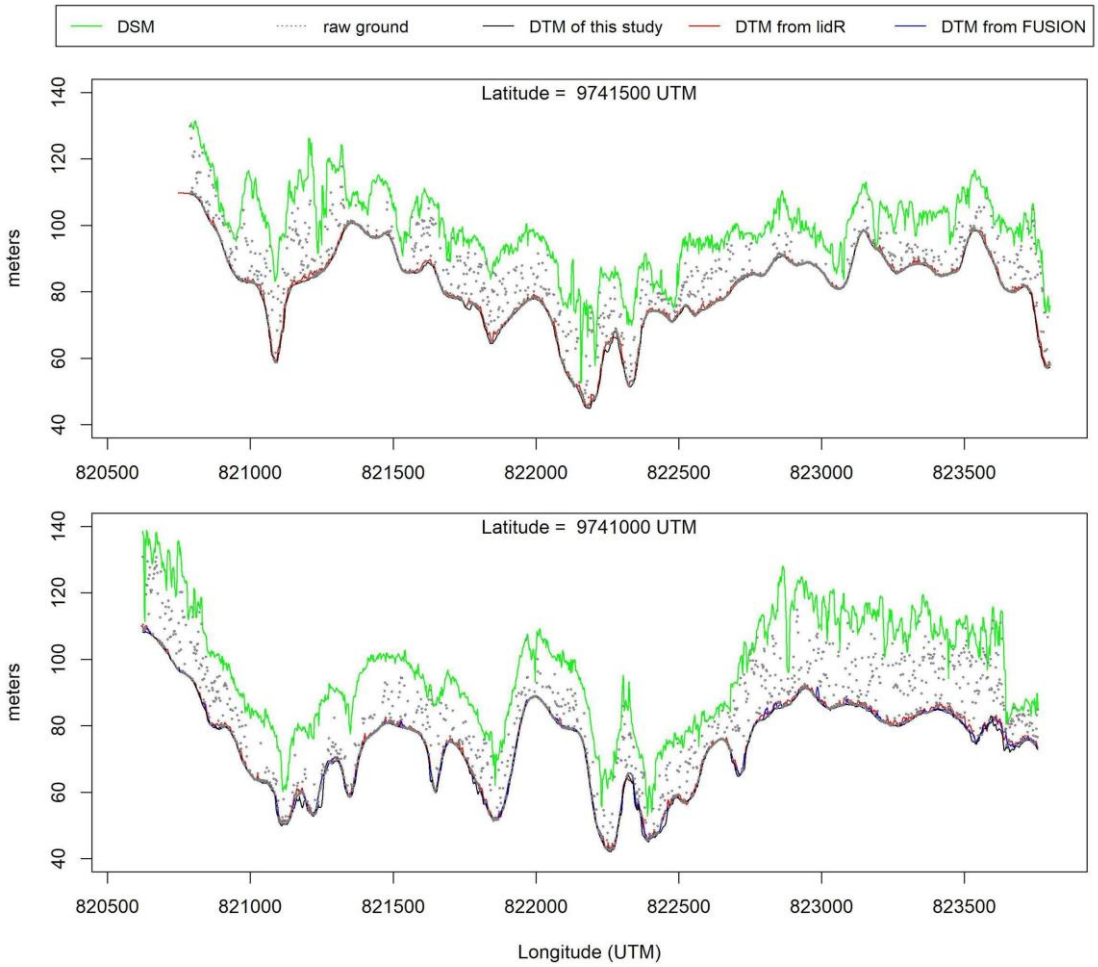

Figure S5. Observational validation process of the DTM (Digital Terrain Model) from transversal cuts in the raster images of DTM and DSM (Digital Surface Model). The black line is the DTM, the green line is the DSM, and the gray points are the lowest returns, every 2 meters, of the lidar returns (raw ground). Close to DTM black line there are two lines: red and blue. These are the DTM derived by "lidR" R package (Roussel & Auty, 2017; using Zhang et al. 2003 ground points filter) and Fusion (McGaughey, 2016; which employs Kraus & Pfeifer 1998 ground points filter) respectively. The histogram of DTM values from this study was tested (Two-sample Kolmogorov-Smirnov test) against the histogram from Fusion and lidR DTM values and them did not present significant differences ($p = 0.55$ and $p = 0.59$ respectively).

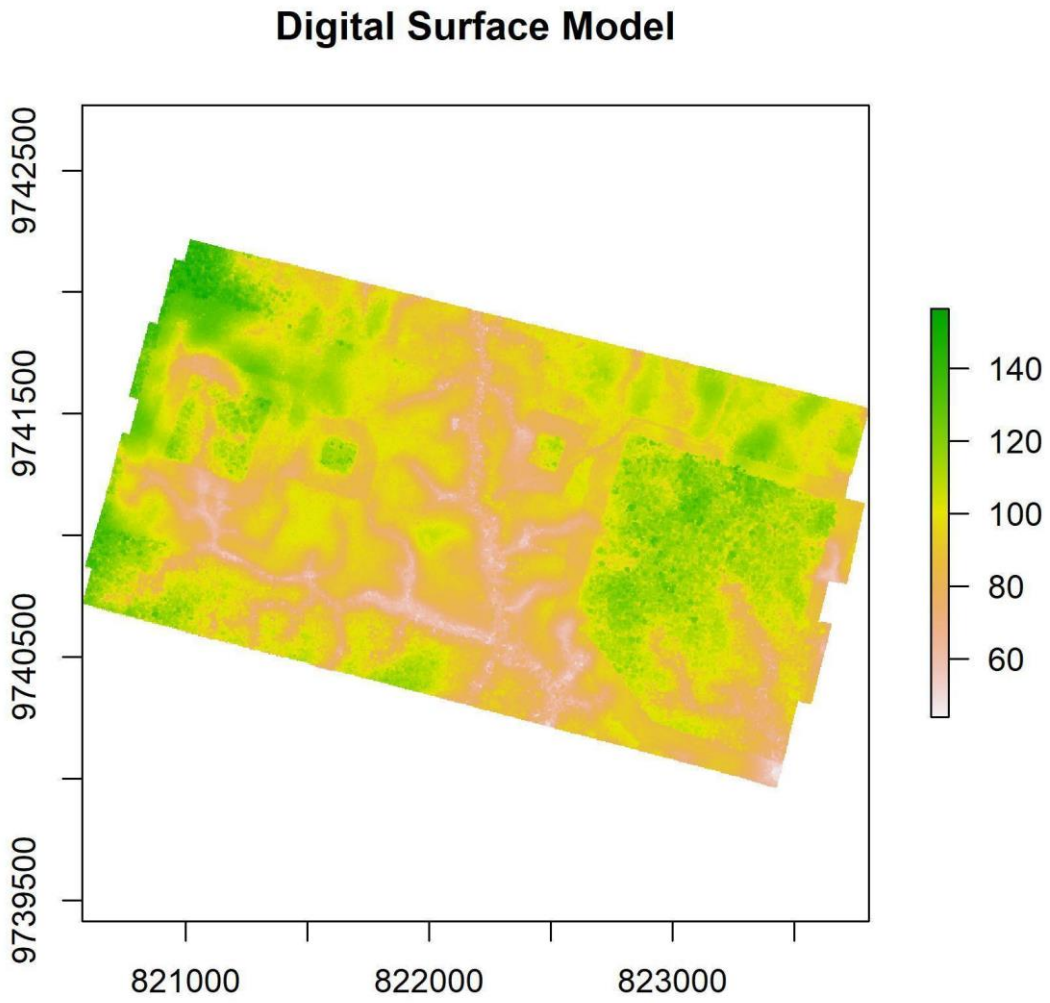

Figure S6. Digital Surface Model (DSM; 2-m grid cell) of “Dimona” site. The axes are UTM and the colors are altitude (meters).

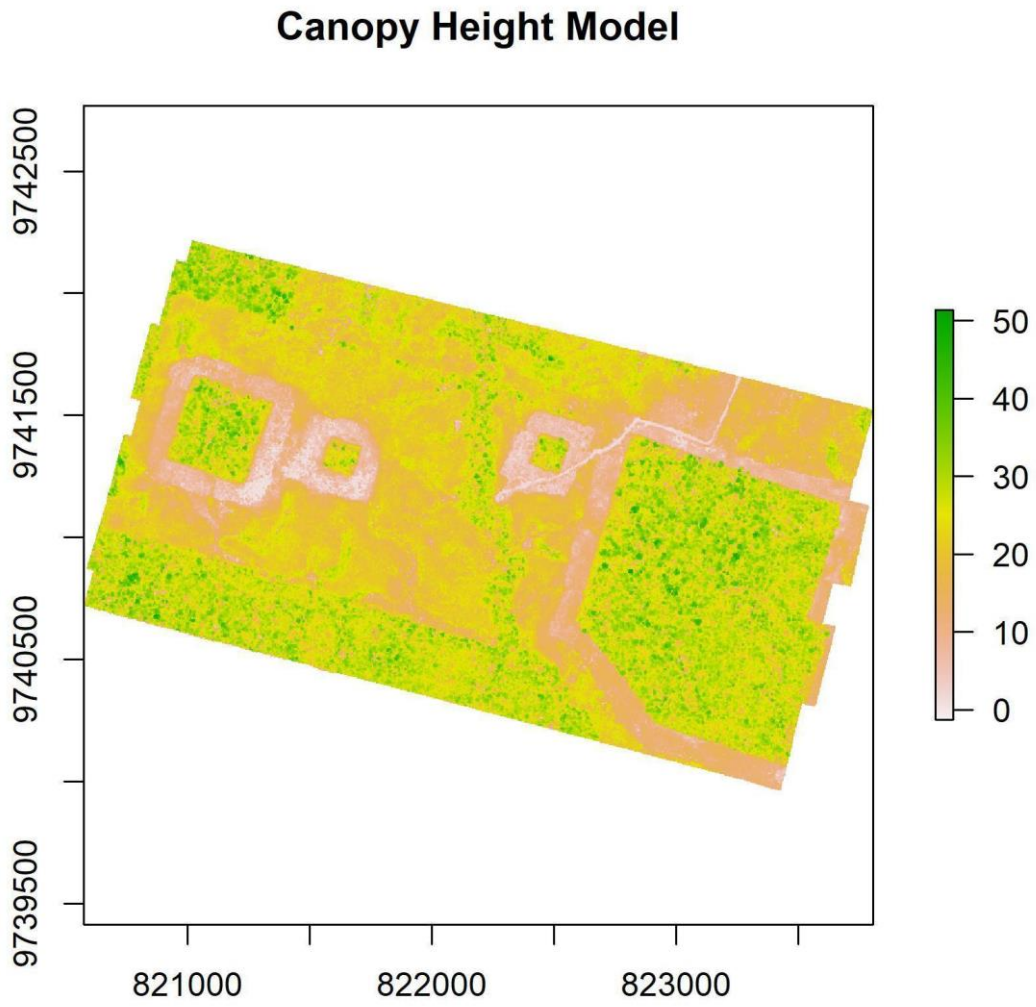

Figure S7. Canopy Height Model (CHM; 2-m grid cell) of “Dimona” site. The axes are UTM and the colors are altitude (meters).

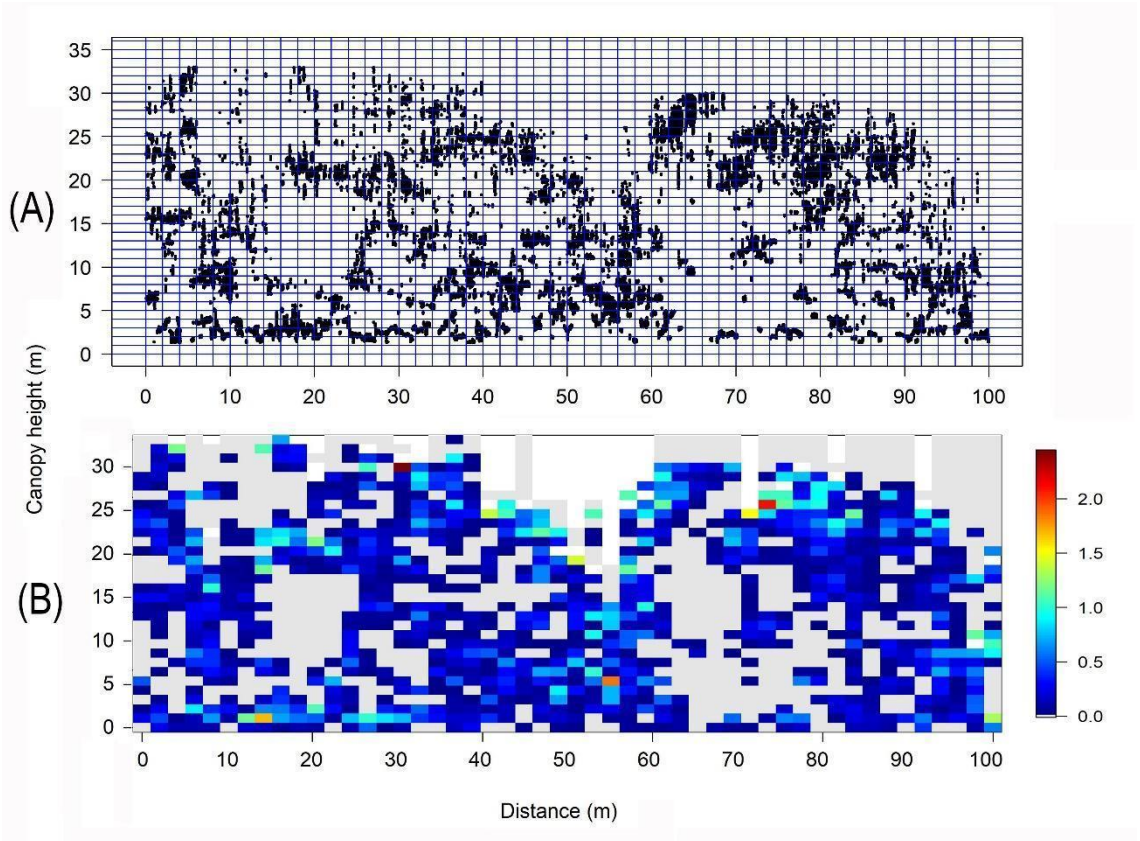

Figure S8. PCL transect data from plot 1 of the 100-ha fragment ("Dimona" site), 80 meters away from the fragment edge (Fig. S1 and Fig S2), showing how lidar pulse returns were separated into 2 m x 1 m pixels (A) and converted into leaf area density (LAD, $m^2 \cdot m^{-3}$) values (B).

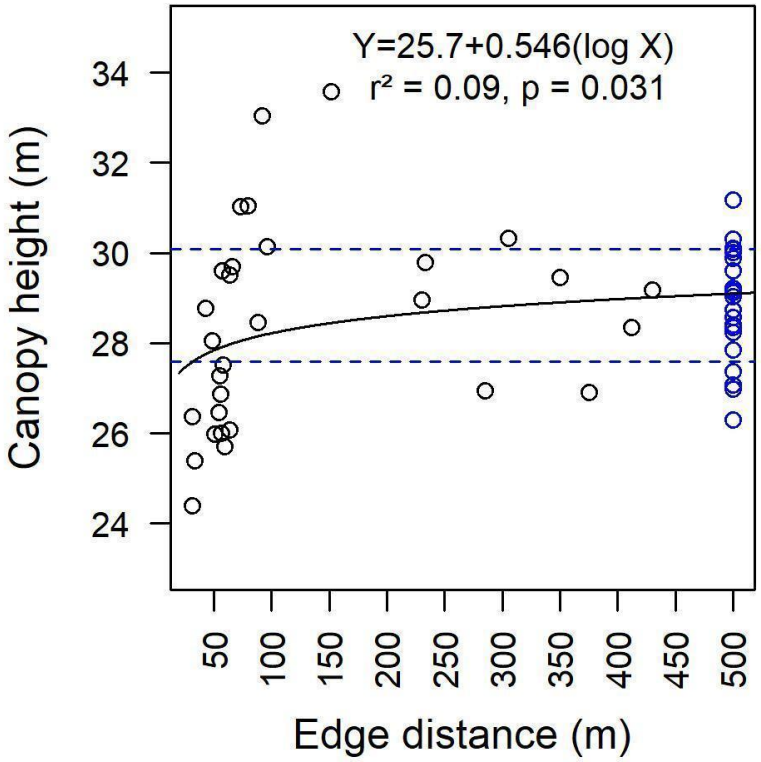

Figure S9. Canopy height as a function of edge distance. The blue points are non-fragmented forest plots more than 500 m away from the edge. The horizontal dashed blue lines represent the interval of 28.83 ± 1.25 (mean ± SD).

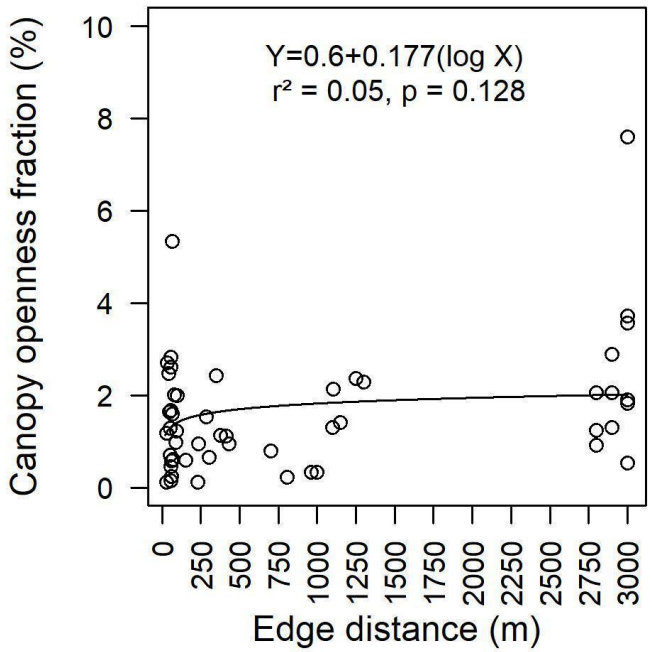

Figure S10. Canopy openness as a function of edge distance.

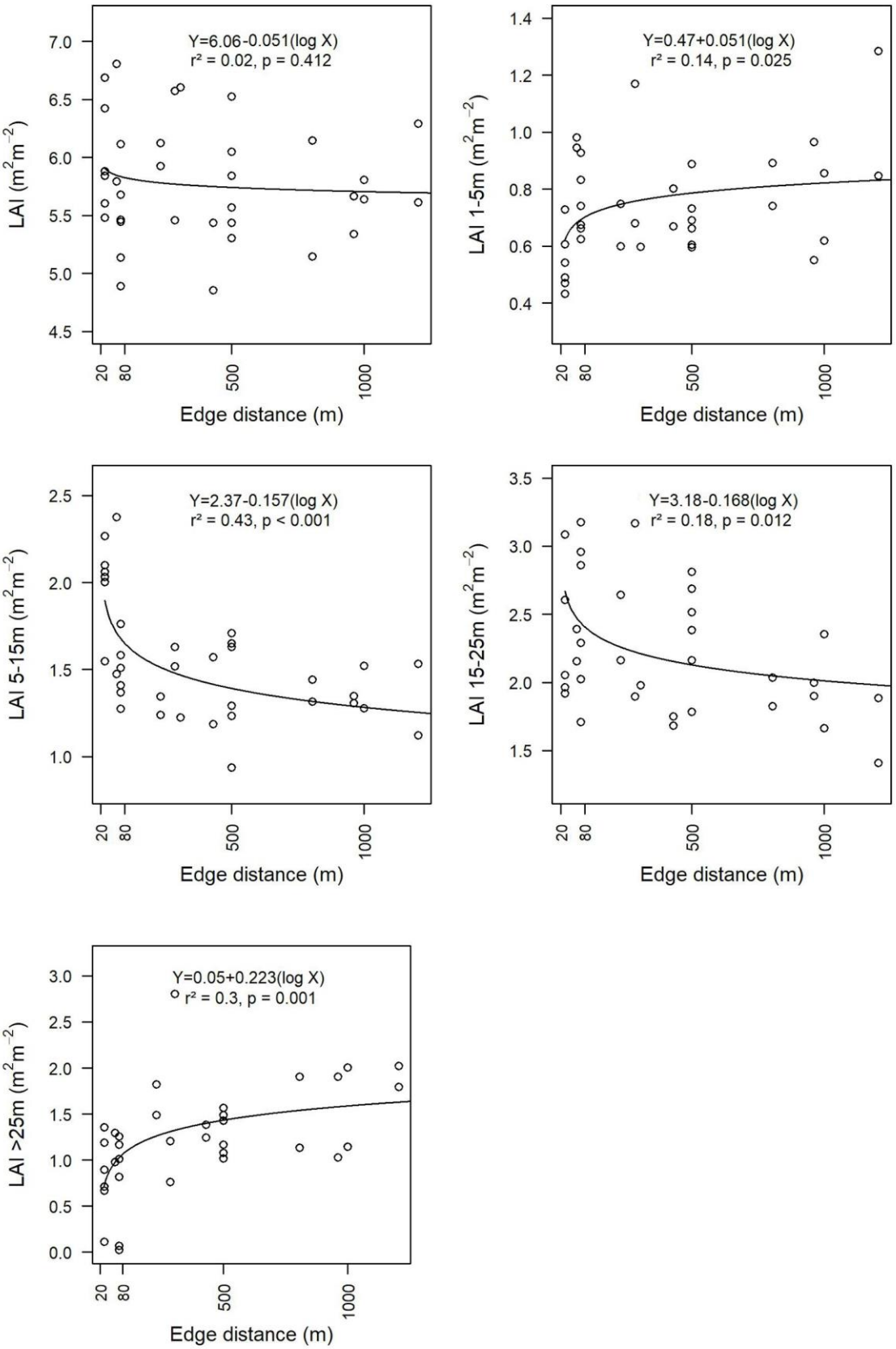

Figure S11. Leaf Area Index as a function of edge distance for all height strata and different vertical strata (ALL, 1-5m , 5-15m, 15-25m, and >25m).

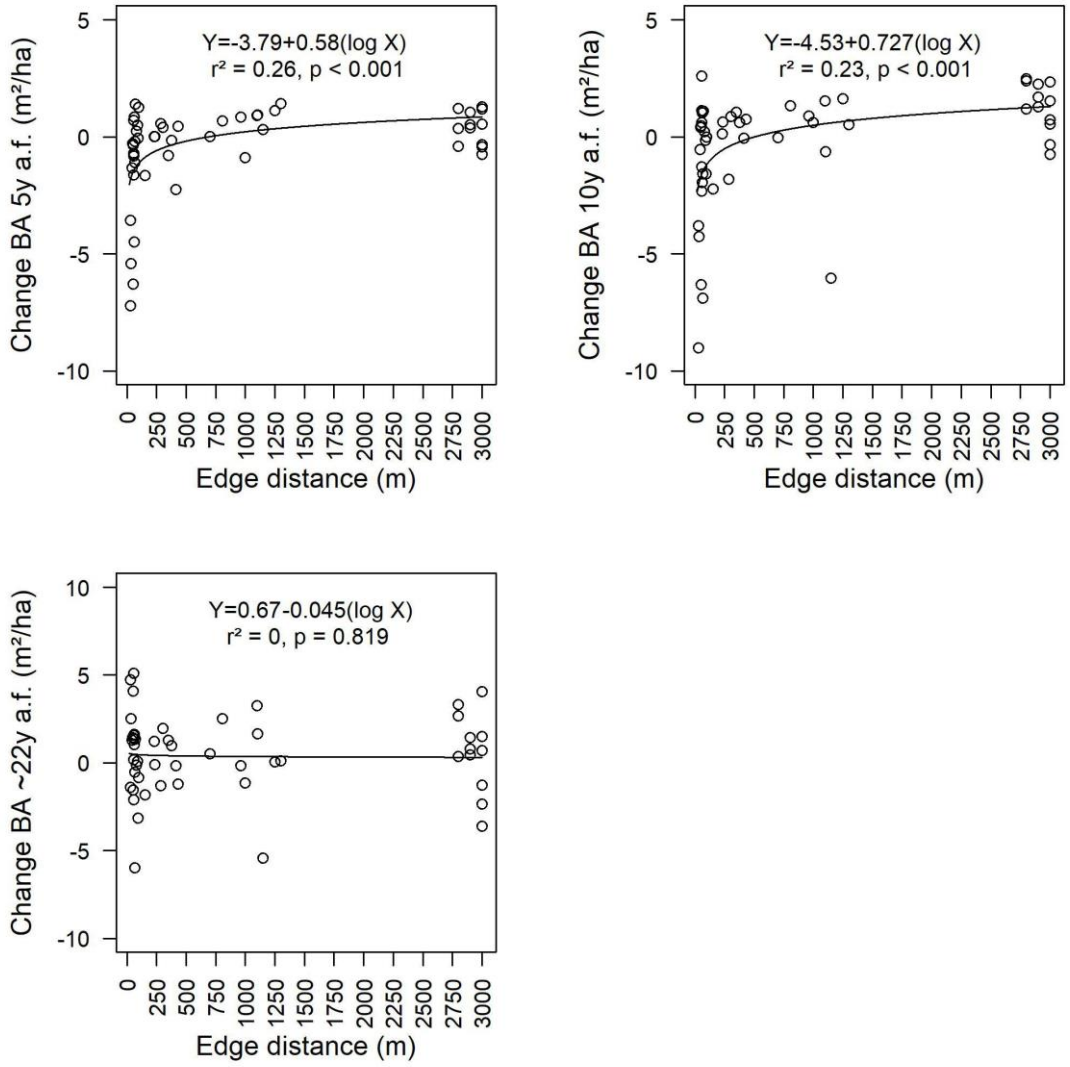

Figure S12. Changes in basal area as a function of edge distance: 5, 10 and ~ 22 years after fragmentation (a.f.).

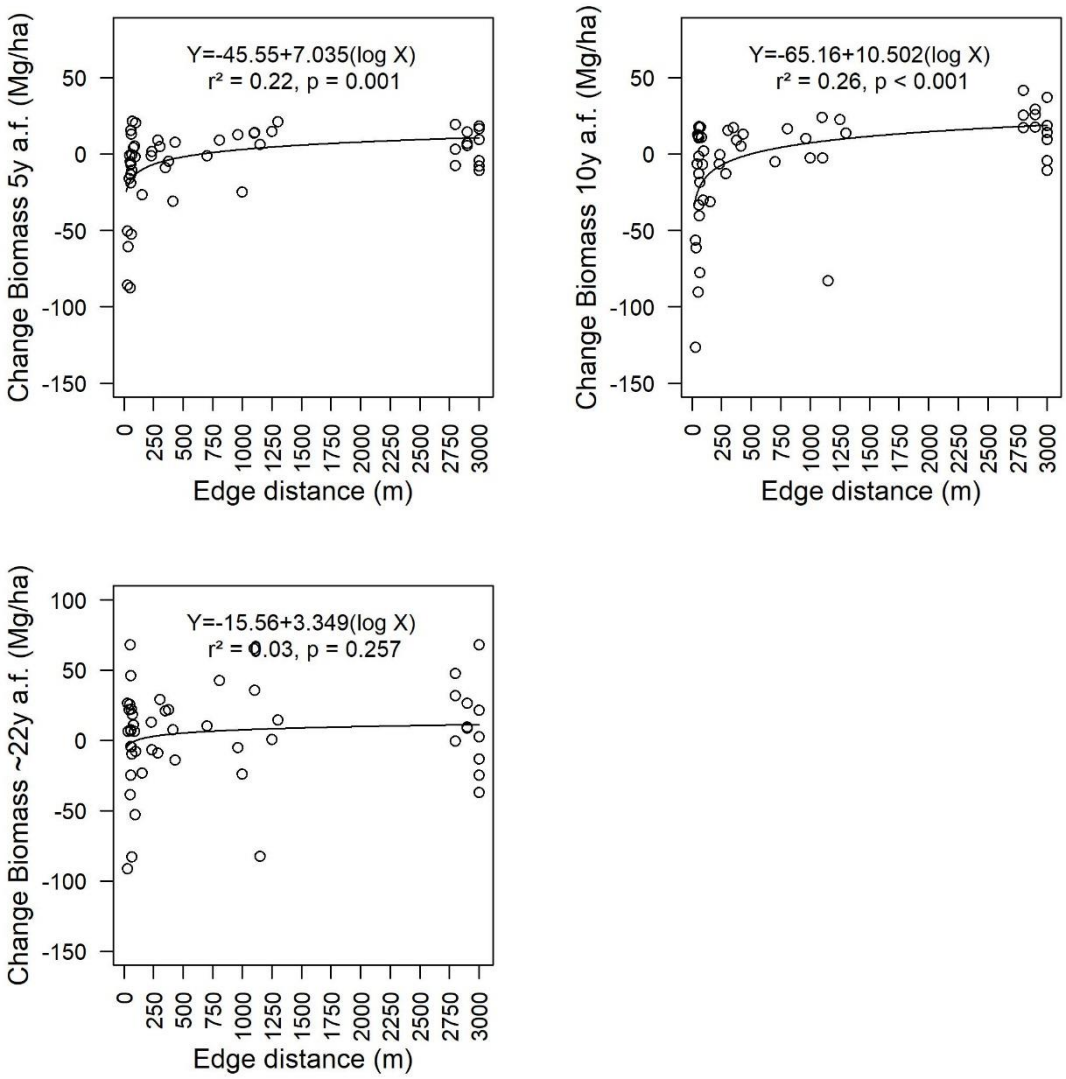

Figure S13. Changes in aboveground biomass as a function of edge distance: 5, 10 and ~ 22 years after fragmentation (a.f.).

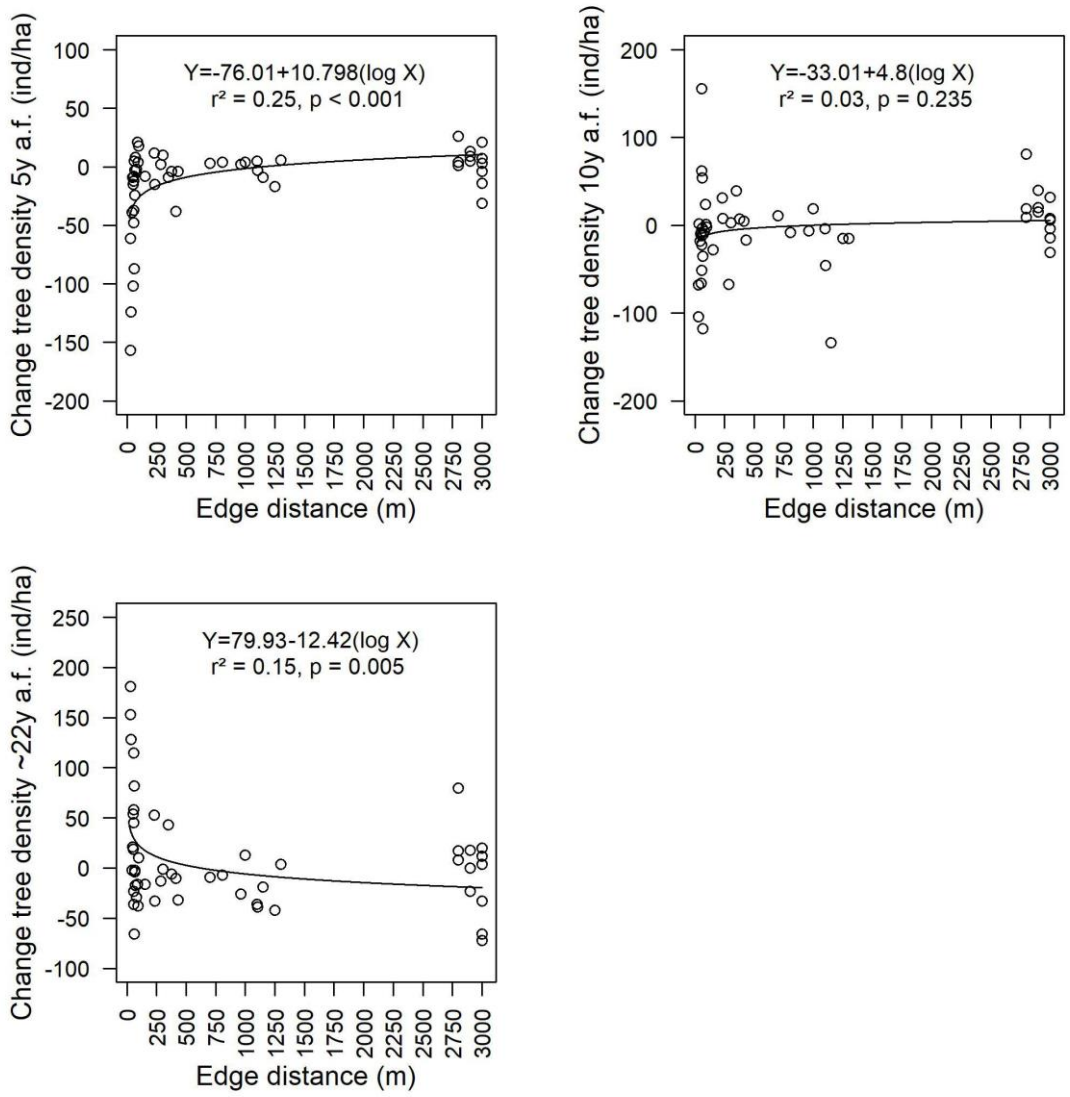

Figure S14. Changes in tree density as a function of edge distance: 5, 10 and ~ 22 years after fragmentation (a.f.).

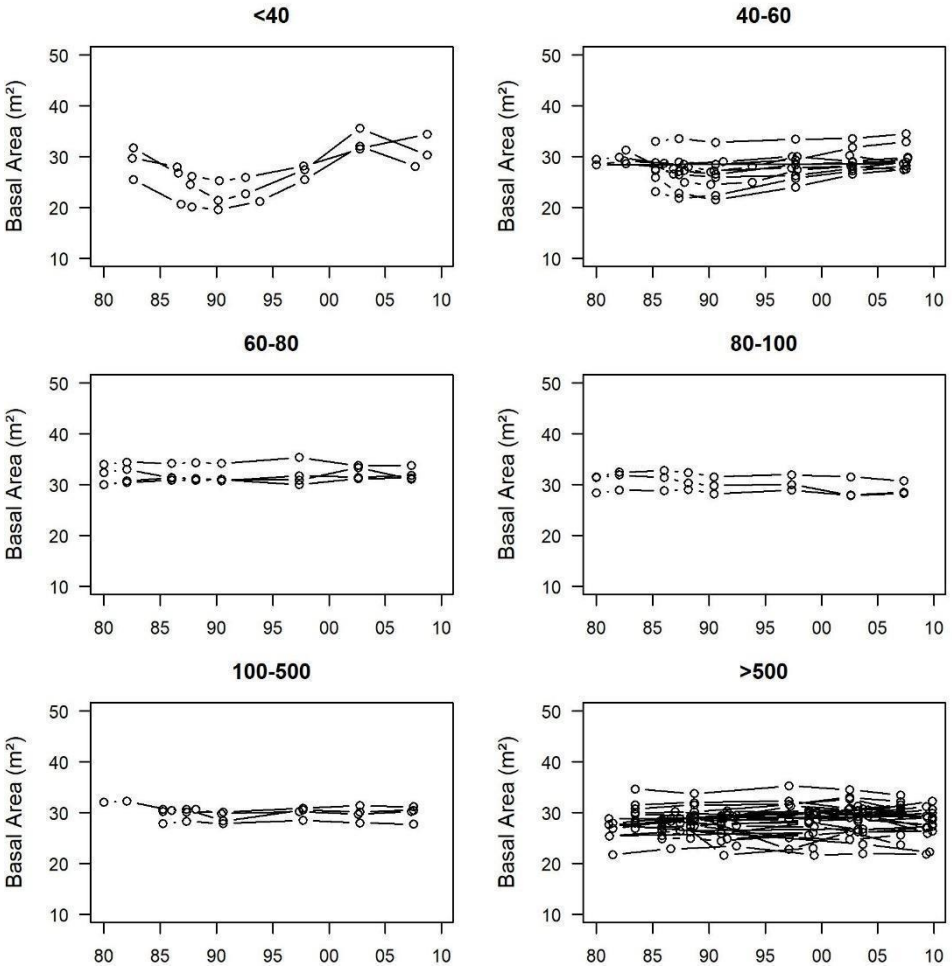

Figure S15. Basal area over time (1980-2010). The graphics are separated into edge-distance classes.

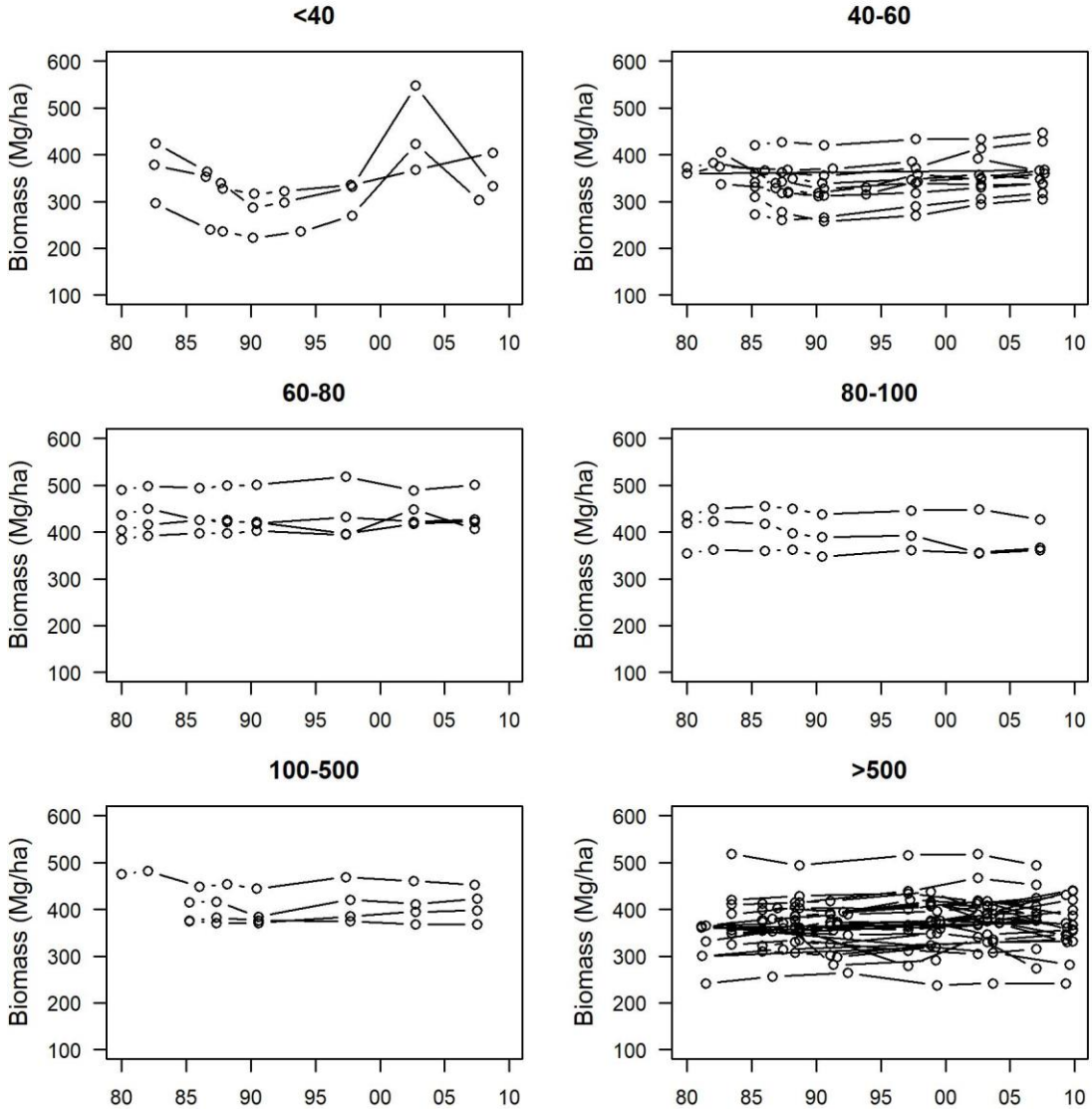

Figure S16. Aboveground biomass over time (1980-2010). The graphics are separated into edge-distance classes.

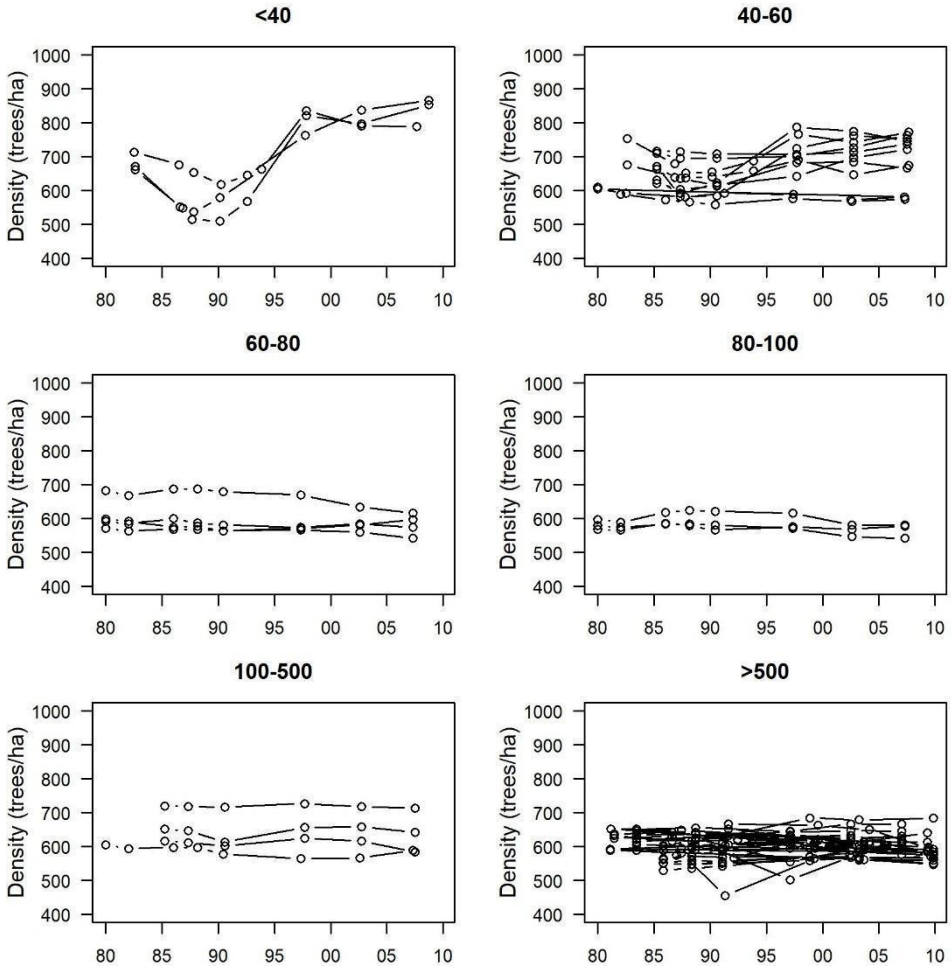

Figure S17. Density of trees (per hectare) in each plot over time (1980-2010). The graphics are separated into edge-distance classes.

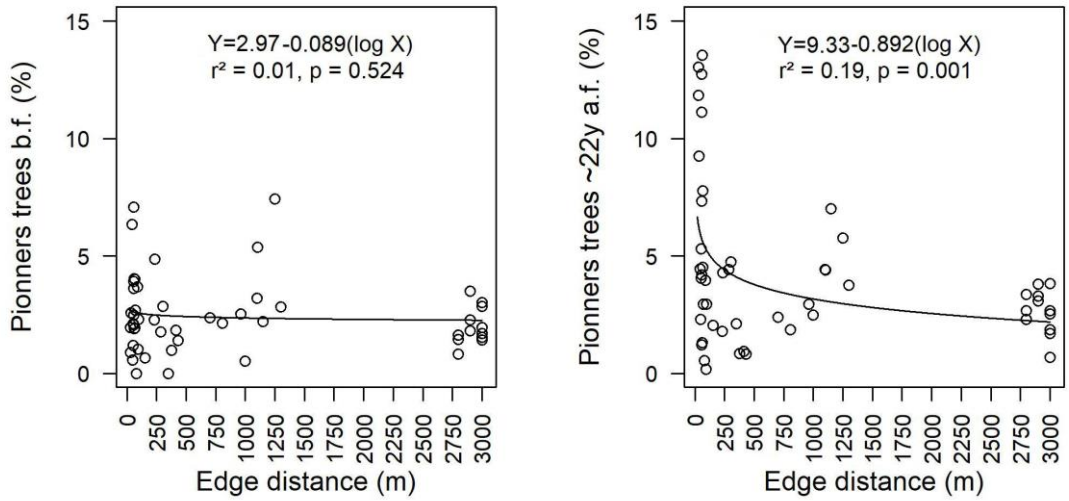

Figure S18. Proportion of pioneer trees species as a function of edge distance: before fragmentation (b.f.) and ~ 22 years after fragmentation (a.f.).

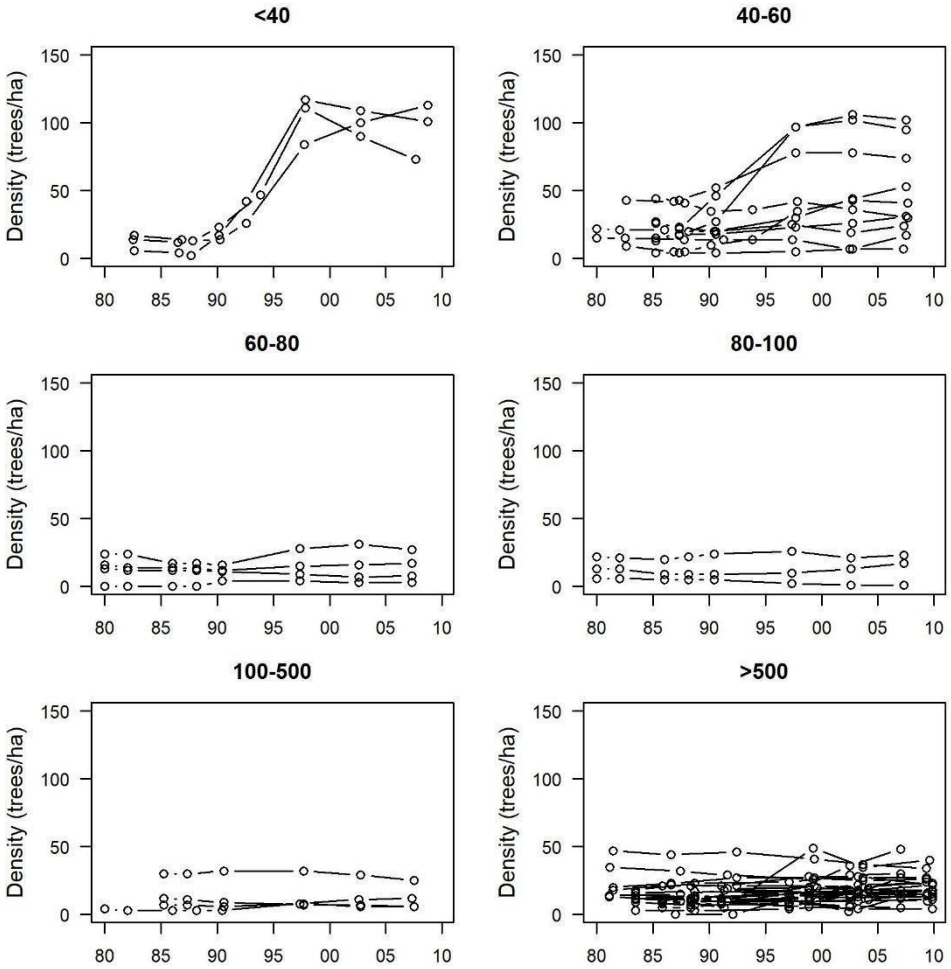

Figure S19. Density of pioneer tree species (per hectare) in each plot over time (1980-2010). The graphics are separated into edge-distance classes.

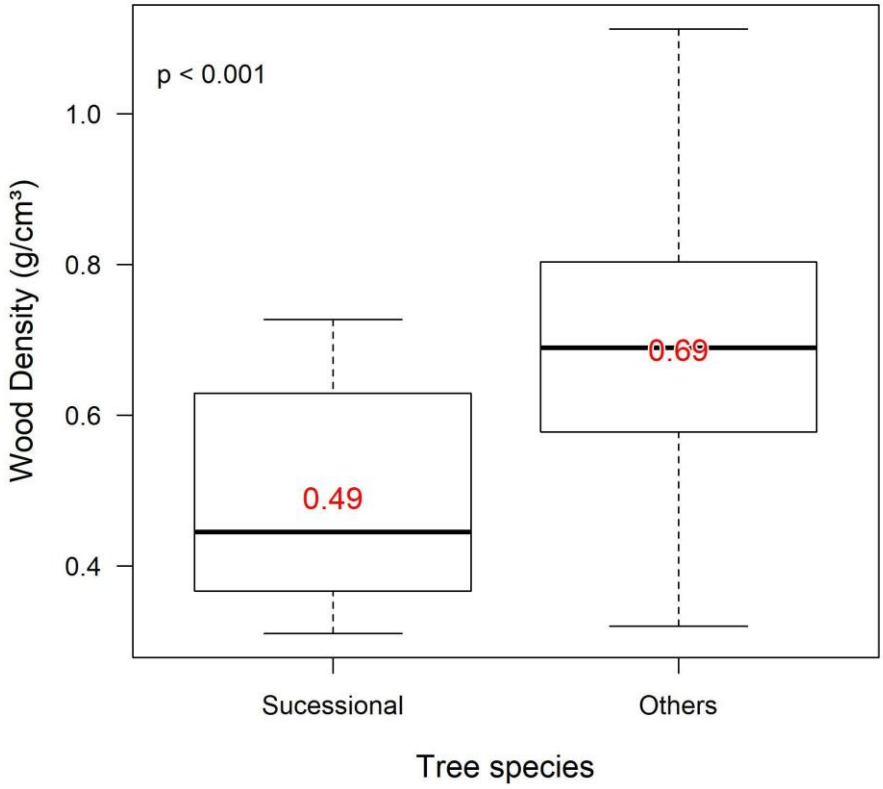

Figure S20. Wood density of the list of early successional species (pioneers) vs. others species. P-value from t-test. The red numbers are the means. Density values are from Zanne et al., 2009.

Table S1 (A). Pearson correlation coefficients (r) between the main structural variables of the canopy and field inventory variables.

	Canopy.height	Rugosity	Canopy.openness	AGB	Pioneers.prop	Delta.dens.5yrs	BA.change
Canopy.height	1.000	0.520	-0.232	0.589	-0.642	0.538	-0.154
Rugosity	0.520	1.000	0.428	0.083	-0.254	0.189	-0.531
Canopy.openness	-0.232	0.428	1.000	-0.339	-0.104	0.051	-0.431
AGB	0.589	0.083	-0.339	1.000	-0.490	0.263	0.270
Pioneers.prop	-0.642	-0.254	-0.104	-0.490	1.000	-0.592	0.192
Delta.dens.5yrs	0.538	0.189	0.051	0.263	-0.592	1.000	0.034
BA.change	-0.154	-0.531	-0.431	0.270	0.192	0.034	1.000

Table S1 (B). p-Values of Pearson correlation coefficients of Table S1(A).

	Canopy.height	Rugosity	Canopy.openness	AGB	Pioneers.prop	Delta.dens.5yrs	BA.change
Canopy.height	NA	0.000	0.102	0.000	0.000	0.000	0.280
Rugosity	0.000	NA	0.002	0.561	0.072	0.183	0.000
Canopy.openness	0.102	0.002	NA	0.015	0.467	0.724	0.002
AGB	0.000	0.561	0.015	NA	0.000	0.062	0.056
Pioneers.prop	0.000	0.072	0.467	0.000	NA	0.000	0.178
Delta.dens.5yrs	0.000	0.183	0.724	0.062	0.000	NA	0.813
BA.change	0.280	0.000	0.002	0.056	0.178	0.813	NA

References

Almeida, D. R. A. de, Nelson, B. W., Schietti, J., Gorgens, E. B., Resende, A. F., Stark, S. C., & Valbuena, R. (2016). Contrasting fire damage and fire susceptibility between seasonally flooded forest and upland forest in the Central Amazon using portable profiling LiDAR. Remote Sensing of Environment, 184, 153–160. doi:10.1016/j.rse.2016.06.017

Asner, G. P., & Mascaro, J. (2014). Mapping tropical forest carbon: Calibrating plot estimates to a simple LiDAR metric. Remote Sensing of Environment, 140, 614–624. doi:10.1016/j.rse.2013.09.023

Bierregaard, R. O., Lovejoy, T. E., Kapos, V., & Hutchings, R. W. (1992). The Biological Dynamics of Tropical Rainforest Fragments. BioScience, 42(11), 859–866. doi:10.2307/1312085

Brinck, K., Fischer, R., Groeneveld, J., Lehmann, S., Dantas De Paula, M., Pütz, S., … Huth, A. (2017). High resolution analysis of tropical forest fragmentation and its impact on the global carbon cycle. Nature Communications, 8, 14855. doi:10.1038/ncomms14855

Broadbent, E. N., Asner, G. P., Keller, M., Knapp, D. E., Oliveira, P. J. C., & Silva, J. N. (2008). Forest fragmentation and edge effects from deforestation and selective logging in the Brazilian Amazon. Biological Conservation, 141(7), 1745–1757. doi:10.1016/j.biocon.2008.04.024

Camargo, J. L. C., & Kapos, V. (1995). Complex edge effects on soil moisture and microclimate in central Amazonian forest. Journal of Tropical Ecology, 11(2), 205–221. doi:10.1017/S026646740000866X

Chambers, J. Q., Asner, G. P., Morton, D. C., Anderson, L. O., Saatchi, S. S., Espírito-Santo, F. D. B., … Souza, C. (2007). Regional ecosystem structure and function: ecological insights from remote sensing of tropical forests. Trends in Ecology and Evolution. doi:10.1016/j.tree.2007.05.001

Chaplin-Kramer, R., Ramler, I., Sharp, R., Haddad, N. M., Gerber, J. S., West, P. C., … King, H. (2015). Degradation in carbon stocks near tropical forest edges. Nature Communications, 6, 10158. doi:10.1038/ncomms10158

Chave, J., Réjou-Méchain, M., Búrquez, A., Chidumayo, E., Colgan, M. S., Delitti, W. B. C., … Vieilledent, G. (2014). Improved allometric models to estimate the aboveground biomass of tropical trees. Global Change Biology, 20(10), 3177–3190. doi:10.1111/gcb.12629

Coomes, D. A., Dalponte, M., Jucker, T., Asner, G. P., Banin, L. F., Burslem, D. F. R. P., … Qie, L. (2017). Area-based vs tree-centric approaches to mapping forest carbon in Southeast Asian forests from airborne laser scanning data. Remote Sensing of Environment, 194, 77–88. doi:10.1016/j.rse.2017.03.017

D'Angelo, S. A., Andrade, A. C. S., Laurance, S. G., Laurance, W. F., & Mesquita, R. C. G. (2004). Inferred causes of tree mortality in fragmented and intact Amazonian forests. Journal of Tropical Ecology, 20(2), 243–246. doi:10.1017/S0266467403001032

De Oliveira, A. A., & Mori, S. A. (1999). A central Amazonian terra firme forest. I. High tree species richness on poor soils. Biodiversity and Conservation, 8(9), 1219–1244. doi:10.1023/A:1008908615271

Didham, R. K., & Lawton, J. H. (1999). Edge Structure Determines the Magnitude of Changes in Microclimate and Vegetation Structure in Tropical Forest Fragments. Biotropica, 31(1), 17. doi:10.2307/2663956

Ewers, R. M., Didham, R. K., Fahrig, L., Ferraz, G., Hector, A., Holt, R. D., … Turner, E. C. (2011). A large-scale forest fragmentation experiment: the Stability of Altered Forest Ecosystems Project. Philosophical Transactions of the Royal Society B: Biological Sciences, 366(1582), 3292–3302. doi:10.1098/rstb.2011.0049

Ferreira, L. V., & Laurance, W. F. (1997). Effects of Forest Fragmentation on Mortality and Damage of Selected Trees in Central Amazonia. Conservation Biology, 11(3), 797–801. doi:10.1046/j.1523-1739.1997.96167.x

Hardiman, B. S., Bohrer, G., Gough, C. M., Vogel, C. S., & Curtis, P. S. (2011). The role of canopy structural complexity in wood net primary production of a maturing northern deciduous forest. Ecology, 92(9), 1818–1827. doi:10.1890/10-2192.1

Hubbell, S. P., & Foster, R. B. (1986). Canopy gaps and the dynamics of a neotropical forest. In Plant Ecology (pp. 77–96).

Jucker, T., Asner, G. P., Dalponte, M., Brodrick, P., Philipson, C. D., Vaughn, N., … Coomes, D. a. (2017). A regional model for estimating the aboveground carbon density of Borneo's tropical forests from airborne laser scanning. In Review, 1–72. doi:10.5194/bg-2018-74

Kapos, V. (1989). Effects of isolation on the water status of forest patches in the Brazilian Amazon. Journal of Tropical Ecology, 5(2), 173–185. doi:10.1017/S0266467400003448

Kraus, K., & Pfeifer, N. (1998). Determination of terrain models in wooded areas with airborne laser scanner data. ISPRS Journal of Photogrammetry and Remote Sensing, 53(4), 193–203. doi:10.1016/S0924-2716(98)00009-4

Larjavaara, M., & Muller-Landau, H. C. (2013). Measuring tree height: A quantitative comparison of two common field methods in a moist tropical forest. Methods in Ecology and Evolution, 4(9), 793–801. doi:10.1111/2041-210X.12071

Laurance, W. F. (2002). Hyperdynamism in fragmented habitats. Journal of Vegetation Science. doi:10.1111/j.1654-1103.2002.tb02086.x

Laurance, W. F., Camargo, J. L. C., Fearnside, P. M., Lovejoy, T. E., Williamson, G. B., Mesquita, R. C. G., … Laurance, S. G. W. (2017). An Amazonian rainforest and its fragments as a laboratory of global change. Biological Reviews. doi:10.1111/brv.12343

Laurance, W. F., Delamônica, P., Laurance, S. G., Vasconcelos, H. L., & Lovejoy, T. E. (2000). Rainforest fragmentation kills big trees. Nature, 404(6780), 836–836. doi:10.1038/35009032

Laurance, W. F., Ferreira, L. V., Merona, J. M. R., & Laurance, S. G. (1998). Rain Forest Fragmentation and the Dynamics of Amazonian Tree Communities. Ecology, 79(6), 2032. doi:10.2307/176707

Laurance, W. F., Laurance, S. G., Ferreira, L. V., Rankin-de Merona, J. M., Gascon, C., & Lovejoy, T. E. (1997). Biomass collapse in Amazonian forest fragments. Science, 278(5340), 1117–1118. doi:10.1126/science.278.5340.1117

Laurance, W. F., Nascimento, H. E. M., Laurance, S. G., Andrade, A. C., Fearnside, P. M., Ribeiro, J. E. L., & Capretz, R. L. (2006). Rain forest fragmentation and the proliferation of successional trees. Ecology, 87(2), 469–482. doi:10.1890/05-0064

Laurance, W. F., Nascimento, H. E. M., Laurance, S. G., Andrade, A., Giraldo, J. P., Lovejoy, T. E., … Angelo, S. D. (2006). Rapid decay of tree-community composition in Amazonian forest fragments, 103(50).

Laurance, W. F., Pérez-Salicrup, D., Delamônica, P., Fearnside, P. M., D'Angelo, S., Jerozolinski, A., … Lovejoy, T. E. (2001). Rain forest fragmentation and the structure of Amazonian liana communities. Ecology, 82(1), 105–116. doi:10.1890/0012-9658(2001)082[0105:RFFATS]2.0.CO;2

Lefsky, M. A., Cohen, W. B., Parker, G. G., & Harding, D. J. (2002). Lidar remote sensing for ecosystem studies. BioScience, 52(1), 19–30. doi:10.1641/0006-3568(2002)052[0019:LRSFES]2.0.CO;2

Longo, M., Keller, M., dos-Santos, M. N., Leitold, V., Pinagé, E. R., Baccini, A., … Morton, D. C. (2016). Aboveground biomass variability across intact and degraded forests in the Brazilian Amazon. Global Biogeochemical Cycles, 30(11), 1639–1660. doi:10.1002/2016GB005465

Lovejoy, T. E., Rankin, J. M., Bierrgaard, R. O., Brown, K. S., Emmons, L. H., & Van der Voort, M. E. (1984). Ecosystem decay of Amazon forest remnants. Extinctions.

MacArthur, R. H., & Horn, H. S. (1969). Foliage Profile by Vertical Measurements. Ecology, 50(5), 802–804. doi:10.2307/1933693

Malcolm, J. R. (1994). Edge effects in central Amazonian forest fragments. Ecology, 75(8), 2438–2445. doi:10.2307/1940897

McGaughey, R. J. (2016). FUSION/LDV: Software for LIDAR data analysis and visualization. US Department of Agriculture, Forest Service, Pacific Northwest Research Station: Seattle, WA, USA, 123(2).

Morton, D. C., Rubio, J., Cook, B. D., Gastellu-Etchegorry, J. P., Longo, M., Choi, H., … Keller, M. (2016). Amazon forest structure generates diurnal and seasonal variability in light utilization. Biogeosciences, 13(7), 2195–2206. doi:10.5194/bg-13-2195-2016

Nascimento, H. E. M., & Laurance, W. F. (2006). Efeitos de área e de borda sobre a estrutura florestal em fragmentos de floresta de terra-firme após 13-17 anos de isolamento. Acta Amazonica, 36(2), 183–192. doi:10.1590/S0044-59672006000200008

Nelson, B. W., Mesquita, R., Pereira, J. L. G., Garcia Aquino De Souza, S., Teixeira Batista, G., & Bovino Couto, L. (1999). Allometric regressions for improved estimate of secondary forest biomass in the central Amazon. Forest Ecology and Management. doi:10.1016/S0378-1127(98)00475-7

Nychka, D., Furrer, R., & Sain, S. (2015). fields: Tools for spatial data. National Center for Atmospheric Research.

Olivas, P. C., Oberbauer, S. F., Clark, D. B., Clark, D. A., Ryan, M. G., O'Brien, J. J., & Ordoñez, H. (2013). Comparison of direct and indirect methods for assessing leaf area index across a tropical rain forest landscape. Agricultural and Forest Meteorology, 177, 110–116. doi:10.1016/j.agrformet.2013.04.010

Parker, G. G., Harding, D. J., & Berger, M. L. (2004). A portable LIDAR system for rapid determination of forest canopy structure. Journal of Applied Ecology, 41(4), 755–767. doi:10.1111/j.0021-8901.2004.00925.x

QGIS Development Team. (2015). QGIS Geographic Information System. Open Source Geospatial Foundation Project. doi:http://www.qgis.org/

R Core Team. (2017). R Core Team (2017). R: A language and environment for statistical computing. R Foundation for Statistical Computing, Vienna, Austria. URL http://www.R-Project.org/., R Foundation for Statistical Computing.

Roussel, J. R., & Auty, D. (2017). lidR: Airborne LiDAR Data Manipulation and Visualization for Forestry Applications.

Runkle, J. R. (1982). Patterns of disturbance in some old-growth mesic forests of eastern North America. Ecology. doi:10.2307/1938878

Simonson, W. D., Allen, H. D., & Coomes, D. A. (2014). Applications of airborne lidar for the assessment of animal species diversity. Methods in Ecology and Evolution. doi:10.1111/2041-210X.12219

Stark, S. C., Enquist, B. J., Saleska, S. R., Leitold, V., Schietti, J., Longo, M., … Oliveira, R. C. (2015). Linking canopy leaf area and light environments with tree size distributions to explain Amazon forest demography. Ecology Letters, 18(7), 636–645. doi:10.1111/ele.12440

Stark, S. C., Leitold, V., Wu, J. L., Hunter, M. O., de Castilho, C. V., Costa, F. R. C., … Saleska, S. R. (2012). Amazon forest carbon dynamics predicted by profiles of canopy leaf area and light environment. Ecology Letters, 15(12), 1406–1414. doi:10.1111/j.1461-0248.2012.01864.x

Tang, H., & Dubayah, R. (2017). Light-driven growth in Amazon evergreen forests explained by seasonal variations of vertical canopy structure. Proceedings of the National Academy of Sciences, 114(10), 2640–2644. doi:10.1073/pnas.1616943114

Tang, H., Dubayah, R., Swatantran, A., Hofton, M., Sheldon, S., Clark, D. B., & Blair, B. (2012). Retrieval of vertical LAI profiles over tropical rain forests using waveform lidar at la selva, costa rica. Remote Sensing of Environment, 124, 242–250. doi:10.1016/j.rse.2012.05.005

Turner, D. P., Cohen, W. B., Kennedy, R. E., Fassnacht, K. S., & Briggs, J. M. (1999). Relationships between leaf area index and Landsat TM spectral vegetation indices across three temperate zone sites. Remote Sensing of Environment, 70(1), 52–68. doi:10.1016/S0034-4257(99)00057-7

Valbuena, R., Heiskanen, J., Aynekulu, E., Pitkänen, S., & Packalen, P. (2016). Sensitivity of Above-Ground Biomass Estimates to Height-Diameter Modelling in Mixed-Species West African Woodlands. PloS One, 11(7), e0158198. doi:10.1371/journal.pone.0158198

Valbuena, R., Maltamo, M., Mehtätalo, L., & Packalen, P. (2017). Key structural features of Boreal forests may be detected directly using L-moments from airborne lidar data. Remote Sensing of Environment, 194, 437–446. doi:10.1016/j.rse.2016.10.024

van Leeuwen, M., & Nieuwenhuis, M. (2010, July 1). Retrieval of forest structural parameters using LiDAR remote sensing. European Journal of Forest Research. doi:10.1007/s10342-010-0381-4

Wu, J., Kobayashi, H., Stark, S. C., Meng, R., Guan, K., Tran, N. N., … Saleska, S. R. (2018). Biological processes dominate seasonality of remotely sensed canopy greenness in an Amazon evergreen forest. New Phytologist. doi:10.1111/nph.14939

Zhang, K., Chen, S. C., Whitman, D., Shyu, M. L., Yan, J., & Zhang, C. (2003). A progressive morphological filter for removing nonground measurements from airborne LIDAR data. IEEE Transactions on Geoscience and Remote Sensing, 41(4 PART I), 872–882. doi:10.1109/TGRS.2003.810682

Zanne, A. E., Lopez-Gonzalez, G., Coomes, D. A. A., Ilic, J., Jansen, S., Lewis, S. L. S. L., … Chave, J. (2009). Global wood density database. Dryad, 235(February), 33. doi:10.5061/dryad.234

4. THE EFFECTIVENESS OF LIDAR REMOTE SENSING FOR MONITORING FOREST COVER ATTRIBUTES IN FOREST AND LANDSCAPE RESTORATION

ABSTRACT

Ambitious pledges to restore over 400 million hectares of degraded lands by 2030 have been made by several countries within the Global Partnership for Forest Landscape Restoration (FLR). Monitoring restoration outcomes at this scale requires cost-effective methods to quantify not only forest cover, but also forest structure and the diversity of useful species. Here we obtain and analyze structural attributes of forest canopies undergoing restoration in the Atlantic Forest of Brazil using a portable ground lidar remote sensing device (that can be a proxy of Airborne Laser Scanner). We assess the ability of these attributes to distinguish forest cover types, to estimate aboveground dry woody biomass (AGB) and to estimate tree species diversity (Shannon index and richness). A set of six canopy structure attributes were able to classify five cover types with an overall accuracy of 75%, increasing to 87% when combining two secondary forest classes. Canopy height and the unprecedent "leaf area height volume" (a cumulative product of canopy height and vegetation density) were good predictors of AGB. An index based on the height and evenness of the leaf area density profile was weakly related to the Shannon Index of tree species diversity and showed no relationship to species richness or to change in species composition. These findings illustrate the potential and limitations of lidar remote sensing for monitoring compliance of FLR goals of landscape multifunctionality, beyond a simple assessment of forest cover gain and loss.

Keywords: Atlantic Forest; Forest canopy; Forest regeneration; Forest succession; Restoration accountability; Restoration monitoring; Tropical forest restoration; Tropical reforestation

4.1. Introduction

Current and future degradation have given rise to global (see Bonn Challenge, 2018) and regional (see WRI, 2018) pledges to restore vast areas of degraded and deforested landscapes, primarily in tropical areas and developing countries (Suding et al., 2015; Holl, 2017). These pledges have placed forests as integral components within a landscape management framework known as Forest Landscape Restoration (FLR). A product of an intergovernmental and interinstitutional dialogue, FLR goals will be accomplished by deliberately managing landscapes to generate a balance of social and ecological benefits (Sabogal et al., 2015). FLR strategies include natural regeneration, assisted natural regeneration, agroforestry, mixed species plantations and commercial monoculture plantations of different species (Laestadius et al., 2015; Aronson et al., 2017), that satisfy different

stakeholders' preferences, ecological objectives and site requirements (Stanturf et al., 2014).

For such large-scale restoration initiatives, the increase in area covered by forest has been the primary indicator of outcome. Though forest cover can be a useful surrogate to evaluate primary productivity (Cao et al., 2016; del Castilho et al., 2018), it may be inadequate to represent other ecosystem functions, such as tree diversity, biogeochemical functions (Meli et al., 2017), or utility for livelihoods (Chazdon et al., 2016; Brancalion & Chazdon, 2017). Monitoring these more complex restoration outcomes requires additional procedures and tools. One logical procedure is, first, to distinguish the different forest cover types in the landscape (e.g., monoculture tree plantations, mixed second-growth forests and old-growth forests) and, second, to determine their respective values in terms of their contributions to biodiversity conservation and ecosystem services, such as carbon uptake and storage (Chazdon et al., 2016). Canopy structural attributes are useful for both distinguishing cover types and as indicators of their respective values. For instance, the aboveground dry wood biomass (AGB) is related to canopy height (Asner & Mascaro, 2014; Longo et al., 2016). Canopy openness has been used to assess tropical forest restoration success (Chaves et al., 2015; Viani et al., 2017). High tree species diversity, which benefits a greater range of stakeholders than monocultures do, may be related to the structural complexity of the vertical canopy profile (Isbell et al., 2011; Sapijanskas et al., 2014; Valbuena et al., 2016a).

A critical step for assessment of forest cover and function in the context of international FLR agreements is to develop replicable standard monitoring protocols that are cost efficient (Holl & Cairns, 2002). Traditional assessments of restoration outcomes rely heavily on field-based methods. Despite recent advances in participatory monitoring of FLR (Evans et al., 2018), these are cost-prohibitive and cannot track progress toward a commitment on the scale of millions of hectares (Holl, 2017). Over the past few years, novel remote sensing technologies such as lidar (light detection and ranging) have emerged as alternatives to monitoring forest structure, composition and function (Bergen et al., 2009; Stark et al., 2012; Hardiman, 2011; 2013. Simonson et al., 2014; Asner & Mascaro, 2014).

Lidar has the potential to penetrate into the forest canopy (Lefsky et al., 2002). This give it the capacity to accurately measure structural canopy parameters such as forest height, canopy openness and leaf area density along the entire

vertical profile (Stark et al., 2012; Almeida et al., 2016). This can be accomplished using either airborne or ground-based platforms. Some studies have used these lidar-derived attributes to distinguish forest types (Stark et al., 2012; Hardiman, 2011; 2013; Valbuena et al., 2013; 2016b), estimate AGB (Asner & Mascaro, 2014), and diversity of plant (Bergen et al., 2009) or animal species (Simonson et al., 2014). The efficacy of lidar for monitoring forest restoration is less known, particularly in tropical forests (Becknell et al., 2018; Mascaro et al., 2012).

The objective of this study is to evaluate the potential of lidar technology (here, a portable ground platform) to estimate key forest cover attributes in Brazil's Atlantic Forest region, an active forest restoration frontier. We quantitatively evaluate lidar's potential to: (i) distinguish different forest cover types; (ii) estimate aboveground biomass; and (iii) estimate four metrics of tree species diversity and composition. Since airborne and ground lidar give similar values for structural metrics when applied to the same sites (Stark et al, 2012, 2015), the PCL system here is taken as an inexpensive proxy for extracting structure metrics that can also be retrieved from airborne laser scanning systems (ALS), since the underlying justification of our study is to evaluate the feasibility of dispensing fully or partially with field inventories to monitor forest restoration outcomes (cover type, biomass and diversity) over very large areas, i.e., using ALS.

4.2. Material and methods

4.2.1. Study sites and experimental design

We selected two locations having forest cover types commonly included in FLR programs (Table 1 and Figure 1). The first three cover types had natural spontaneous species compositions and the last three had planted tree species: (1) old-growth forests ("OG"); (2) second-growth forest established on former pastures ("SGpas"); or (3) on post-harvest *Eucalyptus* plantations with resprouting *Eucalyptus* trees dominating the canopy ("SGeuc"); (4) a set of planted tree species in restoration plantations, each having a different species richness -- 20, 58 or 114 species ("PLdiv"); (5) another set of restoration plantations always having 20 tree species but with a managed range of aboveground biomass ("PLabg") (Campoe et al., 2014); and (6) mature eucalypt monoculture plantations ("Euc").

The three natural forest cover types – OG, SGpas and SGeuc – were seasonal semi-deciduous in the Atlantic Forest Biome in southeastern Brazil, within or near the Corumbataí River Basin (22°20' S, 47°40' W; 470-1060 m elevation). Site details are given by Cesar et al. (2018). The three planted cover types – PLdiv, PLagb, and Euc – were located at the Anhembi Forest Science Experiment Station of the University of São Paulo (22°43' S, 48°11' W, 455 m elevation and < 2% slope). See Ferez et al., (2015) for further Anhembi site description. Both the Corumbataí River basin and the Anhembi field station have a dry winter and a humid summer, mean annual precipitation of 1,100-1,367 mm and average temperature of 20-23°C (climate type: Cwa, Köppen classification) (Alvares et al., 2013).

We established field sample plots in these six cover types (Table 1). We identified species and measured the diameter at breast height (DBH) for all individuals with DBH > 5 cm. Field work was in 2016-2017 and the time between field inventory and lidar measurements of forest structure was less than one year.

Table 1. Location (Corumbataí or Anhembi), forest cover type, sampling design (field plots and lidar data collection), and primary objectives of investigation (forest cover types, aboveground biomass, and tree diversity analysis).

Site	Forest cover types	Design	Objective
Corumbataí	Old-growth Atlantic Coastal Forest ("OG").	4 plots of 900 m² (45x20 m), inventoried in 2016-2017. More than 100 years old. One 45-m Lidar transect in the plot center, collected in 2017.	Tree cover type; Biomass; Diversity
	Second-growth forests, spontaneous succession without human assistance on abandoned (post-harvest) Eucalpytus plantations ("SGeuc").	8 plots of 900 m² (45x20 m), inventoried in 2016-2017. Sucession ages (and number of plots) were 17 (1), 28 (1), 34 (3), and 45 (3) years. One 45-m Lidar transect in the plot center collected in 2017.	
	Second-growth forests, spontaneous succession without human assistance on abandoned cattle pastures of planted grasses ("SGpas").	11 plots of 900 m² (45x20 m), inventoried in 2016-2017. Sucession ages (and number of plots) were 11 (1), 20 (1), 30 (3), 34 (2) and 45 (4) years. One 45-m Lidar transect in the plot center collected in 2017.	
Anhembi	*Eucalyptus sp* plantation. ("Euc").	7 plots of 360 m^2 (45x8 m), inventoried in 2017. There were five plots of *E. urophylla* (three of 26 y and two of 37 y) and two plots of *E. grandis* (both 41 y old). One 45-m Lidar transect in the plot center collected in 2017.	Tree cover type
	Managed restoration plots with a specie richness gradient ("PLdiv").	12 plots of 2,160 m^2 (45x48 m), inventoried in 2016. There were four plots for each of three richness levels (20, 58 and 114 species), all 10 y old. Three parallel and equidistant 45-m Lidar transects in each plot, collected in 2016.	Tree cover type; Diversity
	Managed restoration plots with a biomass gradient ("PLagb").	32 plots of 792 m^2 (36x22 m), inventoried in 2016. All plots had 20 planted tree species and were 13 y old. A factorial experiment of different types of management provided a biomass gradient (more details in Ferez et al., 2015). Two parallel and equidistant 45-m Lidar transects in each plot, collected in 2017.	Biomass

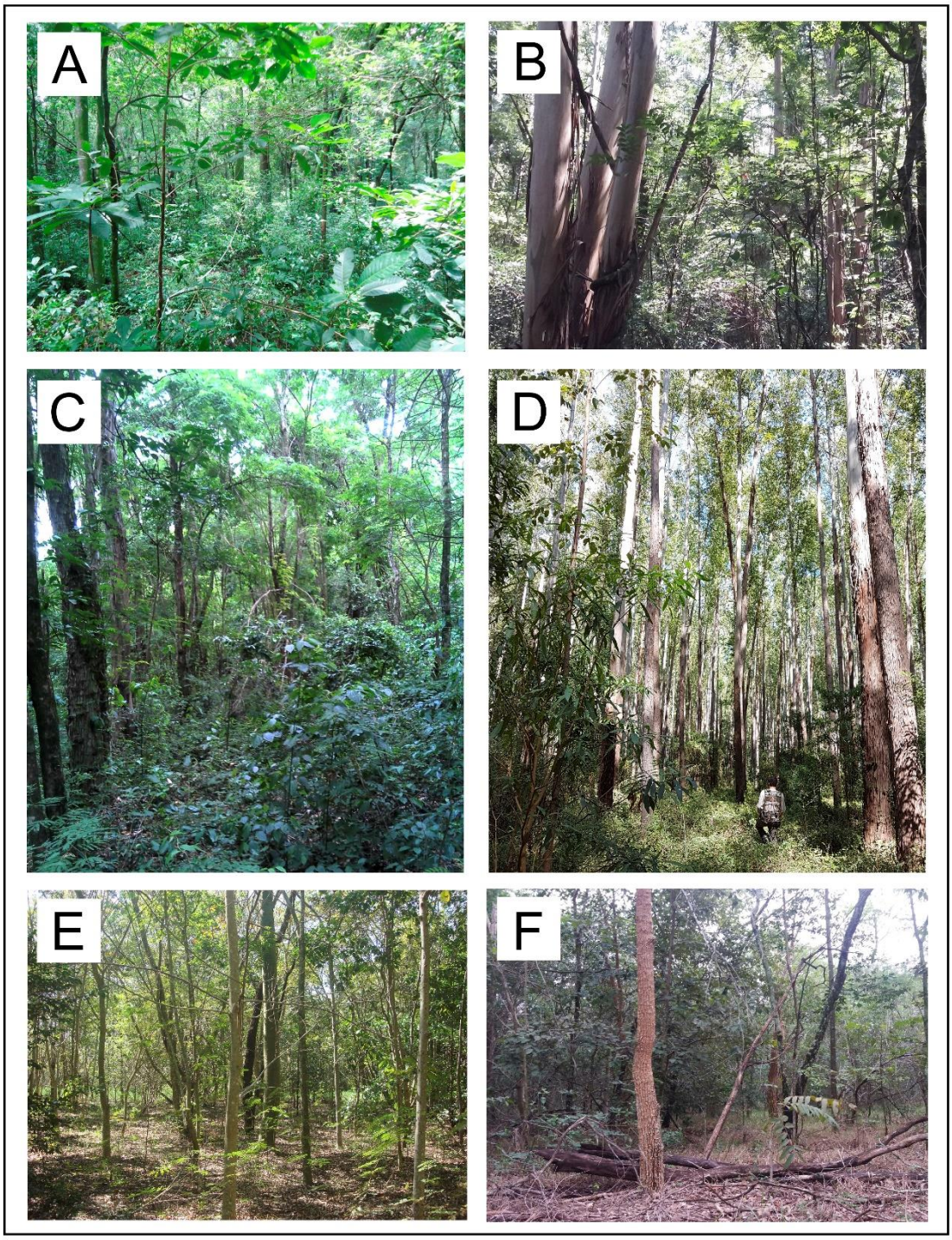

Figure 1. Forest cover types: (A) Old-growth Atlantic Coastal forest (OG); (B) Spontaneous second-growth forests that established after harvest of planted *Eucalyptus* spp. (SGeuc); (C) Spontaneous second-growth forests that established on grass-planted cattle pastures (SGpas); (D) monoculture *Eucalyptus* plantation (Euc); (E) Restoration areas planted with a species richness gradient across plots (PLdiv); and (F) Restoration areas planted with a biomass gradient across plots (PLagb).

4.2.2. Lidar-derived structural attributes

Ground-based lidar data were collected with the Portable Canopy profiling Lidar (PCL) system (Parker et al., 2004; Hardiman, 2011; 2013; Stark et al., 2012;

Almeida et al., 2016). The PCL is a profiling range-finder type laser, model LD90-3100VHS-FLP manufactured by Riegl (Horn, Austria) that is carried by a walking operator along a transect. Surveys were conducted at a constant walking velocity (0.5 m/s), with a vertical upward view, producing a high-density 2D pulse return cloud (2,000 pulses per linear meter) along the transect.

Six continuous variables of forest canopy structure were estimated: (i) canopy height, as the average of the maximum heights from each 2-m along-track interval (Figure S1); (ii) canopy openness, as the fraction of 2-m along-track intervals with a maximum height less than 10 meters; (iii) canopy rugosity, as the standard deviation of maximum height at each 2-m interval; (iv) the mean leaf area index (LAI) of each transect; (v) the understory LAI, as the sum of the LAD at a height ≤ 5 m; and (vi) the leaf area height volume (LAHV, equation 1). For visual comparisons, and for extraction of some of the above variables, we also obtained a mean leaf area density (LAD, $m^2\ m^{-3}$) profile of each transect.

LAD and LAI were estimated using the MacArthur-Horn equation (MacArthur & Horn, 1969) as described in Almeida et al. (2016). There is one mean LAD profile and one mean LAI value per plot transect. The former is a vertical stack of mean LADs, taking the mean of LAD horizontally at each 1-m height interval across all 2-m horizontal sections of transect. LAI is the sum of the mean LAD profile (Almeida et al., 2018).

LAHV, introduced in this study, is the sum of the products of height and mean LAD at that height, for all 1m height intervals in the mean LAD profile. There is one LAHV value per plot transect:

$$LAHV = \sum(i \times LAD_i) \quad (1)$$

where i is the height and LAD_i is the horizontal mean of leaf area densities at the respective canopy height (Figure 2). A geometrical interpretation of LAHV is that it sums the volumes bound by each unit of leaf area and the horizontal plane of the ground over all vertical positions. Biologically, leaf area and basal area are often assumed to be directly proportional, while cross sectional area of branches may be approximately constant over branching generations, and the number of branching generations increases linearly with height (West et al., 1997). Together this suggests that LAHV could be directly proportional to wood volume, and thus AGB (see model in Stark et al. 2015).

4.2.3. Data analysis

The inventory plots were the sampling units, and the lidar transects of these plots provided their structural attributes. For this reason, when multiple transects were made in a plot, we joined them into a single transect corresponding to that plot. For our first objective, to distinguish the forest cover types using only lidar-derived attributes, we used the Random Forests decision tree supervised classification. We included five of the six cover types listed in Table 1, excluding “PLagb” because it was considered not representative of typical restoration managed plots. Only when the purpose was the forest cover type classifications, we also added some lidar transects that were outside of the inventory plots to increase the number of observations per cover type, after ensuring that these transects belong to the same forest type. The sample size (number of transects) for OG, SGeuc, SGpas, PLdiv and Euc forest cover types were 18, 22, 35, 36 and 7, respectively. We report the overall classification accuracy and the accuracies for each cover type in an error matrix. The error matrix was constructed from a jack-knife cross-validation –the optimal decision tree was obtained by including all but one randomly chosen transect in the training data, then seeing if the left-out transect was correctly classified. The RF classifier completed 10,000 iterations using all six continuous variables from lidar. We report the importance ranking of these six variables to overall classification accuracy and to the discrimination of each of the cover types. For a visual interpretation of the importance of each structural variable to the classifier we interpret critical features of the five LAD profiles. We also provide a two-dimensional depiction of the attribute hyperspace using principal components analysis (PCA). The PCA was based on the same six lidar-derived attributes of canopy structure that were used by the classifier, plus AGB from field inventories of the plots.

For our second objective – to examine the potential of lidar to estimate AGB – we used five cover types: three having spontaneously colonized tree plots (old-growth OG forest and two types of secondary growth, SGeu and SGpas), the Eucalyptus monoculture plots (Euc) and the biomass-managed planted tree plots (PLagb). In OG, SGeuc, and SGpas, the AGB of each plot was obtained from their DBH and wood density using the general allometric equation proposed by Chave et al. (2014). To estimate AGB of Eucalyptus spp. trees from their DBH, we used a specific equation developed locally by Campos et al. (1992). For the biomass-

managed planted tree plots we used a multi-species allometric equation, that uses DBH, wood density and tree height, developed from the mix of 20 tree species planted at the Anhembi experiment (Ferez et al. 2015). A multiple linear model was developed to estimate biomass after excluding structural attributes that did not satisfy assumptions of homoscedasticity, symmetric residuals or multi-collinearity. Simple linear regressions are also given for the best predictors of AGB. We computed the absolute and relative Root Mean Square Error (RMSE) for assessing the model accuracy (Eq.S1-S2).

For our third objective, to predict tree biodiversity from forest structure, diversity was represented in four different ways: species density (number of species/area using a fixed area); species richness for a fixed number of trees sampled from each plot by randomized rarefaction; tree community Shannon diversity index; and floristic composition. We considered floristic composition from the viewpoint of the score obtained on a single axis non-metric multidimensional scaling (NMDS). NMDS was in turn based on a triangular matrix containing all plot pairs' Jaccard similarity indices, using presence/absence of each species. All four diversity variables were obtained for the plots for the three cover types that had spontaneous natural colonization (OG, SGeuc, and SGpas). In the plots with 20, 58 or 114 planted tree species (cover type PLdiv) we used only species density, since the tree community Shannon index and the composition there was sensitive to the species density treatments. The single species monoculture (Euc) and the fixed 20-species biomass-managed plots (PLagb) were not included in the diversity prediction analyses.

The potential of lidar to provide a proxy for tree diversity was examined with an additional variable, the structure-based "canopy Shannon index" (Stark et al., 2012). The canopy Shannon Index is based on the mean LAD profile of a transect. It increases with the number of heights having vegetation present and with the equitability of LAD among those vegetated heights (McArthur & McArthur, 1961; Valbuena et al., 2012). We hypothesized that this index may be related to alpha species diversity at plot scale because the index would increase in older succession stages which are taller, having more vegetation strata, and because in OG forest dynamics allow specific tree species to colonize different canopy strata (Williams et al., 2017). Spearman correlations were obtained for the canopy Shannon index against each of the four tree biodiversity metrics (species density, species richness,

tree community Shannon index, and floristic composition represented by NMDS score).

4.3. Results

Lidar-derived structural attributes performed well as predictors of forest cover type and of the tree biomass of a plot, weakly as predictors of tree species evenness, and poorly as predictors of richness and difference in floristic composition between plots.

4.3.1. Discrimination of forest cover types using lidar

Using six lidar-derived structure attributes, the Random Forests classifier identified the five forest cover types with an overall 75% accuracy (Table 2). The largest misidentifications were mutual between the two secondary forests; overall accuracy improved to 87% when these were combined as a single class. The importance of each structure variable to overall accuracy and to correct prediction of each forest cover type is shown in Table 3.

Table 2. Error matrix from a jack-knife validation of the Random Forests classifier of five forest cover types that used the six lidar-derived canopy structure variables shown in Table 3. Percent correct classification of each type is in bold on the diagonal; percent errors are off-diagonal. Types are: monoculture *Eucalyptus* plantations (*Euc*), old-growth forests (*OG*), planted forests with three levels tree diversity combined here in a single class (PLdiv), spontaneous second-growth after harvest of a *Eucalyptus* plantation (*SGeuc*), and spontaneous second-growth on abandoned planted-grass cattle pastures (*SGpas*).

		True class				
		OG	*SGeuc*	*SGpas*	*PLdiv*	*Euc*
Classified As:	*OG*	**77**	9	7		
	SGeuc	23	**51**	15		
	SGpas		40	**61**	2	
	PLdiv			17	**98**	
	Euc					**100**

Overall accuracy = 75%

Lumping two secondary forests, overall accuracy = 87%

Table 3. Variable importance to classification accuracy. First column gives the mean decrease in overall percent accuracy of the classifier if just that variable is scrambled. Other cells, scaled 0-1 with red color ramp, indicate importance of each structural variable in classifying each forest cover type. Types are: monoculture *Eucalyptus* plantations (*Euc*), old-growth forests (*OG*), planted forests with three levels tree diversity combined here in a single class (PLdiv), spontaneous second-growth after harvest of a *Eucalyptus* plantation (*SGeuc*), and spontaneous second-growth on abandoned planted-grass cattle pastures (*SGpas*). LAI is the Leaf Area Index and LAHV is Leaf Area Height Volume.

		OG	SGeuc	SGpas	PLdiv	Euc
Canopy height	32,5	0,88	0,32	0,42	0,93	0,88
Canopy rugosity	31	0,13	0,94	0,35	0,96	0,34
Canopy openness	27	0,82	0,00	0,35	1,00	0,62
Understory LAI	23	0,31	0,05	0,42	0,79	0,77
LAI	20	0,36	0,26	0,36	0,51	0,63
LAHV	12	0,44	0,11	0,33	0,23	0,30

Forest cover types classified with highest accuracy had distinguishing features in their LAD profiles (Figure 2). Monoculture *Eucalyptus* plantations were classified with 100% accuracy and had the most distinctive profile: a tall canopy with low LAI and low canopy openness. The set of plots containing a range of diversity of planted trees (PLdiv) were identified with 95% accuracy. Compared with all the other forest cover types, these have a smoother canopy (single dominant height), low stature, and thus high fraction below 10m (high openness). The two second-growth forest types had very similar LAD profiles, and thus the RF classifier had difficulty in separating them.

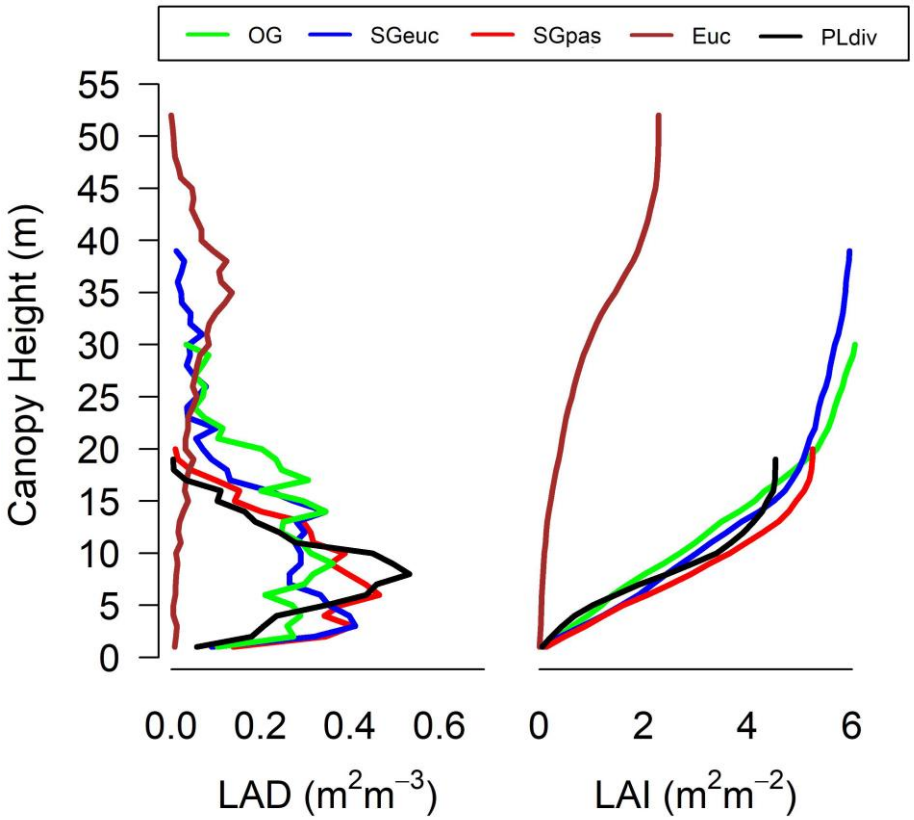

Figure 2. Mean leaf area density (LAD) profiles (left) and cumulative leaf area (LAI) (right) for the five forest cover types used in the classification accuracy assessment. Types are: monoculture *Eucalyptus* plantations (*Euc*), old-growth forests (*OG*), planted forests with three levels tree diversity combined here in a single class (PLdiv), spontaneous second-growth after harvest of a *Eucalyptus* plantation (*SGeuc*), and spontaneous second-growth on abandoned planted-grass cattle pastures (*SGpas*).

Further insights into how each lidar-derived structure variable contributes to the separation of cover classes by the classifier are evident in the scatterplot of sores for the first two PCA components (Figure 3), which explained 72% of total variance in the structural attribute hyperspace. The *Eucalyptus* plots, easily discriminated by the classifier, form a dense isolated cluster in the two-dimensional depiction. This is due to the odd combination of tall canopy but a low total LAI, with almost no understory (Table 3). Old-growth forest plots, classified with 88% accuracy, are pulled away from other cover types by their high aboveground biomass, tall canopy and low fraction of heights below 10m (low openness). Some of the plots of secondary forest developed on post-harvest *Eucalyptus*, are very rugose due to tall *Eucalyptus* stump sprouts; this attribute was useful to the best decision trees.

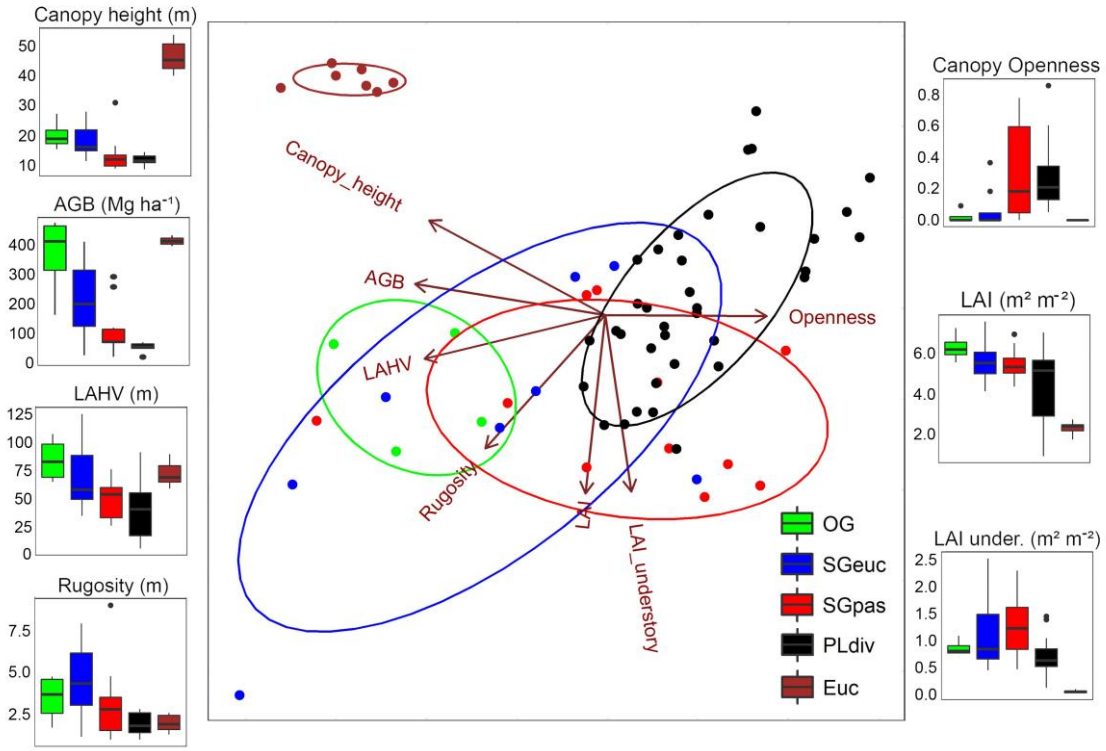

Figure 3. Biplot of the first two axes of a principal component analysis and boxplots of the seven canopy structural attributes used in the PCA (six lidar-derived plus the aboveground dry woody biomass). Forest cover types are coded by the same colors used in Fig. 2. Types are: monoculture *Eucalyptus* plantations (*Euc*), old-growth forests (*OG*), planted forests with three levels tree diversity combined here in a single class (PLdiv), spontaneous second-growth after harvest of a *Eucalyptus* plantation (*SGeuc*), and spontaneous second-growth on abandoned planted-grass cattle pastures (*SGpas*).

4.3.2. Predicting aboveground biomass from lidar

Across the three non-planted forest cover types, AGB was significantly correlated in simple regressions with three lidar-derived canopy structure attributes: LAHV, canopy height and LAI. Respective correlations with AGB were 0.84, 0.75, and 0.54 (Figure S2). Among the planted tree plots which have a biomass-managed gradient (PLagb), AGB was correlated with these same three structural attributes, with r = 0.75, 0.78, and 0.51, respectively (Figure S3). Canopy openness was discarded as it showed a strongly heteroscedastic, non-linear and saturated relationship with AGB.

While LHAV and canopy height each showed high explanatory value in simple regressions for the two sets of plots just described (Figure 4), they were highly correlated within each of these sets (r > 0.70). With all four forest cover types plus the *Eucalyptus* plantation in the same model, collinearity was reduced. Both

predictors could be included in a multiple linear regression (Figure 5), obtaining r^2 = 0.84 (versus r^2 = 0.69 using only canopy height, r^2 = 0.68 using only LAHV).

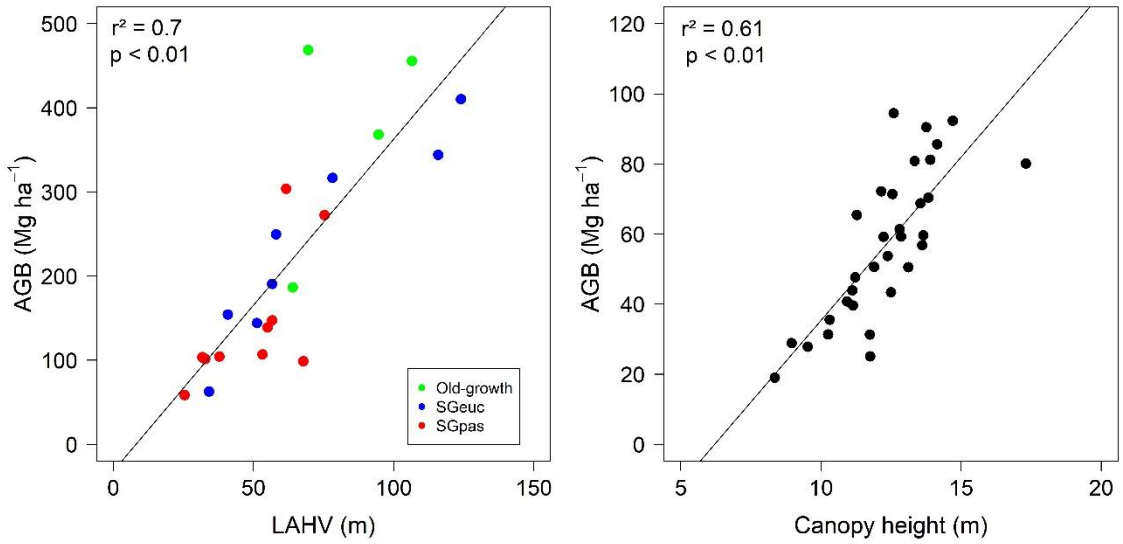

Figure 4. Aboveground biomass as a function of LAHV (left) for spontaneous vegetation (old-growth forests and two second-growth forests) (r^2 = 0.7, RMSE = 72.6, relative RMSE = 34.1%); and as a function of Canopy Height (right) for planted forest, (biomass-managed plots with 20 tree species) (r^2 = 0.61, RMSE = 13.5, relative RMSE = 23.8%).

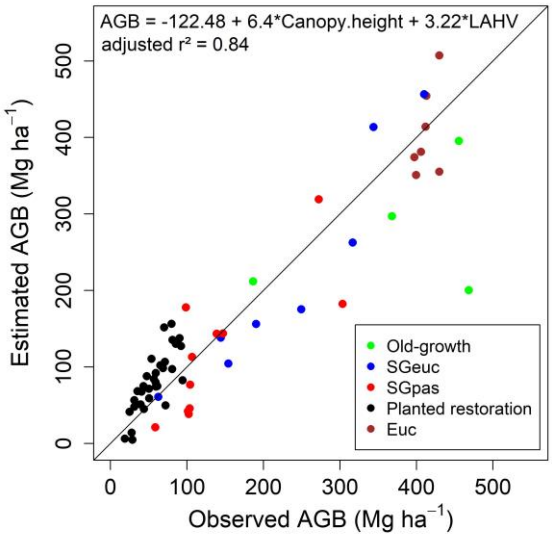

Figure 5. Multiple linear regression model using LAHV and Canopy Height as predictors of aboveground biomass (r^2 = 0.84, RMSE = 57, relative RMSE = 36,8%) of plots from five forest cover types: three spontaneous (old-growth plus two second growth types) and two planted (biomass-managed plots with 20 species and *Eucalyptus* monoculture).

4.3.3. Predicting tree diversity from lidar

About 25% of the variance in tree community Shannon diversity index could be explained using the purely structural “canopy Shannon index”, when considering

the set of plots in the three natural, spontaneously colonized forest cover types (Figure 6). The other three measures of biological diversity -- species density, richness and composition NMDS score -- were not significantly related to canopy Shannon index (Figures S4 and S5).

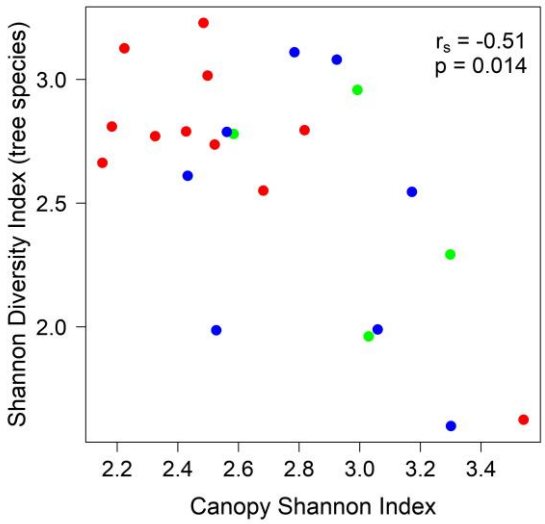

Figure 6. Scatterplot and Spearman's correlation between the canopy structure Shannon index derived from lidar and the floristic Shannon index for the set of three spontaneously colonized forest cover types: old-growth forests (green), secondary forest on former *Eucalyptus* plantation (blue), and second growth on former planted-grass pasture (red).

4.4. Discussion

In this study, we characterized different restoration outcomes based on structural attributes derived from PCL. Those attributes were capable to distinguish forest cover types and their associated AGB stocks and tree diversity level. Previous studies have used Airborne Laser Scanner metrics to estimate AGB (Long et al., 2016) and distinguish forest types (Stark et al., 2012; Gorgens et al., 2016) in patches and landscapes covered by old-growth native forests. However, few studies have analyzed forest restoration areas with discrete return lidar metrics (Becknell et al., 2018). The lack of studies analyzing the effectiveness of lidar technology for monitoring restoration is a critical limitation, as the structural and compositional heterogeneity of forest cover are expected to increase with different reforestation approaches, the existence of forest patches at different successional development stages, and the adoption of different management practices (Chazdon et al., 2016), and these approaches must be adequately compared.

The attributes of canopy structure and LAD profiles provided important indicators of structure and potential ecosystem functions of forest restoration components. The range of forest management and history was reflected in canopy structure. Second-growth forests originating from natural regeneration after 20-40 years showed attributes closer to old-growth forest. The restoration plantations, despite having high taxonomic diversity, are still an even-aged tree community with a more homogeneous canopy with vegetation density concentrated between about 5 and 12 m height. On the other hand, disturbances, succession, and longer time spans create a more heterogeneous canopy, as consequence of the differential growth rates, turnover rates, and sensitivity to disturbances among tree species (Chazdon et al., 2014).

In the old-growth forests, LAD was better distributed throughout the vertical canopy profile, diversifying the environments, impacting tree growth and survival, and generating more possibilities of niches for animals that live in different heights of the canopy (McDonnell, 1986; Zahawi et al., 2015), all factors with potential impacts on canopy ecosystem functions. The spread of the vegetation along the vertical profile can also be observed in LAI accumulation, where the old-growth forests had a constant variation when compared to the other forest cover types. SGeuc presented a structure similar to old-growth forest. Eucalypt trees can consolidate a closed upper canopy in less than a decade, quickly generating a shaded environment in which shade-tolerant native species can grow. Second-growth from pasture (SGpas) may take longer to reach such taller canopy structure with shaded understory. Some studies have already demonstrated the contribution, or at least the lack of negative effects, of Eucalypts in the regeneration of native tree species in the Atlantic Forest region (Cesar et al., 2018; Amazonas et al., 2018). The structure of intensively managed, monoculture eucalypt plantations was, however, markedly different from the other forest cover types, without vegetation at low or medium vertical stratum. Although eucalypt plantations had a taller canopy, the LAHV (leaf area height volume) was higher in old-growth.

LAHV, a novel canopy structure metric presented for the first time in this study, displayed promising results as a potential metric of qualifying forest cover and assess its functions. LAHV may be a powerful variable for generalist equations, since it included the LAD information in its computation. Many studies have already demonstrated the potential of canopy-derived metrics from lidar cloud to estimate

forest biomass (Longo et al., 2016; Mascaro & Asner, 2015). However, the relation between height and biomass is not always consistent. In our study, old- and second-growth forests (>100 and 20-40 years old, respectively) presented different relationships than the restoration plantation/biomass experiment (13 years old) (see Figure 4).

Other variables also showed significant relationships with AGB. For airborne lidar data, the canopy openness was an important metric for estimating AGB and assessing canopy dynamics (Mascaro & Asner, 2015; Leitold et al., 2018). Airborne lidar has the potential to measure the canopy structure continuously, on a fine scale and in large areas (millions of hectares). The spatial information provided by the Airborne lidar may also improve the classification accuracy of the forest cover types from the information of neighboring pixels.

Our results highlight the need to consider different models to estimate AGB in the context of FLR, particularly for the species-rich, structurally complex forests found in tropical regions. We chose to use site and taxa specific AGB allometries in this study because universal relationships (e.g., Chave et al., 2014) may have likely lower accuracy. Likewise, the relationship between AGB and canopy structural characteristics is a function of the specific architectures and allometries that relate leaf area and its vertical positions to basal area, wood volume, and with wood density biomass (Stark et al., 2015). Species and taxonomic differences cannot be completely factored out to produce accurate AGB estimates from lidar, and field inventory approaches can never completely fulfill the needs of forest restoration monitoring alone. Taxonomic and functional information, particularly wood density, improves AGB estimates. These factors may have contributed to our finding that different forest cover types were best predicted by separate metrics and equations. Still, we note that a combined model of canopy height and LAHV were able to predict over 80 % of estimated biomass differences over these heterogeneous forests, suggesting that forest architectural rules have a great capacity to unify estimation over vegetation types.

The estimation of tree diversity is one of the greatest challenges of remote sensing (Turner et al., 2003; Bergen et al., 2009; Simonson et al., 2015). Some studies have linked tree diversity with vegetation structure in temperate forests (Bergen et al., 2009), and the combination of lidar and hyperspectral data has shown promising results towards this objective (Asner et al., 2015). We found a nonlinear

relation between the canopy Shannon index and the Shannon index of tree species diversity, which increases with both richness and equitability, representing vertical positions occupied by leaf area and evenness in the LAD over these positions. Therefore, we expected a positive relationship between species and canopy Shannon index, since the occupancy of more strata could indicate a diversity of growth rates, or maximum heights, or shade tolerance. Richness *per se* was not related to canopy diversity independently. Additional work is required, encompassing a broader range of diversity, to validate this relationship, explore evenness and richness independently, and investigate potential mechanistic relationships driving the interaction between tree diversity and canopy structure (Sapijanskas et al., 2014; Williams et al., 2017).

Qualitative as well as quantitative indicators of forest recovery are needed to support policies that successfully protect, sustain, and recover forests at multiple scales and for different objectives (Chazdon et al., 2016). Our results may help to understand patterns of carbon recovery in restoration contexts, although we found a limited potential of lidar to estimate tree diversity. This is noteworthy given the growing global interest in FLR and the need for the associated services that forests could provide to mitigate climate changes (Grassi et al., 2017; Griscom et al., 2017). Current ambitious restoration goals require the combination of different methodological approaches being implemented under strong financial constraints. To address this challenge, cost-efficient solutions must be developed for monitoring restoration at large spatial and temporal scales, and at lower costs, to help FLR programs. One possibility is to expand terrestrial lidar monitoring. However, to achieve rapid and broad geographic scopes, airborne lidar may be best. Here, we provide insights for the further adoption and application of PCL as a powerful complementary data stream to improve understanding of the consequences of restoration for carbon stocks and forest services, which could be further developed with airborne lidar (Stark et al., 2012).

The PCL beam has an oval footprint that samples about 4% and 11% of each 1 m deep (across-track) voxel at 5 m and 25 m in canopy height, respectively. The minimum number of PCL transects needed to characterize a sample plot depends of the forest structure, such the width of treetops. For instance, in the eucalyptus plantation, where width of treetops was smaller than others forest cover types, we used an 8-m-wide plot, whereas for the old- and second-grow canopy forest types we

used a 20-m wide plot. Also, for the high diversity plantation canopy forest type, we used two equidistant transects to cover a plot of 48-m-wide. Other studies used PCL in 20-m-wide plots in the Amazon rainforest and obtained satisfactory results (Almeida et al., 2016; Stark et al., 2012). However, regardless of plot size a reasonable number of sub-samples (columns of voxels) must be collected for feasible estimates of LAD and canopy openness.

Lidar data can likely bring additional insight to monitoring recovery of forest functionality at large-scales in the future. Stark et al. (2015) used vegetation profiles to estimate the demographic distribution of trees, which is key to know the successional stage of the forest. In addition, lidar data, when collected on airborne platforms, enables the preparation of digital terrain models with high accuracy (Leitold et al., 2015), useful for the planning of restoration projects (Schulz et al. 2016). Although we use a portable profiling system, all the canopy structural attributes used in this study can also be estimated using an airborne system (Stark et al., 2012; Almeida et al., *in press*).

Our study provides insights to monitoring forest restoration outcomes beyond those available from forest cover extent or gain, in a more integrated approach including indicators of diversity and potentially of ecosystem functions. Even though we evaluated these outcomes at a local scale, our results may significantly contribute to the discussion at landscape scale regarding the need of FLR needs to include the full heterogeneous mosaic of forest cover types expected. For example, assessing potential relationships between different forest types and tree diversity (i.e. beta diversity) and forest structure at landscape scales may prove challenging, but nevertheless is a promising avenue. The effective monitoring of FLR programs is not only important for accountability and tracking progress towards national, regional, and international restoration commitments, it is also a key step to improve current restoration approaches and to develop novel methods that are better suited for the different socio-ecological conditions in which FLR will be implemented. Our results can help address realistic restoration goals and actions in the context of global change.

4.5. Conclusion

Lidar-derived structural variables performed well for discriminating forest cover types. Canopy height, rugosity and openness were the most useful attributes. Leaf area height volume (LAHV) was of low value for classification but improved estimation of biomass. The structural attribute “canopy Shannon Index”, which was tested as the single predictor of tree diversity, proved to be of limited value for this purpose. Combining classification outputs with the canopy Shannon Index would, however, improve biodiversity estimation as the low diversity monoculture was identified with 100% accuracy. We have shown lidar to be a promising tool for monitoring multiple of forest restoration project objective outcomes, beyond a simple binary classification of forest cover. Further evaluation is recommended as the next step, including a broader range of cover types and ages.

4.6. Supplementary material

Absolute and relative Root Mean Square Error (RMSE) were computed according with the equation below:

$$RMSE\ (Mg \cdot ha^{-1}) = \sqrt{\sum_{i=1}^{n}(y_i - \hat{y}_i)^2 / n} \qquad \text{(Eq.S1)}$$

$$RMSE\ (\%) = 100 * \frac{RMSE\ (Mg \cdot ha^{-1})}{\bar{y}} \qquad \text{(Eq.S2)}$$

Where n is the number of observations, y_i is the observed aboveground biomass value for plot *i*, and $\hat{y}_i$ is the predicted aboveground biomass value for plot i and $\bar{y}$ is the average of the observed aboveground biomass values.

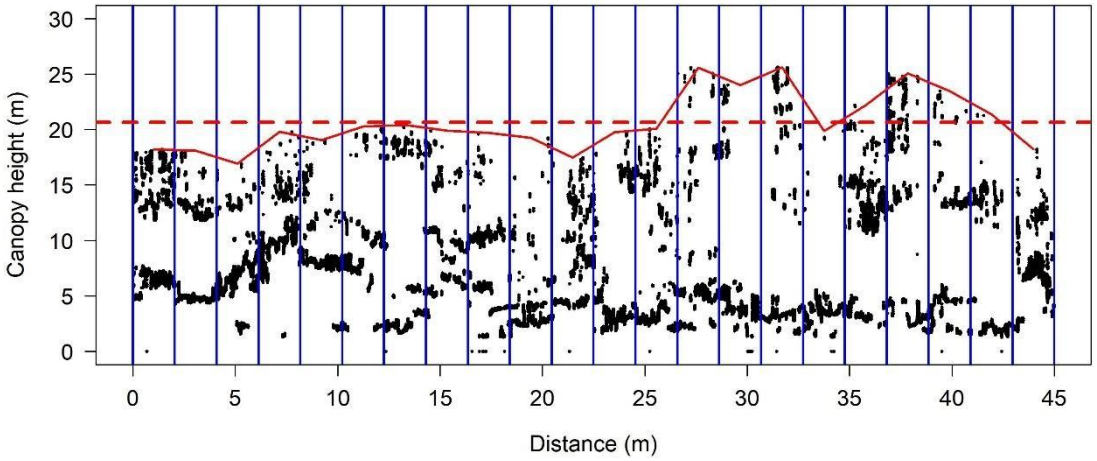

Figure S1. Example of a transect of PCL data (from an Old-growth forest). Division of data into columns two meters long (vertical blue lines), the maximum points in each column (red solid line) and its average (red dashed horizontal line), which corresponds to canopy height attribute. The canopy rugosity attribute is the standard deviation of the maximum points. The attribute of canopy openness is the fraction of columns where the maximum point is less than 10 meters in height. In this example, since there are no columns with a maximum height lower than the 10-meter threshold, the canopy opening fraction is equal to zero (0/22 columns).

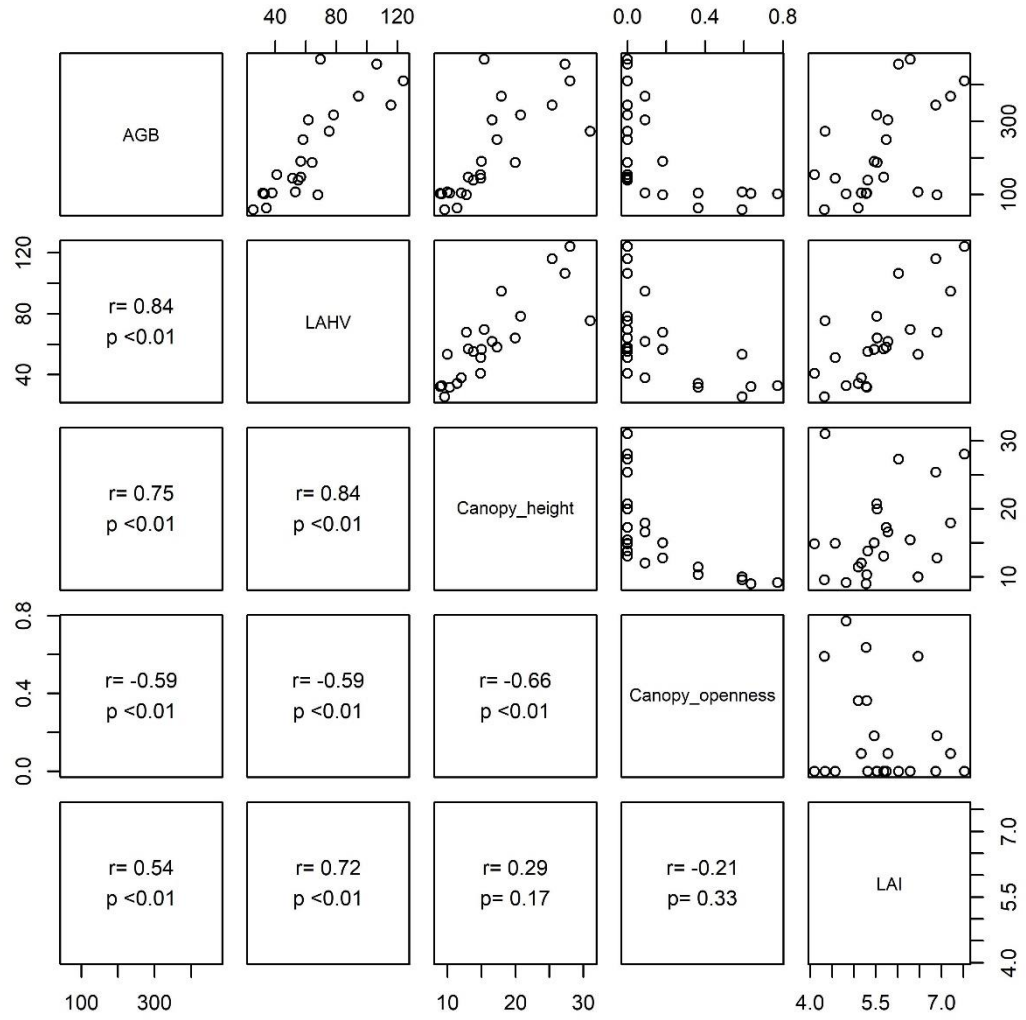

Figure S2. Correlogram between AGB and the structural attributes of the canopy (derived from lidar) in Corumbataí study area with "Old-growth", "SGeuc" and "SGpas" typologies using Pearson correlation.

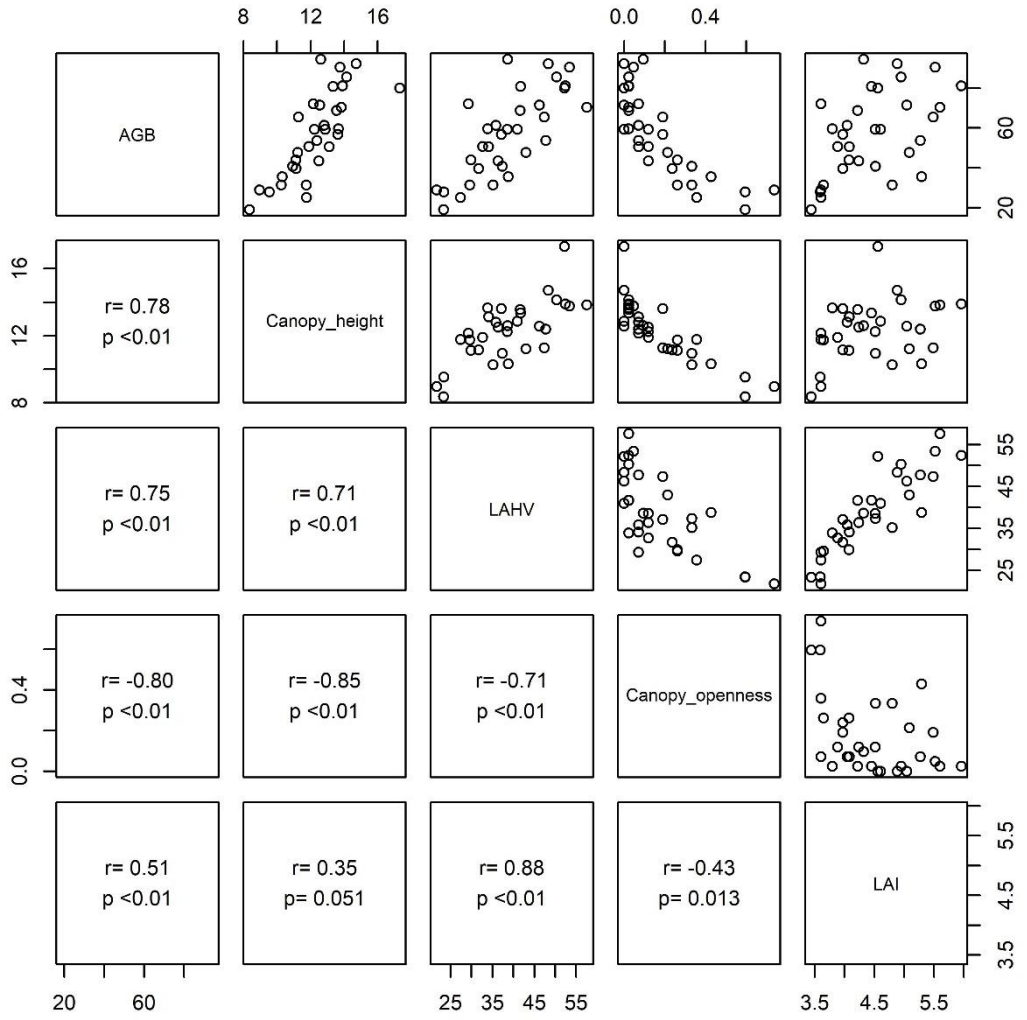

Figure S3. Correlogram between AGB and the structural attributes of the canopy (derived from the lidar) in the forest restoration plantation with biomass gradient, using the Pearson correlation.

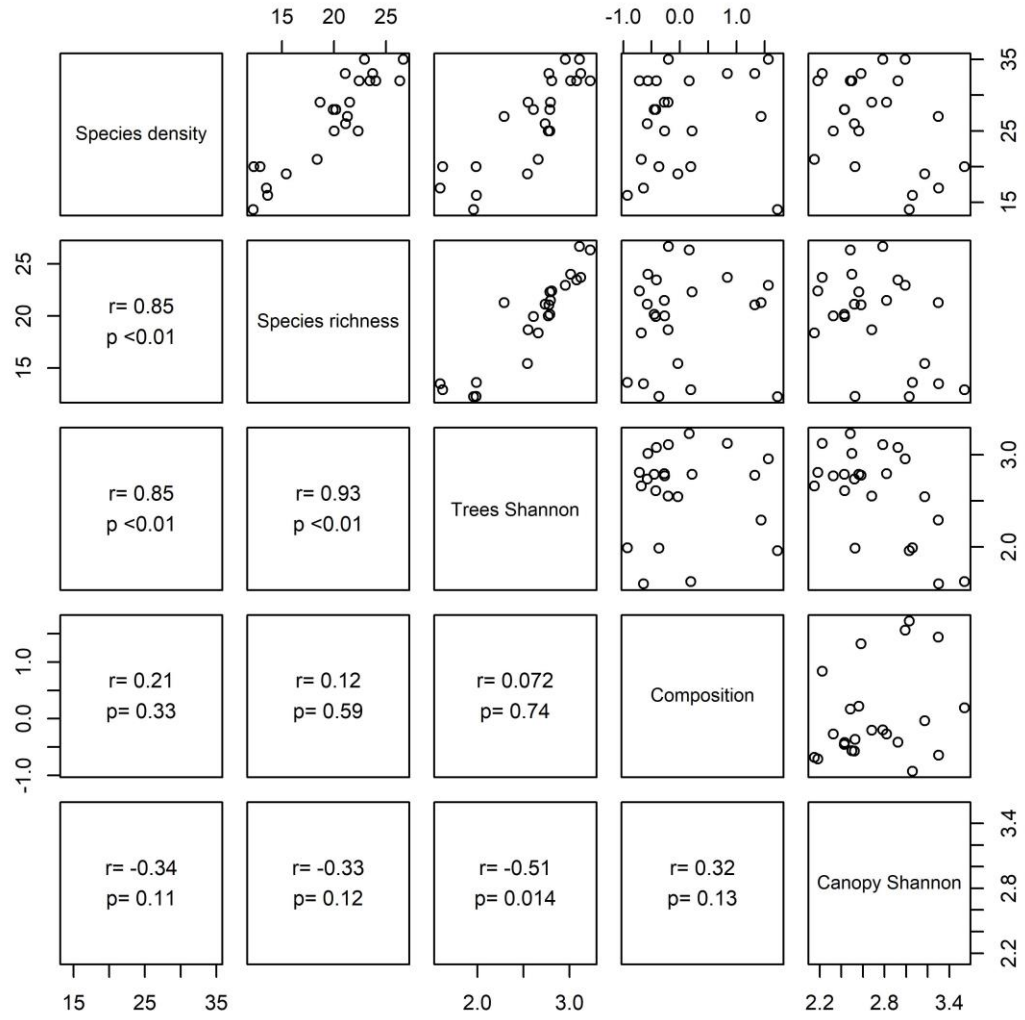

Figure S4. Correlation between the tree species diversity variables (Species density, Richness, Shannon index and composition dissimilarity) and the structural attribute Canopy Shannon index (lidar-derived) in the Corumbataí study area with the "Old-growth", "SGeuc" and "SGpas" using the Spearman correlation.

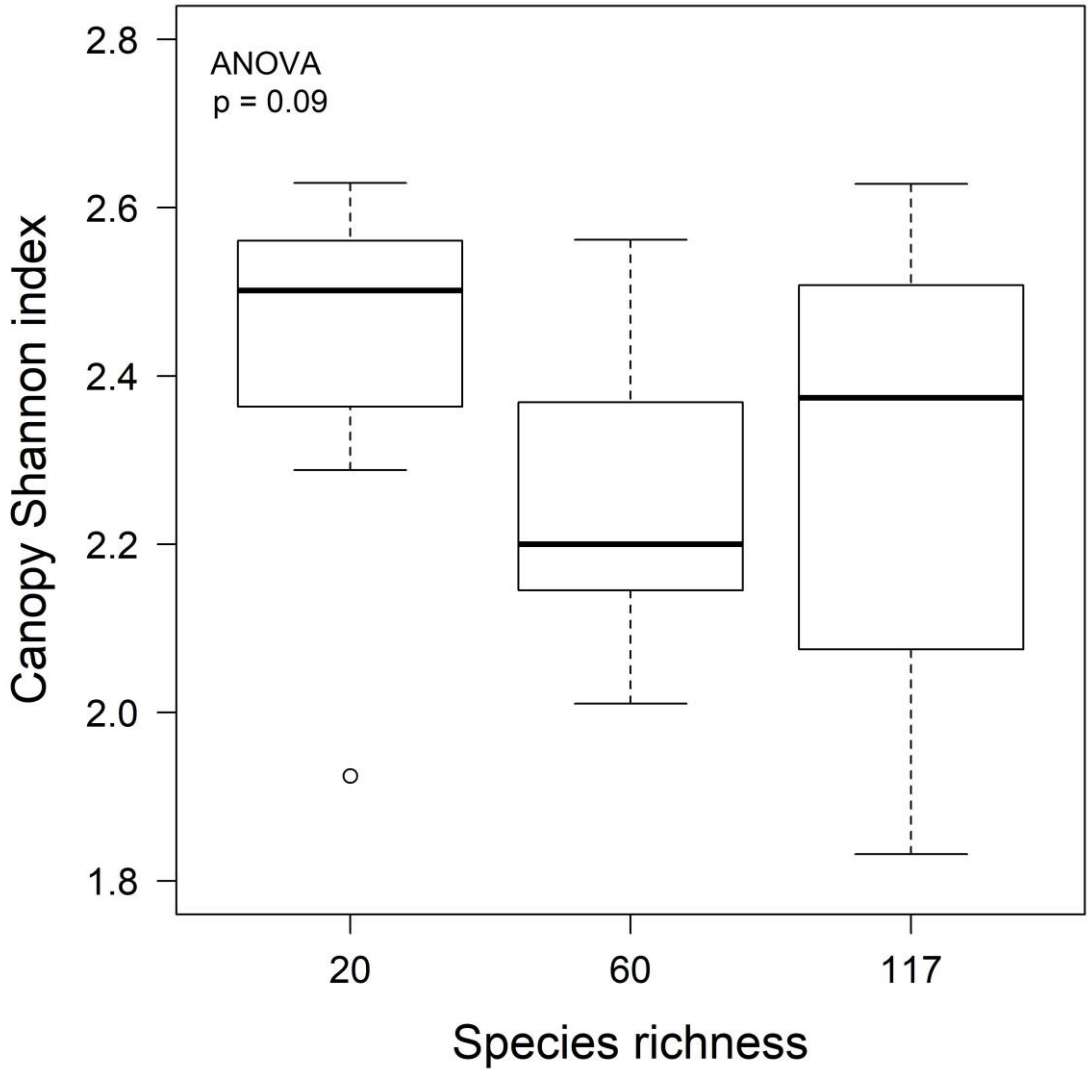

Figure S5. Canopy Shannon index for different richness levels in the restoration plantation with species richness gradient ("PLdiv" forest cover type).

References

Abshire, J. B., Sun, X., Riris, H., Sirota, J. M., McGarry, J. F., Palm, S., … Liiva, P. (2005). Geoscience Laser Altimeter System (GLAS) on the ICESat mission: On-orbit measurement performance. Geophysical Research Letters, 32(21), 1–4. doi:10.1029/2005GL024028

AICHI TARGETS. Link: https://www.cbd.int/sp/targets/. Acceded em 21/05/2018.

Alexander, S., Nelson, C. R., Aronson, J., Lamb, D., Cliquet, A., Erwin, K. L., … Murcia, C. (2011). Opportunities and Challenges for Ecological Restoration within REDD+. Restoration Ecology. doi:10.1111/j.1526-100X.2011.00822.x

Almeida, D. R. A. de, Nelson, B. W., Schietti, J., Gorgens, E. B., Resende, A. F., Stark, S. C., & Valbuena, R. (2016). Contrasting fire damage and fire susceptibility between seasonally flooded forest and upland forest in the Central Amazon using portable profiling LiDAR. Remote Sensing of Environment, 184, 153–160. doi:10.1016/j.rse.2016.06.017

Alvares, C. A., Stape, J. L., Sentelhas, P. C., De Moraes Gonçalves, J. L., & Sparovek, G. (2013). Köppen's climate classification map for Brazil. Meteorologische Zeitschrift. doi:10.1127/0941-2948/2013/0507

Amazonas, N. T., Forrester, D. I., Silva, C. C., Almeida, D. R. A., Rodrigues, R. R., & Brancalion, P. H. S. (2018). High diversity mixed plantations of Eucalyptus and native trees: An interface between production and restoration for the tropics. Forest Ecology and Management, 417, 247–256. doi:10.1016/j.foreco.2018.03.015

Aronson, J., Blignaut, J. N., & Aronson, T. B. (2017). Conceptual Frameworks and References for Landscape-scale Restoration: Reflecting Back and Looking Forward ,. Annals of the Missouri Botanical Garden, 102(2), 188–200. doi:10.3417/2017003

Asner, G. P., Mascaro, J., Muller-Landau, H. C., Vieilledent, G., Vaudry, R., Rasamoelina, M., ... & Van Breugel, M. (2012). A universal airborne LiDAR approach for tropical forest carbon mapping. Oecologia, 168(4), 1147-1160. doi: 10.1007/s00442-011-2165-z

Asner, G. P., & Mascaro, J. (2014). Mapping tropical forest carbon: Calibrating plot estimates to a simple LiDAR metric. Remote Sensing of Environment, 140, 614–624. doi:10.1016/j.rse.2013.09.023

Asner, G. P., Ustin, S. L., Townsend, P. A., Martin, R. E., & Chadwick, K. D. (2015). Forest biophysical and biochemical properties from hyperspectral and LiDAR remote sensing. Land Resources Monitoring, Modeling and Mapping with Remote Sensing. CRC Press, Taylor & Francis Group, 429–448.

Becknell, J. M., Keller, M., Piotto, D., Longo, M., Nara dos-Santos, M., Scaranello, M. A., … Porder, S. (2018). Landscape-scale lidar analysis of aboveground biomass distribution in secondary Brazilian Atlantic Forest. Biotropica. doi:10.1111/btp.12538

Bergen, K. M., Goetz, S. J., Dubayah, R. O., Henebry, G. M., Hunsaker, C. T., Imhoff, M. L., … Radeloff, V. C. (2009). Remote sensing of vegetation 3-D structure for biodiversity and habitat: Review and implications for lidar and radar spaceborne missions. Journal of Geophysical Research: Biogeosciences. doi:10.1029/2008JG000883

Bonn Challenge. Link: http://www.bonnchallenge.org/. Acceded in 21/05/2018

Bonner, M. T. L., Schmidt, S., & Shoo, L. P. (2013). A meta-analytical global comparison of aboveground biomass accumulation between tropical secondary forests and monoculture plantations. Forest Ecology and Management, 291, 73–86. doi:10.1016/j.foreco.2012.11.024

Brancalion, P. H. S., & Chazdon, R. L. (2017). Beyond hectares: four principles to guide reforestation in the context of tropical forest and landscape restoration. Restoration Ecology. doi:10.1111/rec.12519

Brancalion, P. H. S., Schweizer, D., Gaudare, U., Mangueira, J. R., Lamonato, F., Farah, F. T., … Rodrigues, R. R. (2016). Balancing economic costs and ecological outcomes of passive and active restoration in agricultural landscapes: the case of Brazil. Biotropica, 48(6), 856–867. doi:10.1111/btp.12383

Brancalion, P. H. S., Viani, R. A. G., Calmon, M., Carrascosa, H., & Rodrigues, R. R. (2013). How to Organize a Large-Scale Ecological Restoration Program? The Framework Developed by the Atlantic Forest Restoration Pact in Brazil. Journal of Sustainable Forestry, 32(7), 728–744. doi:10.1080/10549811.2013.817339

Campoe, O. C., Iannelli, C., Stape, J. L., Cook, R. L., Mendes, J. C. T., & Vivian, R. (2014). Atlantic forest tree species responses to silvicultural practices in a degraded pasture restoration plantation: From leaf physiology to survival and initial growth. Forest Ecology and Management. doi:10.1016/j.foreco.2013.11.016

Campos, J. C. C., J. A. Silva, and B. R. Vital. 1992. Volume e biomassa do tronco e da copa de eucalipto de grande porte. Revista Árvore 16:319–336.

Cao, S., Sanchez-Azofeifa, G. A., Duran, S. M., & Calvo-Rodriguez, S. (2016). Estimation of aboveground net primary productivity in secondary tropical dry forests using the Carnegie-Ames-Stanford approach (CASA) model. Environmental Research Letters, 11(7). doi:10.1088/1748-9326/11/7/075004

César, R. G., Moreno, V. S., Coletta, G. D., Chazdon, R. L., Ferraz, S. F. B., De Almeida, D. R. A., & Brancalion, P. H. S. (2018). Early ecological outcomes of natural regeneration and tree plantations for restoring agricultural landscapes. Ecological Applications, 28(2). doi:10.1002/eap.1653

Chave, J., Réjou-Méchain, M., Búrquez, A., Chidumayo, E., Colgan, M. S., Delitti, W. B. C., … Vieilledent, G. (2014). Improved allometric models to estimate the aboveground biomass of tropical trees. Global Change Biology, 20(10), 3177–3190. doi:10.1111/gcb.12629

Chaves, R. B., Durigan, G., Brancalion, P. H. S., & Aronson, J. (2015). On the need of legal frameworks for assessing restoration projects success: new perspectives from São Paulo state (Brazil). Restoration Ecology. doi:10.1111/rec.12267

Chazdon, R. L. (2014). Second Growth: The Promise of Tropical Forest Regeneration in an Age of Deforestation. Journal of Chemical Information and Modeling. doi:10.1017/CBO9781107415324.004

Chazdon, R. L., Brancalion, P. H. S., Laestadius, L., Bennett-Curry, A., Buckingham, K., Kumar, C., … Wilson, S. J. (2016). When is a forest a forest? Forest concepts and definitions in the era of forest and landscape restoration. Ambio, 45(5), 538–550. doi:10.1007/s13280-016-0772-y

Chazdon, R. L., Brancalion, P. H. S., Lamb, D., Laestadius, L., Calmon, M., & Kumar, C. (2017). A Policy-Driven Knowledge Agenda for Global Forest and Landscape Restoration. Conservation Letters, 10(1), 125–132. doi:10.1111/conl.12220

del Castillo, E. G., Sanchez-Azofeifa, A., Gamon, J. A., Avendaño, M. Q., & others. (2018). Integrating proximal broad-band vegetation indices and carbon fluxes to model gross primary productivity in a tropical dry forest. Environmental Research Letters. doi: 10.1088/1748-9326/aac3f0

Don, A., Schumacher, J., & Freibauer, A. (2011). Impact of tropical land-use change on soil organic carbon stocks - a meta-analysis. Global Change Biology. doi:10.1111/j.1365-2486.2010.02336.x

Evans, K., Guariguata, M. R., & Brancalion, P. H. S. (2018). Participatory monitoring to connect local and global priorities for forest restoration. Conservation Biology. doi:10.1111/cobi.13110

Ferez, A. P. C., Campoe, O. C., Mendes, J. C. T., & Stape, J. L. (2015). Silvicultural opportunities for increasing carbon stock in restoration of Atlantic forests in Brazil. Forest Ecology and Management, 350, 40-45. doi: 10.1016/j.foreco.2015.04.015

FLR. Link: http://www.forestlandscaperestoration.org/. Acceded in 21/05/2018

Grassi, G., House, J., Dentener, F., Federici, S., Den Elzen, M., & Penman, J. (2017). The key role of forests in meeting climate targets requires science for credible mitigation. Nature Climate Change. doi:10.1038/nclimate3227

Griscom, B. W., Adams, J., Ellis, P. W., Houghton, R. A., Lomax, G., Miteva, D. A., … Fargione, J. (2017). Natural climate solutions. Proceedings of the National Academy of Sciences. doi:10.1073/pnas.1710465114

GEDI. https://science.nasa.gov/missions/gedi. Acceded in 05/25/2018.

Görgens, E. B., Soares, C. P. B., Nunes, M. H., & Rodriguez, L. C. E. (2016). Characterization of Brazilian forest types utilizing canopy height profiles derived from airborne laser scanning. Applied Vegetation Science, 19(3), 518–527. doi:10.1111/avsc.12224

Hardiman, B. S., Bohrer, G., Gough, C. M., Vogel, C. S., & Curtis, P. S. (2011). The role of canopy structural complexity in wood net primary production of a maturing northern deciduous forest. Ecology, 92(9), 1818–1827. doi:10.1890/10-2192.1

Hardiman, B. S., Gough, C. M., Halperin, A., Hofmeister, K. L., Nave, L. E., Bohrer, G., & Curtis, P. S. (2013). Maintaining high rates of carbon storage in old forests: A mechanism linking canopy structure to forest function. Forest Ecology and Management. doi:10.1016/j.foreco.2013.02.031

Helmer, E. H., Lefsky, M. A., & Roberts, D. A. (2009). Biomass accumulation rates of Amazonian secondary forest and biomass of old-growth forests from Landsat time series and the Geoscience Laser Altimeter System. Journal of Applied Remote Sensing, 3(1), 33505. doi:https://doi.org/10.1117/1.3082116

Holl, K. D., & Cairns, J. (2002). Monitoring and appraisal. In: M. R. Perrow, & A. J. Davy (Eds.). Handbook of ecological restoration (pp. 411–432). Cambridge, England: Cambridge University Press.

Holl, K. D. (2017). Restoring tropical forests from the bottom up. Science. doi:10.1126/science.aam5432

IBEMA. https://www.funcate.org.br/msa/projetos/mudanca-de-uso-da-terra. Acceded in 05/25/2018.

Laestadius, L., Buckingham, K., Maginnis, S., & Saint-Laurent, C. (2015). Back to Bonn and beyond: A history of forest landscape restoration and an outlook for the future. Unasylva, 245, 11–18.

Lefsky, M. A., Cohen, W. B., Parker, G. G., & Harding, D. J. (2002). Lidar remote sensing for ecosystem studies. BioScience, 52(1), 19–30. doi:10.1641/0006-3568(2002)052[0019:LRSFES]2.0.CO;2

Leitold, V., Michael Keller, Douglas C Morton, Bruce D Cook, & Yosio E Shimabukuro. (2014). Airborne lidar-based estimates of tropical forest structure in complex terrain: Opportunities and trade-offs for REDD+. Carbon Balance and Management, 10(1). doi:10.1186/s13021-015-0013-x

Longo, M., Keller, M., dos-Santos, M. N., Leitold, V., Pinagé, E. R., Baccini, A., … Morton, D. C. (2016). Aboveground biomass variability across intact and degraded forests in the Brazilian Amazon. Global Biogeochemical Cycles, 30(11), 1639–1660. doi:10.1002/2016GB005465

McArthur, R.H. & McArthur, J.W. (1961). On bird species diversity. Ecology 42, 594–598.

McDonnell, M. J. (1986). Old field Vegetation Height and the Dispersal Pattern of Bird-Disseminated Woody Plants. Bulletin of the Torrey Botanical Club, 113(1), 6. doi:10.2307/2996227

Mascaro, J., Asner, G. P., Dent, D. H., DeWalt, S. J., & Denslow, J. S. (2012). Scale-dependence of aboveground carbon accumulation in secondary forests of Panama: A test of the intermediate peak hypothesis. Forest Ecology and Management, 276, 62–70. doi:10.1016/j.foreco.2012.03.032

Meli, P., Holl, K. D., Benayas, J. M. R., Jones, H. P., Jones, P. C., Montoya, D., & Mateos, D. M. (2017). A global review of past land use, climate, and active vs. passive restoration effects on forest recovery. PLoS ONE. doi:10.1371/journal.pone.0171368

Menz, M. H. M., Dixon, K. W., & Hobbs, R. J. (2013). Hurdles and opportunities for landscape-scale restoration. Science. doi:10.1126/science.1228334

Pistorius, T., & Freiberg, H. (2014). From target to implementation: Perspectives for the international governance of forest landscape restoration. Forests, 5(3), 482–497. doi:10.3390/f5030482

Saatchi, S. S., Harris, N. L., Brown, S., Lefsky, M., Mitchard, E. T. A., Salas, W., … Morel, A. (2011). Benchmark map of forest carbon stocks in tropical regions across three continents. Proceedings of the National Academy of Sciences, 108(24), 9899–9904. doi:10.1073/pnas.1019576108

Sabogal, C., Besacier, C., & McGuire, D. (2015). Forest and landscape restoration: concepts, approaches and challenges for implementation. Unasylva, 66(245), 3.

Sapijanskas, J., Paquette, A., Potvin, C., Kunert, N., & Loreau, M. (2014). Tropical tree diversity enhances light capture through crown plasticity and spatial and temporal niche differences. Ecology. doi:10.1890/13-1366.1

Schulz, J. J., & Schröder, B. (2017). Identifying suitable multifunctional restoration areas for Forest Landscape Restoration in Central Chile. Ecosphere, 8(1). doi: 10.1002/ecs2.1644

Silva, C. A., Hudak, A. T., Vierling, L. A., Klauberg, C., Garcia, M., Ferraz, A., … Saatchi, S. (2017). Impacts of airborne lidar pulse density on estimating biomass stocks and changes in a selectively logged tropical forest. Remote Sensing, 9(10). doi:10.3390/rs9101068

Simonson, W. D., Allen, H. D., & Coomes, D. A. (2014). Applications of airborne lidar for the assessment of animal species diversity. Methods in Ecology and Evolution. doi:10.1111/2041-210X.12219

Souza Jr, C. M., Siqueira, J. V., Sales, M. H., Fonseca, A. V., Ribeiro, J. G., Numata, I., ... & Barlow, J. (2013). Ten-year Landsat classification of deforestation and forest degradation in the Brazilian Amazon. Remote Sensing, 5(11), 5493-5513. doi:10.3390/rs5115493

Stanturf, J. A., Palik, B. J., & Dumroese, R. K. (2014). Contemporary forest restoration: A review emphasizing function. Forest Ecology and Management. doi:10.1016/j.foreco.2014.07.029

Suding, K., Higgs, E., Palmer, M., Callicott, J. B., Anderson, C. B., Baker, M., … Schwartz, K. Z. S. (2015). Committing to ecological restoration. Science, 348(6235), 638–640. doi:10.1126/science.aaa4216

Tang, H., Dubayah, R., Swatantran, A., Hofton, M., Sheldon, S., Clark, D. B., & Blair, B. (2012). Retrieval of vertical LAI profiles over tropical rain forests using waveform lidar at la selva, costa rica. Remote Sensing of Environment, 124, 242–250. doi:10.1016/j.rse.2012.05.005

Tilley, B. K., Munn, I. A., Evans, D. L., Parker, R. C., & Roberts, S. D. (2005). Cost considerations of using LiDAR for timber inventory. The 2004 Annual Southern Forest Economics Workshop., 43–50. Retrieved from http://sofew.cfr.msstate.edu/papers/0504tilley.pdf

Turner, W., Spector, S., Gardiner, N., Fladeland, M., Sterling, E., & Steininger, M. (2003). Remote sensing for biodiversity science and conservation. Trends in Ecology and Evolution. doi:10.1016/S0169-5347(03)00070-3

Valbuena, R., Packalén, P., Martín-Fernández, S., & Maltamo, M. (2012). Diversity and equitability ordering profiles applied to study forest structure. Forest Ecology and Management 276(0): 185–195. doi:10.1016/j.foreco.2012.03.036.

Valbuena R., Packalen P., García-Abril A., Mehtätalo L. & Maltamo M. (2013) Characterizing Forest Structural Types and Shelterwood Dynamics from Lorenz-based Indicators Predicted by Airborne Laser Scanning. Canadian Journal of Forest Research 43: 1063-1074. doi: 10.1139/cjfr-2013-0147

Valbuena R., Maltamo M. & Packalen P. (2016a) Classification of Multi-Layered Forest Development Classes from Low-Density National Airborne Lidar Datasets. Forestry 89: 392-341. doi: 10.1093/forestry/cpw010

Valbuena R., Eerikäinen K., Packalen P. & Maltamo M. (2016b) Gini Coefficient Predictions from Airborne Lidar Remote Sensing Display the Effect of Management Intensity on Forest Structure. Ecological Indicators 60: 574-585. doi: 10.1016/j.ecolind.2015.08.001

Viani, R. A., Holl, K. D., Padovezi, A., Strassburg, B. B., Farah, F. T., Garcia, L. C., ... & Brancalion, P. H. (2017). Protocol for monitoring tropical forest restoration: perspectives from the Atlantic forest restoration pact in Brazil. Tropical Conservation Science, 10. doi: 10.1177/1940082917697265.

West, G. B., Brown, J. H., & Enquist, B. J. (1997). A general model for the origin of allometric scaling laws in biology. Science. doi:10.1126/science.276.5309.122

Williams, L. J., Paquette, A., Cavender-Bares, J., Messier, C., & Reich, P. B. (2017). Spatial complementarity in tree crowns explains overyielding in species mixtures. Nature Ecology and Evolution. doi:10.1038/s41559-016-0063

WRI, 2018. Initiative 20x20. World Resources Institute. http://www.wri.org/our-work/project/initiative-20x20/about-initiative-20x20#project-tabs. Acceded in 05/28/2018.

Zahawi, R. A., Dandois, J. P., Holl, K. D., Nadwodny, D., Reid, J. L., & Ellis, E. C. (2015). Using lightweight unmanned aerial vehicles to monitor tropical forest recovery. Biological Conservation, 186, 287–295. doi:10.1016/j.biocon.2015.03.031

5. MONITORING THE STRUCTURE OF FOREST RESTORATION PLANTATIONS WITH A DRONE-LIDAR SYSTEM

ABSTRACT

We are living a unprecedented moment for promoting forest restoration globally, with international and regional pledges to restore at least 350 million hectares by 2030. To achieve these ambitious goals, it is necessary to develop cost-effective technologies to monitor the structure and functions of restored forests at much broader scales, going beyond the traditional plot-scale assessments. Light detection and ranging (lidar) is a remote sensing technology that has proven to be effective for continuous and broad-scale forest measurements, yet its application to tropical forest restoration remains poorly explored. The use of lidar in unmanned aerial vehicle (UAV) platforms have the potential to be an agile and autonomous method for monitoring forest restoration projects and support decision making, especially in conditions and scales were using an airplane-borne lidar system is not financially viable. Here, we explored the potential of an UAV-borne lidar system to assess the outcomes of a mixed-species restoration plantation experiment designed to maximize aboveground biomass (AGB) accumulation. The experiment was established in Brazil's Atlantic Forest with 20 native tree species, by combining two levels of planting density (high and low, 3,333 and 1,667 plants ha^{-1}, respectively) and two management levels (usual and intensive), totaling four treatments and a control (plots left over for natural regeneration). We analyzed three structural variables from lidar (canopy height, gap fraction and leaf area index) and one from field inventory (AGB). Structural differences between the treatments and the control plots were reliably distinguished by the UAV-borne lidar system. AGB was strongly correlated with canopy height, allowing the elaboration of a prediction equation to use the UAV-borne lidar system for monitoring other restoration plantations in the region. Both intensive weed management/fertilization and high seedling density planting maximized AGB accumulation, but the combination of these two silvicultural approaches did not result in higher AGB than that promoted by these approaches in separation. UAV-borne lidar systems showed enormous potential for monitoring large-scale forest restoration projects, being an important tool to aid decision making and accountability in forest landscape restoration.

Keywords: Drone; Atlantic Forest; Leaf area index; Leaf area density; Tropical forest restoration; Forest landscape restoration; Tropical silviculture; Aboveground biomass; Forest structure

5.1. Introduction

We are living in an unprecedented moment for promoting forest landscape restoration (FLR) globally, with international (see Bonn Challenge, 2018) and regional (see WRI, 2018) restoration pledges to restore at least 350 million hectares by 2030 of degraded and deforested lands (Suding et al., 2015). Achieving these pledges can result in diverse benefits to society, such as biodiversity conservation, climate change mitigation, watershed protection, soil recovery, and recreation (Chazdon et al., 2017). Although FLR has been promoted as a multipurpose activity,

its accountability is still limited to the simplistic quantification of how much land has been restored. It is timely and important to develop cost-effective innovations to monitore restoration functions at large scales, going beyond the quantification of forest areas and advancing in the direction of the qualification of forest attributes (Brancalion and Chazdon, 2017). Moreover, it is critical to assess the outcomes of different restoration approaches in order to disseminate best-practices and promote cost-efficient silvicultural solutions to overcome the ecological barriers for forest development in degraded site conditions (Holl. 2017; Brancalion and van Melis, 2017).

The restoration strategy used to restore a degraded site would depend on its past land-use history and levels of degradation and resilience (Holl and Aide 2011). In sites with lower degradation levels and thus higher resilience, the most cost-effective restoration strategy is usually the isolation of the site from disturbances for further natural regeneration (Chazdon and Guariguata, 2016). In sites with intermediate degradation level, natural regeneration may have to be assisted, such as through the control of lianas and ruderal plants, and enrichment planting (Brancalion et al., 2016). Finally, more degraded and less resilient sites may require more intense interventions (i.e., active restoration), which usually come in the form of a combination of soil preparation and fertilization, weed control, and tree seedling plantation or direct seeding to reoccupy the entire area with desired plant species (Molin et al., 2018). In active restoration, planting density, soil fertilization and weed control intensity may play a key role in the success and viability of forest restoration strategies (Campoe et al., 2010; Brancalion et al., in press). These decisions are critically important given the limited resources available for restoration and the challenge of reestablishing tropical forests in highly degraded sites (Rodrigues et al., 2011; Shoo et al., 2016).

In this context, monitoring both restoration outcomes and processes is crucial to better support the development of novel and more effective restoration strategies. Usually, monitoring forest restoration outcomes is done through field inventories evaluating forest structure parameters, such as canopy openness, tree diameter and height (which also allow biomass and carbon stock estimations), and diversity parameters (Ruiz-Jaen and Aide, 2005; Wortley et al., 2013; Viani et al., 2017). Aboveground biomass (AGB), in particular, is a critical variable measured in restoration projects as it express one of the most important restoration outcomes

targeted in tropical forest regions (i.e., climate change mitigation potential) (Griscom et al., 2017; Locatelli et al., 2015), and represents a good surrogate of many other indicators associated to tropical forest successional development (Chazdon, 2014; Lennox et al., 2018). In restoration plantations, canopy openness is a key ecological indicator as it is associated to the suppression of ruderal grasses and understory recolonization by shade-tolerant, late-successional species that are essential for tropical forest development (Viani et al., 2017).

Monitoring forest structure through field inventories at large spatial scales is economically and operationally limited. Current active remote sensing technologies such as lidar (Light Detection and Ranging) have the potential to describe the three-dimensional forest structure, allowing the estimation of AGB and canopy openness for large areas (Longo et al., 2016; Leitold et al., 2018). Lidar has been increasingly used in forested areas (van Leeuwen & Nieuwenhuis, 2010), yet usually presents a high cost and dependence on companies owning airplanes to carry out data collection. Unmanned aerial vehicles (UAV, aka, drones) platforms represent a low-cost, agile, and autonomous opportunity for data collection in areas much larger than plots but at the same time not so large to justify data collection with airplane-borne systems. At present, the use of UAV for natural resource management is increasing (Shahbazi et al., 2014) and there are UAVs capable of carrying lidar systems (Sankey et al., 2017; GatorEye, 2018). However, little is known about the potential use of these new systems in the context of forest restoration projects and their efficiency in monitoring forest structure parameters in mixed-species plantations.

Here, we explored the potential of an UAV-borne lidar system to assess the outcomes of a mixed-species restoration plantation experiment designed to maximize AGB accumulation. We used the UAV-borne lidar system to quantify forest structure variables that are difficult to measure in forest inventories (eg., gap fraction, mean canopy height, leaf area index and leaf area density), and associated these variables with AGB stocks measured by field inventories to assess the reliability of using Lidar to monitor forest AGB in restoration plantations. In addition to compare different silvicultural treatments according to their impacts in the development of forest structured, we aimed to test the usefulness of an UAV-borne lidar system for monitoring forest landscape restoration projects at an appropriate scale, going beyond plot-scale measurements while also avoiding expensive, airplane-borne systems.

5.2. Material and methods

5.2.1. Study area and experimental design

The study was conducted at the Anhembi experimental station of forest sciences of the Luiz de Queiroz College of Agriculture, University of São Paulo (ESALQ/USP), located in southeastern Brazil (22° 43'S, 48° 11'W, 455 m above sea level of the sea and land slope <5%) (Figure 1). The climate is dry in the winter and humid in the summer with average annual precipitation of 1,300 mm (average of 48 mm per month in the dry period between April and September). The average annual temperature is 20.6° C with averages of 16.8° C in July and 23.5° C in February.

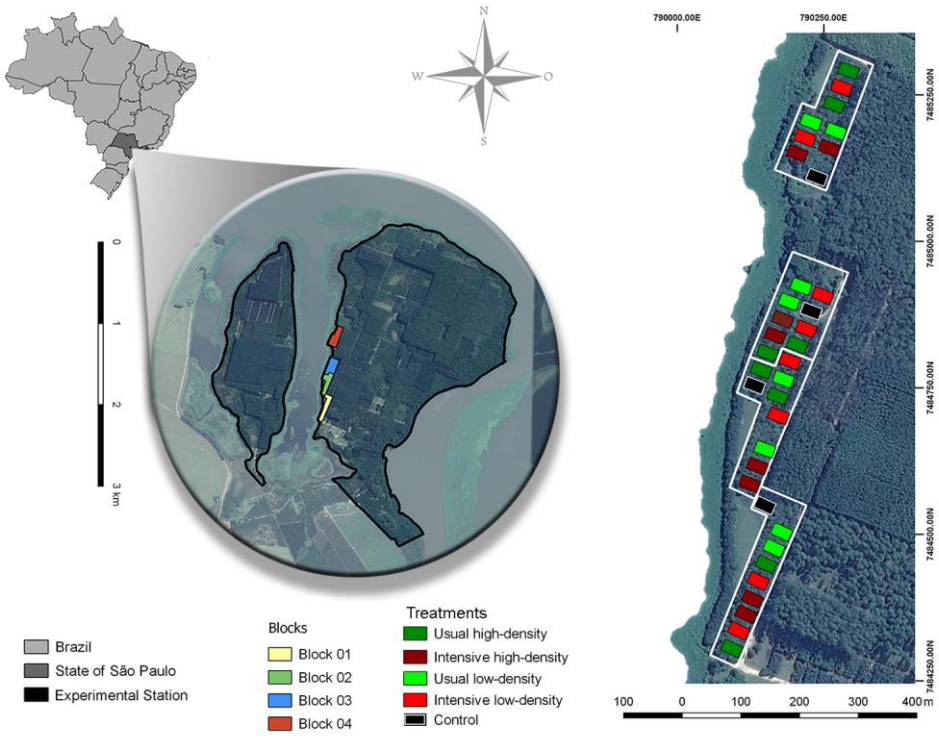

Figure 1. Study area and experimental blocks and plots where tree plantations were established according to different silvicultural management intensities to maximize aboveground biomass accumulation in the Atlantic Forest of Brazil.

In March 2004, a 3-level factorial design (2^3) experiment was established based on the following treatments and levels: (i) pioneer/non-pioneer species proportion (50:50 and 67:33), (ii) planting density, (1,667 and 3,333 individual.ha^{-1}), and (iii) silvicultural management intensity (traditional: mechanical mowing and moderate levels of fertilization, intensive: herbicide spraying and high levels of fertilization; see Campoe et al., 2010 and Brancalion et al., in press for more details).

We also included four control plots, fenced for livestock exclusion and without any tree planting or management activity. Since previous studies have not found a significant effect of the proportion of pioneers in AGB accumulation (Brancalion et al., in press), we did not consider this factor to increase the number of replicates in the others. By doing so, the experiment was assessed based on two factors (*i.e*., planting density and management intensity) with eight replicates each, and four replicates for control plots. The experiment was established with 20 native tree species in 42×30 m (1,260 m^2) plots (Figure 1), in an area previously occupied by a pasture of the African fodder grass *Urochloa decumbens* (Stapf) R.D. Webster, the most important weed species in the region (Brancalion et al., 2016).

5.2.2. Data collection

Twelve years after planting (2016), we measured tree height and diameter (0.3 m aboveground) for all trees within the effective area of each plot (36×22 m, 792 m^2), excluding border lines to avoid edge effects. Plot AGB was estimated based on an equation developed for this same experiment when it was five years old (Ferez et al., 2015), using wood density data obtained at the time of tree harvesting for the development of the equation. Fourteen years after planting (2018), we collected lidar data using a UAV platform (GatorEye Unmanned Flying Laboratory; Figure 2) at 60 m flying height aboveground and 10 $m.s^{-1}$ speed, with an approximate horizontal distance between adjacent flight lines of 50 meters, producing a lidar point cloud density of 193 returns m^{-2}.

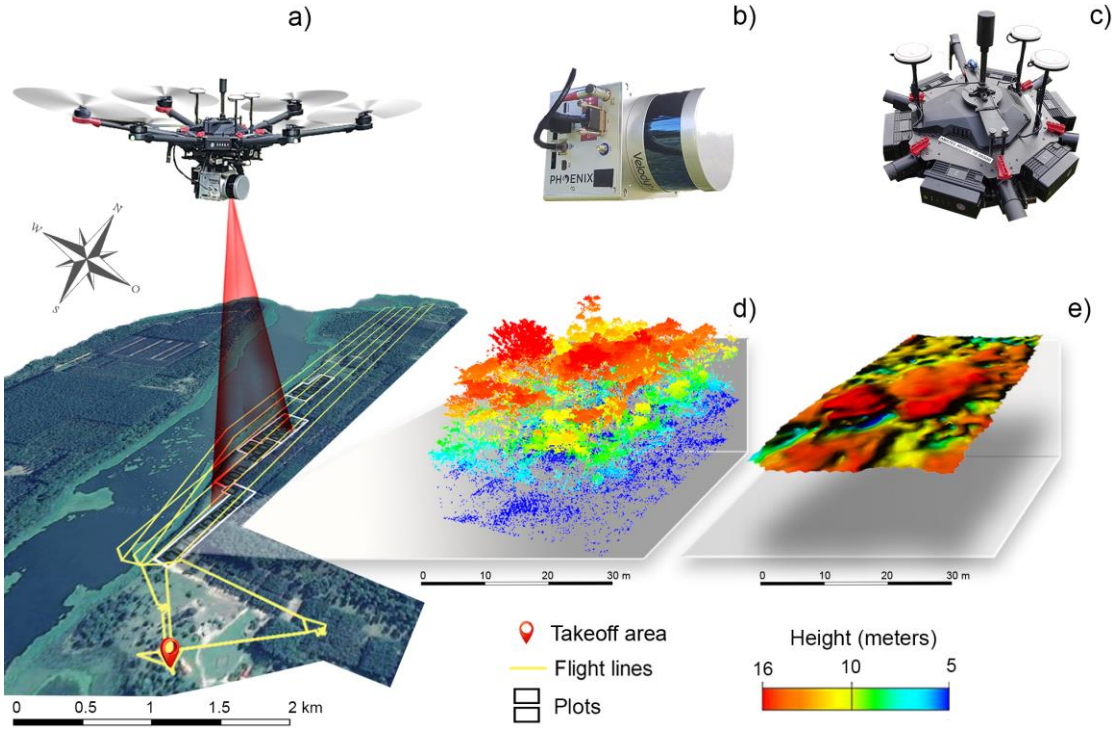

Figure 2. GatorEye system and data: (a) illustration of the unmanned aerial vehicle flying over the experimental sites; (b) lidar-hardware system; (c) georeference system; (d) cloud lidar data of one plot (treatment low-density intensive); (e) canopy height model of the plot.

The GatorEye system (www.gatoreye.org) includes a vertical takeoff and landing (VTOL) DJI Matrice 600 Pro hexacopter capable of 16-22 minutes flight times for smaller areas (<15 hectares per flight, and with five sets of batteries for multiple flights per day), and a 5 km telemetry/control range. The Phoenix LiDAR systems sensor suite consists of a Velodyne VLP-16 dual-return laser scanner head, capable of 600,000 returns per second with Phoenix live and post-processing software. The sensor is geolocated to ± 2.5 cm using a dual-frequency GNSS receiver and a tactical grade Inertial Measurement Unit (IMU) (STIM300), with geolocation data post-processed relative to a local base station (X900S-OPUS) using Novatel Inertial Explorer software. The location of the base station itself was determined using the online Trimble CenterPoint RTX post-processing platform for 8+ hours of combined location data collected over 2 days.

5.2.3. Data processing and analysis

Lidar data processing and analysis were performed in the R environment (R Core Team, 2017) using the software LAStools (Isenburg, 2018). First, from the raw 3D lidar point cloud, we classify the ground returns and generate the raster digital

terrain model (DTM) with 0.5 m resolution. Then, also from the raw lidar cloud, we performed a spurious-return filter and generated the raster digital surface model (DSM) with 0.5 m resolution. Finally, with DTM and DSM we removed the lower and upper spurious data from the raw lidar point cloud and generated the normalized lidar point cloud and the canopy height model (CHM) with a 0.5 m resolution. The CHM and the normalized point cloud were clipped from the polygons of the georeferenced field plots. We georeferenced the four corners of each rectangular plot in the field with a high-precision RTK GNSS system. Three structural variables of the canopy were estimated (two derived from the CHM and one from the normalized cloud) for each plot: (i) canopy height (mean of the CHM), (ii) gap fraction (CHM area fraction with height less than five meters, considering only gaps ≥10 m^2), and (iii) leaf area index (LAI – calculated by the sum of leaf area density profile). The leaf area density (LAD) profile was estimated by the MacArthur-Horn equation (MacArthur and Horn, 1969) using methods described in Almeida et al. (in press). In summary, the method was based on the rates at which ranging pulses pass through (vs. are reflected) within units of canopy volume, providing a basis to estimate volumetric variation in vegetation density from optical transmission rates (MacArthur & Horn 1969; Parker et al., 2004; Stark et al., 2012). LAD was estimated at 1 m of ground height (to avoid possible ground returns) with voxel resolution of 1 m3 using only the first returns within 10° of scan nadir view angle. We fixed K = 1 (from MacArthur-Horn equation), so we calculated an “effective LAD” and “effective LAI”. For convenience, these are hereafter referred to as simply LAD and LAI.

After checking data normality and homoscedasticity (using Shapiro-wilk and Bartlett tests, respectively) (using “shapiro.test” and “bartlett.test” functions in R Core Team 2017), the three canopy variables and AGB were tested by analysis of variance (ANOVA) and posthoc Tukey-HSD ($\alpha = 0.05$). The LAD profile was analyzed both graphically and using ANOVA and posthoc Tukey-HSD tests in certain canopy vertical strata (e.g. LAIunderstory, sum of the LAD where canopy height 1-4 m). Furthermore, we developed equation for AGB estimation from the lidar-derived canopy metrics using linear regression and least-squares method. For model assessment, we computed leave-one-out cross-validation. A hypothesis test testing whether observed and predicted values follow the 1:1 correspondence line (Valbuena et al., 2017), was assessed from the intercept (α) and slope (β) of the linear regression model between the observed and leave-one-out predicted values (obsi =

α + β·predi). Which is proven by not rejecting the null hypotheses that H0: α = 0 and H0: β = 1. Absolute and relative bias from the model was assessed by residuals distribution (Figure S1, Supplementary Material).

5.3. Results

Both intensive weed management/fertilization and high seedling density planting maximized AGB accumulation, but the combination of these two silvicultural approaches did not result in higher AGB than that promoted by these approaches in separation, whereas AGB was significantly lower for plots planted at lowed seedling density and submitted to low intensity management (Figure 3A). Canopy height showed similar results, being lower in the usual low-density treatment, but no significantly different in intensive low-density (Figure 3B). Natural regeneration plots showed significantly lower canopy height and gap fraction values than planting treatments, which did not differ among their selves (Figure 3B, C). Leaf area index was lowest under natural regeneration and showed an increasing trend with respect most to the management type (from traditional to intensive) than to planting density (from high to low), as follows: natural regeneration < traditional-high < intensive -high < traditional-low < intensive-low (Figure 3D).

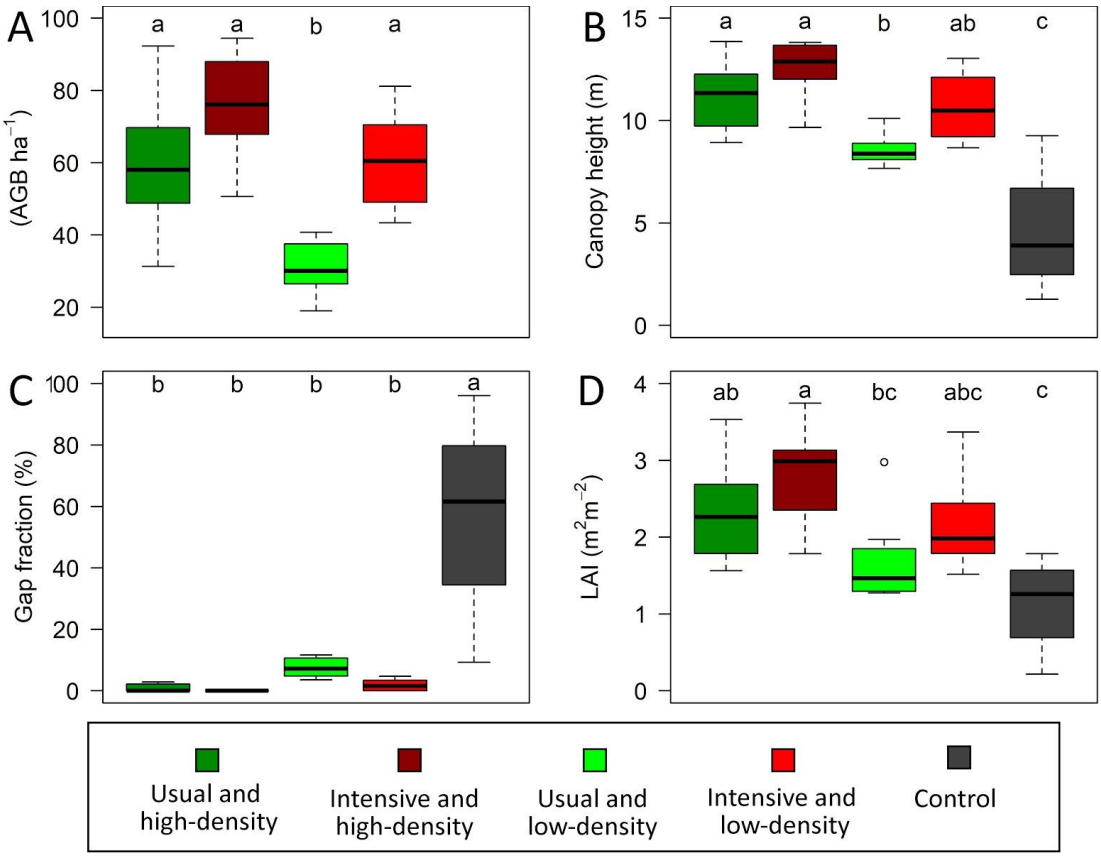

Figure 3. Boxplot of the structural variables in function of different silvicultural intensity treatments applied to experimental tree plantations established in the Atlantic Forest of Brazil. Variables: AGB (aboveground dry wood biomass; A), canopy height (B), gap fraction (C), and LAI (leaf area index; D). The silviculture treatments were established based on a combination between usual and intensive management with high (3,333 plants ha-1) and low (1,667 plants ha^{-1}) planting density; control plots were lef over for natural regeneration, without tree planting or any type of silvicultural intervention. All variables had a significant ANOVA test with $p < 0.001$. *Posthoc* Tukey-HSD ($\alpha = 0.05$) results are the letters "abc" in the graphs.

The LAD profile was also different among silvicultural treatments (Figure 4). The usual low-density treatment had lower $LAI_{above7m}$ (sum of the LAD where canopy height ≥ 7 m) than the high-density treatments (p-value < 0.001; Figure S2). All treatments showed similar $LAI_{understory}$ ($p = 0.09$; Figure S2). Natural regeneration showed an evident difference in the LAD profile (Figure 4).

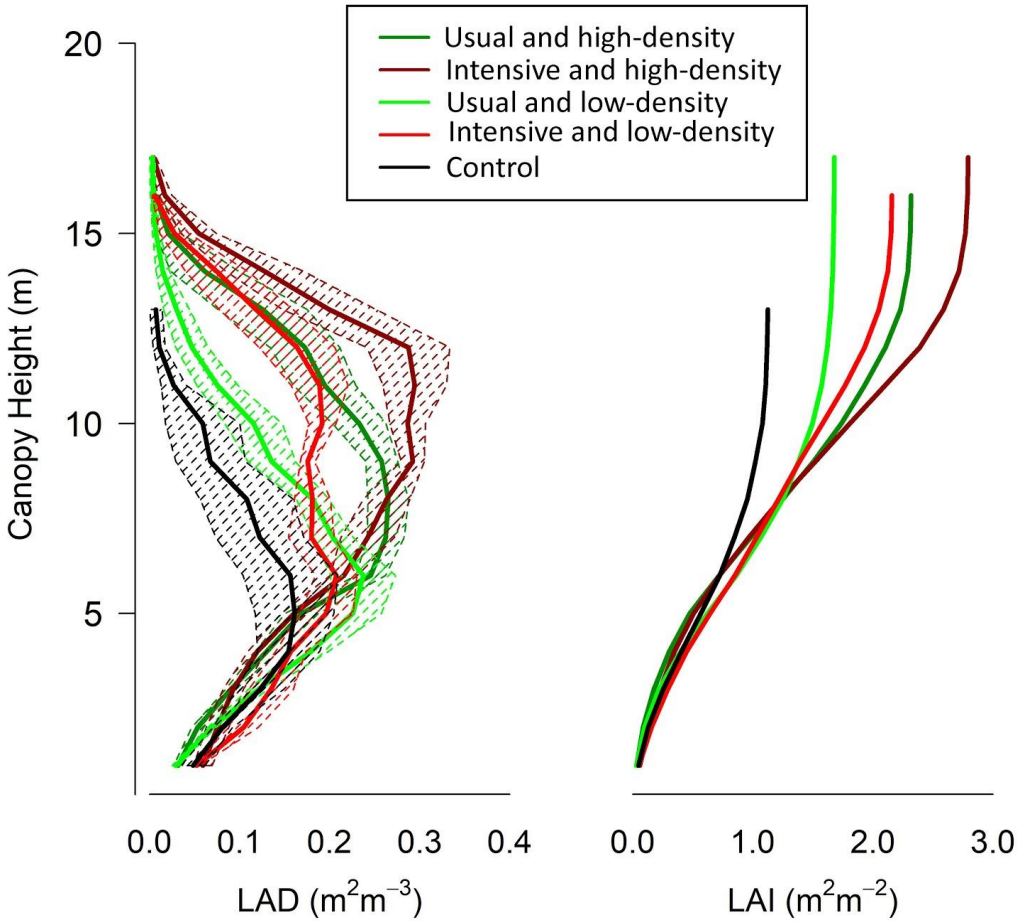

Figure 4. Vertical profiles of Leaf Area Density (LAD) and accumulated Leaf Area Index (LAI) obtained with a UAV-borne lidar for experimental tree plantations managed under different silvicultural intensity treatments in the Atlantic Forest of Brazil.

The best prediction model (higher r^2) for AGB produced with lidar-derived canopy variables was a simple linear regression using canopy height ($r^2 = 0.84$, $p < 0.001$) (Figure 5A). Observed and leave-one-out predicted values follow the 1:1 correspondence (Figure 5B). The model presented a normal distribution of residuals (Shapiro test $p = 0.069$, after outlier removal), non-tendentious and with the presence of one single outlier (Figure S1, Supplementary Material). With the outlier removal the coefficient of determination (r^2) increased from 0.75 to 0.84. LAI also showed a significant correlation with AGB (Figure S3, Supplementary Material), but because of its high correlation with canopy height, it was not significant in the multiple linear model.

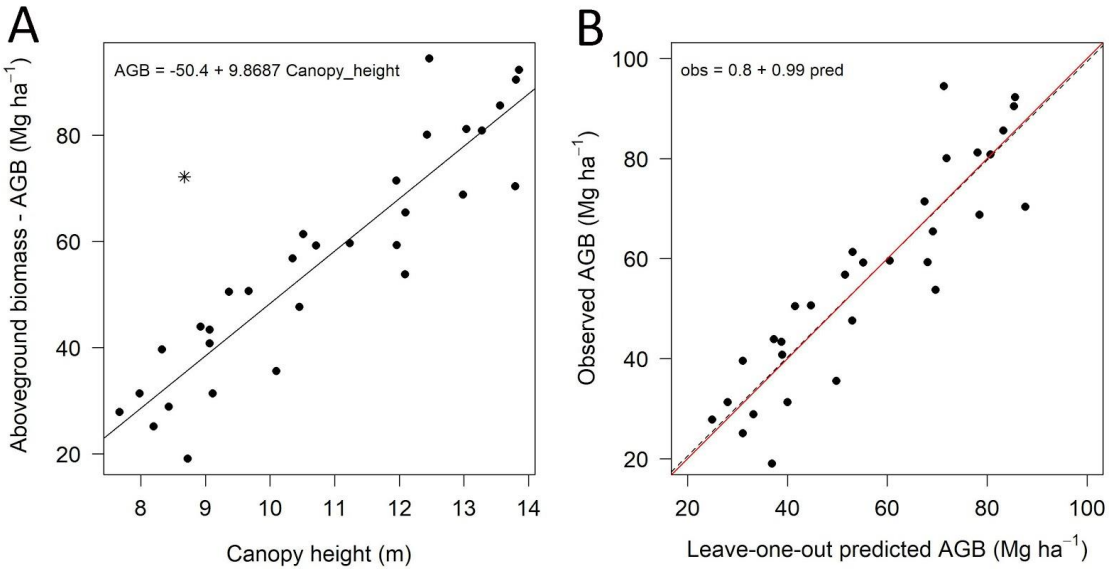

Figure 5. Best prediction model of AGB in relation to canopy variables (lidar-derived) resulting from different silvicultural intensity treatments applied to experimental tree plantations established in the Atlantic Forest of Brazil. On the left is scatterplot of AGB as function of canopy height ($r^2 = 0.84$, $p < 0.001$). The "*" point is an outlier not considered in the equation. On the right is the leave-one-out validation: the solid red line represents the 1:1 correspondence. Dashed line is the linear regression fit between observed and leave-one-out predicted ($obs_i = \alpha + \beta \cdot pred_i$). The values of α and β showed no significant difference of 0 and 1 respectively.

5.4. Discussion and conclusion

We used a UAV-borne lidar system to monitor the structure of forest restoration plantations established according to different silviculture strategies in the Atlantic Forest of Southeastern Brazil. One previous study used an UAV and photogrammetric techniques from RGB images to monitor the differential outcomes of tree plantations, nucleation, and natural regeneration in the restoration tropical forests in Costa Rica (Zahawi et al. 2015), but to the best of our knowledge, ours is the first study using a UAV-borne lidar system to monitor tropical forest restoration. Photogrammetry techniques allow the production of three-dimensional clouds from photographs (RGB images) allowing the estimation of vegetation height from DSM and DTM. However, in closed canopy forests this technique is limited to estimate the DTM (Zahawi et al., 2015). The main advantage of lidar is the potential to cross the forest canopy and produce a DTM with high accuracy. For example, Sankey et al. (2017) used a UAV-borne lidar system to characterize forest plots in Arizona (southwestern United States), and also a hyperspectral sensor (272 spectral bands ranging 400-1000 nm) to allow the distinction and classification of plant species.

We monitored both field and lidar-derived forest structure variables in plots established with different silvicultural management intensities. We also produced a

model of AGB estimation for forest restoration plots in the Atlantic Forest using lidar data. Although presenting a high r^2 (0.84), this equation can be certainly improved if developed with field inventory data collected at the same moment of lidar data collection (in this work, forest inventories were performed two years before drone flights) and if a better AGB equation is used (we quantified AGB for the 10-year-old plantation with an equation developed for the 5-year-old plantation and used wood density data collected in the 5-year-old plantation too). Plantation AGB was higher in high-planting density plots regardless management intensity. This suggests that the denser plantations provided greater AGB accumulation, independently of mechanical or chemical control of weeds and differential fertilization. However, at lower planting density, intensive fertilization and weed control with herbicide spraying resulted in higher AGB stocks. Consequently, restoration practitioners can choose both planting higher seedling density with lower silvicultural inputs or planting lower seedling density with higher silvicultural inputs to maximize carbon sequestration. Deciding on which strategy to use will rely on factors like seedling and planting costs, restrictions for herbicide use, and project specific objectives, like producing timber. A more detailed discussion about the impacts of these silvicultural treatments in AGB accumulation, implementation costs, and recolonization of plantation understory by native woody species can be found in Brancalion et al. (in press).

The use of an UAV-lidar system allowed for the evaluation of forest structure metrics that were never assessed before in this experiment (Campoe et al. 2010; Ferez et al. 2015; Brancalion et al. in press). Gap fraction and the leaf area index are important variables to diagnose the success of the forest restoration, as they represent how efficient restoration interventions were in reestablishing a forest physiognomy and creating a favorable habitat for for native biota while detrimental to invasive grasses (Viani et al., 2017). In this work, all silvicultural treatments resulted in plantations with a gap fraction of less than 15%, whereas natural regeneration resulted in much higher values. As a recognition of the importance of these variables for assessing restoration success, the Environmental Secretary of São Paulo State in southeastern Brazil (where the project was established) included canopy cover as one of the three ecological indicadors that have to be monitored to assess the quality of restoration projects established with public funds or as means of legal compliance (Chaves et al., 2015). According to this legal instrument, forest restoration projects must achieve a canopy cover of at least 80%. The official method for measuring

canopy cover is placing a 25-m tape over the ground and measuring the area of the tape covered by the projection of the tree canopies, which has also been used by the Atlantic Forest Restoration Pact (Viani et al. 2017). This method has as one of its main limitations the high costs and operational difficulty to be used in very large areas, as it relies on the work of field teams that have to walk all over the restoration sites. Another important limitation is that the average canopy cover is calculated based on samples, so its accuracy is highly dependent on the use of an appropriate number and allocation of samples, which has proven to be challenging (Viani et al., 2018). The UAV-lidar system allows to obtain a census of the restoration sites, which allows for more robust and reliable assessments of restoration quality and compliance with legal instruments.

The obtention of LAI and LAD profiles is also another advantage of the UAV-lidar system. Although planting treatments showed different LAD profile distribution, it is possible to observe that in general they have a monomodal LAD distribution (similar to a normal distribution) with a greater accumulation of vegetation at certain canopy height stratum. This should occur because it is a relatively young forest plantation (14 years), where the great majority of the individuals present the same age and height, and consequently, greater accumulation of vegetation in a certain vertical stratum. LAD profiles in primary forests normally showed the vegetation homogeneously distributed along the LAD profile (Stark et al., 2012; Almeida et al., 2016). We expect that the LAD profile of these restoration plantations will change in the next years as forest succession proceeds, with the senescence of pioneer trees, regeneration of colonizing species in the understory, and a more pronounced growth differentiation among the non-pioneer tree species of the forest. Consequently, the use of LAD profiles can be more useful for monitoring older restoration sites.

In this work we limit the estimation of structural attributes of the forest. The young structure of the forest plantation and the similar diversity among the treatments made it impossible to infer about tree species diversity. Some studies have used lidar to estimate tree diversity in temperate forests (Bergen et al., 2009). However, for species-rich forests such as tropical forests, estimating diversity from the vegetation structure is still a major challenge. Fusion of lidar and hyperspectral data is great promise in this direction (Asner et al., 2015; Sankey et al., 2017). The UAV system used in this work is also equipped with a hyperspectral sensor (Headwall Photonics Nano-Hyperspec sensor with 270 spectral bands in the VISNIR

region, 400-100nm), which data can be combined with lidar data to assess tree diversity patterns in the forest. We collected lidar and hyperspectral data with the same system in a neighboring restoration experiment established with 20, 60 and 120 native tree species, and collected the spectral data for the species (ASD Fieldspec 4 sensor field colletion), in order to combine these data to test if this UAV-lidar-hyperspectral system is able to distinguish the tree diversity levels of this controlled experiment.

The use of UAV-borne remote sensors in applied to forestry and ecological issues is increasing (Anderson and Gaston 2013; Goodbody et al., 2017), as it enables the collection of data in suitable climatic situations, and in greater frequencies when compared to airplanes or satellites platforms (Anderson and Gaston 2013). The UAV-borne sensors present an enormous potential for use in rural properties and can be a crucial tool to aid decision making and accountability in forest landscape restoration. Up-scaling tropical forest restoration relies on the development of disruptive innovations to increase the efficiency and reduce costs of planning, implementation, and monitoring activities, and may certainly not happen through the massive replication of plot-scale, traditional restoration approaches (Holl. 2017; Brancalion and van Melis, 2017). The UAV-lidar system is one of these potential disruptive technologies with potential to revolutionize forest landscape restoration and will certainly be a protagonist in future research and development projects in this field.

5.5. Supplementary material

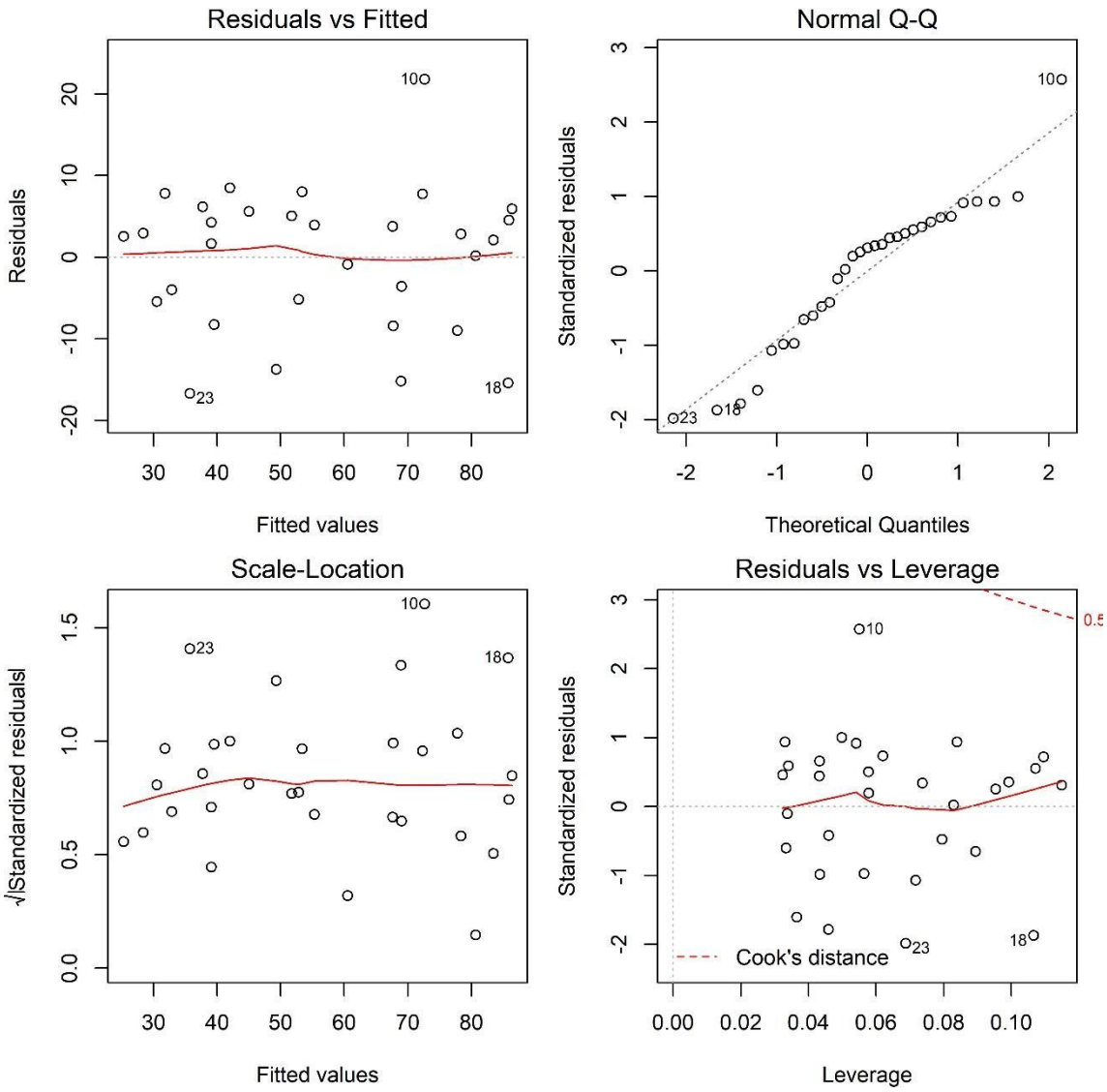

Figure S1. Graphics for quality analysis of the AGB prediction model.

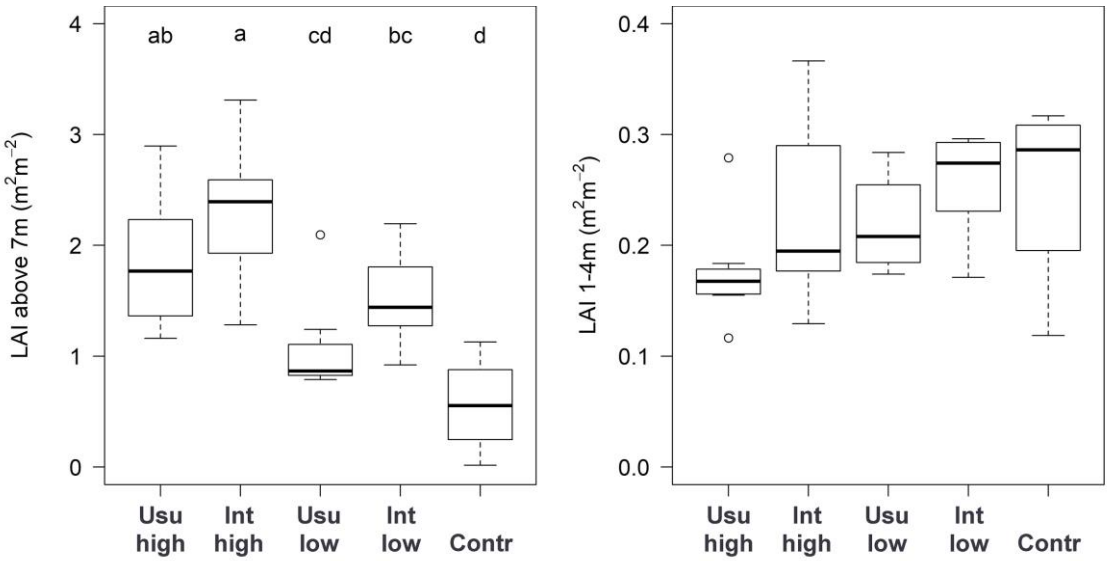

Figure S2. LAI above 7 m (ANOVA p-value < 0.001) and LAI understory (1-4 m) (ANOVA p-value = 0.091) as function of treatments.

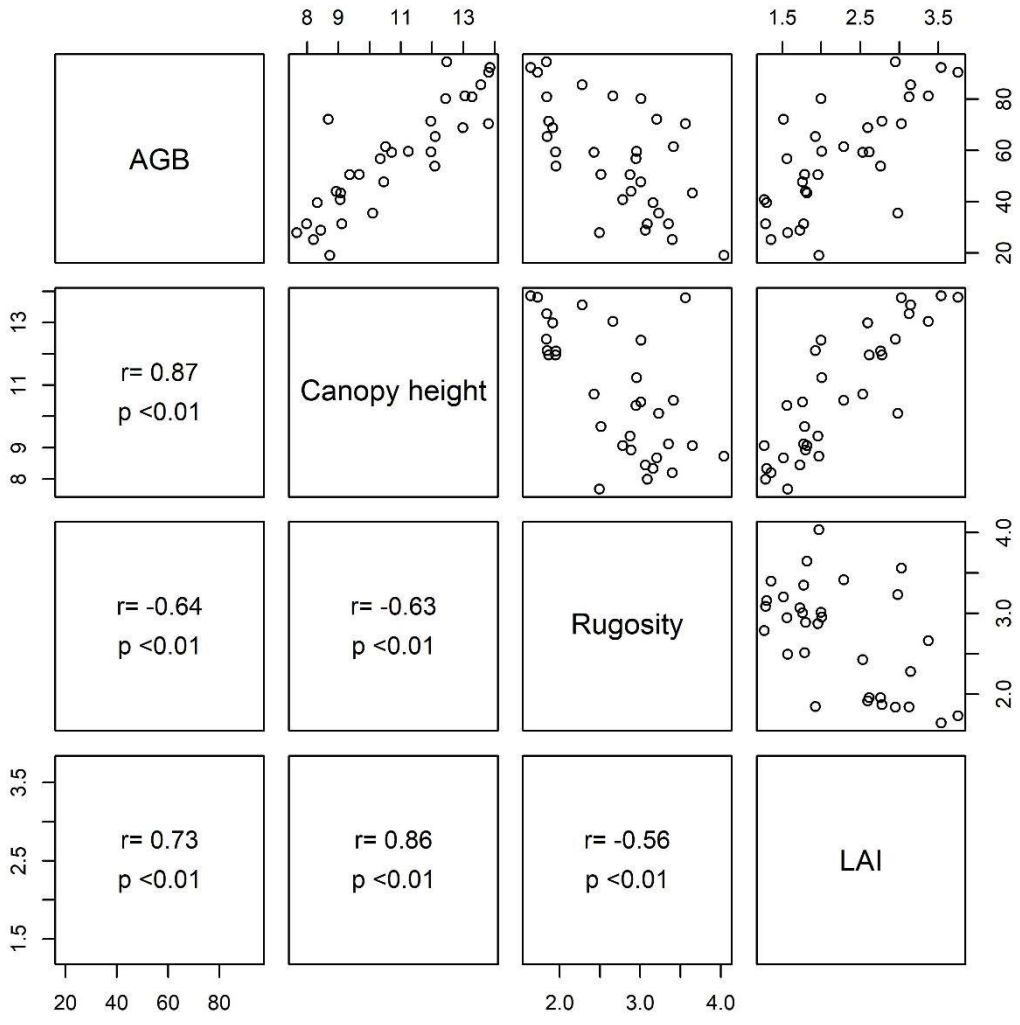

Figure S3. Correlogram between AGB and the structural attributes of the canopy (lidar-derived).

References

Almeida, D.R.A. de, Nelson, B.W., Schietti, J., Gorgens, E.B., Resende, A.F., Stark, S.C., Valbuena, R., 2016. Contrasting fire damage and fire susceptibility between seasonally flooded forest and upland forest in the Central Amazon using portable profiling LiDAR. Remote Sens. Environ. 184, 153–160. doi:10.1016/j.rse.2016.06.017

Almeida, D. R. A.; Stark, S. C.; Shao, G.; Schietti, J.; Nelson, B. W.; Silva, C. A.; Gorgens, E. B.; Valbuena, R; Papa, D. A.; Brancalion, P. H. S. Optimizing the remote detection of tropical rainforest structure with airborne lidar: leaf area profile sensitivity to pulse density and spatial sampling. Remote Sensing.

Anderson, K., Gaston, K.J., 2013. Lightweight unmanned aerial vehicles will revolutionize spatial ecology. Front. Ecol. Environ. doi:10.1890/120150

Asner, G.P., Ustin, S.L., Townsend, P.A., Martin, R.E., Chadwick, K.D., 2015. Forest biophysical and biochemical properties from hyperspectral and LiDAR remote sensing. L. Resour. Monit. Model. Mapp. with Remote sensing. CRC Press. Taylor Fr. Gr. 429–448.

Bergen, K.M., Goetz, S.J., Dubayah, R.O., Henebry, G.M., Hunsaker, C.T., Imhoff, M.L., Nelson, R.F., Parker, G.G., Radeloff, V.C., 2009. Remote sensing of vegetation 3-D structure for biodiversity and habitat: Review and implications for lidar and radar spaceborne missions. J. Geophys. Res. Biogeosciences. doi:10.1029/2008JG000883

Bonn Challenge. Link: http://www.bonnchallenge.org/. Acceded in 20/10/2018

Brancalion, P.H.S., Schweizer, D., Gaudare, U., Mangueira, J.R., Lamonato, F., Farah, F.T., Nave, A.G., Rodrigues, R.R., 2016. Balancing economic costs and ecological outcomes of passive and active restoration in agricultural landscapes: the case of Brazil. Biotropica 48, 856–867. doi:10.1111/btp.12383

Brancalion, P.H.S., Chazdon, R.L., 2017. Beyond hectares: four principles to guide reforestation in the context of tropical forest and landscape restoration. Restor. Ecol. doi:10.1111/rec.12519

Brancalion, P. H. S.; Campoe, O.; Mendes, J. C. T.; Noel, C.; Moreira, G. G.; van Melis, J.; Stape, J. L.; Guillemot, J., in press. Intensive silviculture enhances biomass accumulation and tree diversity recovery in tropical forest restoration. Ecological applications.

Campoe, O. C., Stape, J.L., Mendes, J.C.T., 2010. Can intensive management accelerate the restoration of Brazil's Atlantic forests? For. Ecol. Manage. doi:10.1016/j.foreco.2009.06.026

Chaves, R.B., Durigan, G., Brancalion, P.H.S., Aronson, J., 2015. On the need of

legal frameworks for assessing restoration projects success: new perspectives from São Paulo state (Brazil). Restor. Ecol. doi:10.1111/rec.12267

Chazdon, R.L., 2014. Second Growth: The Promise of Tropical Forest Regeneration in an Age of Deforestation, Journal of Chemical Information and Modeling. doi:10.1017/CBO9781107415324.004

Chazdon, R.L., Guariguata, M.R., 2016. Natural regeneration as a tool for large-scale forest restoration in the tropics: prospects and challenges. Biotropica 48, 716–730. doi:10.1111/btp.12381

Chazdon, R.L., Brancalion, P.H.S., Lamb, D., Laestadius, L., Calmon, M., Kumar, C., 2017. A Policy-Driven Knowledge Agenda for Global Forest and Landscape Restoration. Conserv. Lett. 10, 125–132. doi:10.1111/conl.12220

GatorEye. Link: http://www.speclab.org/gatoreye.html Acceded in 20/10/2018

Goodbody, T.R.H., Coops, N.C., Marshall, P.L., Tompalski, P., Crawford, P., 2017. Unmanned aerial systems for precision forest inventory purposes: A review and case study. For. Chron. doi:10.5558/tfc2017-012

Griscom, B.W., Adams, J., Ellis, P.W., Houghton, R.A., Lomax, G., Miteva, D.A., Schlesinger, W.H., Shoch, D., Siikamäki, J. V., Smith, P., Woodbury, P., Zganjar, C., Blackman, A., Campari, J., Conant, R.T., Delgado, C., Elias, P., Gopalakrishna, T., Hamsik, M.R., Herrero, M., Kiesecker, J., Landis, E., Laestadius, L., Leavitt, S.M., Minnemeyer, S., Polasky, S., Potapov, P., Putz, F.E., Sanderman, J., Silvius, M., Wollenberg, E., Fargione, J., 2017. Natural climate solutions. Proc. Natl. Acad. Sci. doi:10.1073/pnas.1710465114

Holl, K.D., Aide, T.M., 2011. When and where to actively restore ecosystems? For. Ecol. Manage. doi:10.1016/j.foreco.2010.07.004

Holl, K.D., 2017. Restoring tropical forests from the bottom up. Science (80-.). doi:10.1126/science.aam5432

Isenburg, M. "LAStools - efficient LiDAR processing software" (version 1.8, licensed), obtained from http://rapidlasso.com/LAStools

Leitold, V., Morton, D.C., Longo, M., dos-Santos, M.N., Keller, M., Scaranello, M., 2018. El Niño drought increased canopy turnover in Amazon forests. New Phytol. doi:10.1111/nph.15110

Locatelli, B., Catterall, C.P., Imbach, P., Kumar, C., Lasco, R., Marín-Spiotta, E., Mercer, B., Powers, J.S., Schwartz, N., Uriarte, M., 2015. Tropical reforestation and climate change: Beyond carbon. Restor. Ecol. doi:10.1111/rec.12209

Longo, M., Keller, M., dos-Santos, M.N., Leitold, V., Pinagé, E.R., Baccini, A.,

Saatchi, S., Nogueira, E.M., Batistella, M., Morton, D.C., 2016. Aboveground biomass variability across intact and degraded forests in the Brazilian Amazon. Global Biogeochem. Cycles 30, 1639–1660. doi:10.1002/2016GB005465

MacArthur, R.H., Horn, H.S., 1969. Foliage Profile by Vertical Measurements. Ecology 50, 802–804. doi:10.2307/1933693

Molin, P.G., Chazdon, R., Frosini de Barros Ferraz, S., Brancalion, P.H.S., 2018. A landscape approach for cost-effective large-scale forest restoration. J. Appl. Ecol. doi:10.1111/1365-2664.13263

Parker, G.G., Harding, D.J., Berger, M.L., 2004. A portable LIDAR system for rapid determination of forest canopy structure. J. Appl. Ecol. 41, 755–767. doi:10.1111/j.0021-8901.2004.00925.x

R core Team, 2017. R: A Language and Environment for Statistical Computing, R Foundation for Statistical Computing, Austria, 2015.

Rodrigues, R.R., Gandolfi, S., Nave, A.G., Aronson, J., Barreto, T.E., Vidal, C.Y., Brancalion, P.H.S., 2011. Large-scale ecological restoration of high-diversity tropical forests in SE Brazil. For. Ecol. Manage. doi:10.1016/j.foreco.2010.07.005

Ruiz-Jaen, M.C., Aide, T.M., 2005. Restoration success: How is it being measured? Restor. Ecol. doi:10.1111/j.1526-100X.2005.00072.x

Sankey, T., Donager, J., McVay, J., Sankey, J.B., 2017. UAV lidar and hyperspectral fusion for forest monitoring in the southwestern USA. Remote Sens. Environ. doi:10.1016/j.rse.2017.04.007

Shahbazi, M., Théau, J., Ménard, P., 2014. Recent applications of unmanned aerial imagery in natural resource management. GIScience Remote Sens. doi:10.1080/15481603.2014.926650

Shoo, L.P., Freebody, K., Kanowski, J., Catterall, C.P., 2016. Slow recovery of tropical old-field rainforest regrowth and the value and limitations of active restoration. Conserv. Biol. doi:10.1111/cobi.12606

Stark, S.C., Leitold, V., Wu, J.L., Hunter, M.O., de Castilho, C. V., Costa, F.R.C., Mcmahon, S.M., Parker, G.G., Shimabukuro, M.T., Lefsky, M.A., Keller, M., Alves, L.F., Schietti, J., Shimabukuro, Y.E., Brandão, D.O., Woodcock, T.K., Higuchi, N., de Camargo, P.B., de Oliveira, R.C., Saleska, S.R., 2012. Amazon forest carbon dynamics predicted by profiles of canopy leaf area and light environment. Ecol. Lett. 15, 1406–1414. doi:10.1111/j.1461-0248.2012.01864.x

Suding, K., Higgs, E., Palmer, M., Callicott, J.B., Anderson, C.B., Baker, M., Gutrich, J.J., Hondula, K.L., LaFevor, M.C., Larson, B.M.H., Randall, A., Ruhl, J.B., Schwartz, K.Z.S., 2015. Committing to ecological restoration. Science (80-.). 348, 638–640. doi:10.1126/science.aaa4216

Valbuena, R., Hernando, A., Manzanera, J.A., Görgens, E.B., Almeida, D.R.A.,

Mauro, F., García-Abril, A., Coomes, D.A., 2017. Enhancing of accuracy assessment for forest above-ground biomass estimates obtained from remote sensing via

van Leeuwen, M., Nieuwenhuis, M., 2010. Retrieval of forest structural parameters using LiDAR remote sensing. Eur. J. For. Res. doi:10.1007/s10342-010-0381-4

Viani, R.A.G., Holl, K.D., Padovezi, A., Strassburg, B.B.N., Farah, F.T., Garcia, L.C., Chaves, R.B., Rodrigues, R.R., Brancalion, P.H.S., 2017. Protocol for monitoring tropical forest restoration: Perspectives from the atlantic forest restoration pact in Brazil. Trop. Conserv. Sci. doi:10.1177/1940082917697265

WRI, 2018. Initiative 20x20. World Resources Institute. http://www.wri.org/our-work/project/initiative-20x20/about-initiative-20x20#project-tabs. Acceded in 05/28/2018.

Wortley, L., Hero, J.M., Howes, M., 2013. Evaluating ecological restoration success: A review of the literature. Restor. Ecol. 21, 537–543. doi:10.1111/rec.12028

Zahawi, R.A., Dandois, J.P., Holl, K.D., Nadwodny, D., Reid, J.L., Ellis, E.C., 2015. Using lightweight unmanned aerial vehicles to monitor tropical forest recovery. Biol. Conserv. 186, 287–295. doi:10.1016/j.biocon.2015.03.031

6. FINAL CONSIDERATIONS

The present study investigated new frontiers of lidar technology aplication to assessing tropical forest degradation and restoration. Chapter 2 provided important insights on the modeling of leaf area density profiles in relation to density of returns and sample resolution of modeling. Estimates of leaf area index (LAD) profiles have great potential to understanding aspects such as the light and water environments and microclimate. The methods for estimating the LAD profile using the MacArthur-Horn equation are relatively recent and more studies needs to be done to verify effects of other parameters of the lidar data (e.g. lidar pulse angle) and other vegetation types.

Chapter 3 showed, by an unprecedented way and in the oldest tropical rainforest fragmentation experiment, the significant relationships of edge effects to changes in the functional composition of species and consequently changes in the canopy structure. In addition to the capacity to estimate aboveground biomass stocks and accumulation, the lidar data presented a correlation with aspects of the dynamics of the fragments such as the tree mortality after the fragmentation and the regeneration of pioneer species. Thus, it was possible to estimate aspects of the forest dynamics using lidar data from only one moment of collection. Multitemporal data can provide even more potential to investigate forest dynamics. Our results demonstrated the biomass resilience at the edges of forest fragments.

Chapter 4 provided important insights on how the structural parameters of the canopy can characterize and differentiate forest types. We presented an unpublished canopy structural variable (“leaf area heigh volume”) that has great potential for AGB models. In this chapter we also investigated the potential of the structural variables of the canopy to estimate diversity. Therefore, the use of lidar data to estimate tree richness in tropical forests is still a great challenge. The high richness and complexity of tropical forests possibly saturates relationships between canopy structure and tree diversity. The combination of remote sensing lidar (measuring biophysical aspects) and hyperspectral (measuring biochemical aspects) are a great promise for a more comprehensive assessment of forest landscapes attributes.

Finally, chapter 5 presented a novel and efficient lidar UAV-borne system – the GatorEye system − for monitoring forest restoration projects. One of the great advantages of UAV is the autonomy for data collection. The costs of UAV-borne lidar

technologies are still expensive, reaching values of up to fifty thousand dollars (https://www.phoenixlidar.com/). It is important to note that the potential contribution of this system is not simply independent outcomes of the UAV and lidar equipments. The entire system is composed of a set of hardware's and software's that allows data collection in an optimal quality to be used. For example, a high-precision georeferencing system and an inertial measurement unit are required to estimate the correct position of the lidar returns. The GatorEye system used in Chapter 5, for example, has a georeferencing system composed of three antennas. If one of the antennas miss the correct positioning, there are still other two to estimate the correct location. With two or only one antenna this correction would not be possible. Despite the high costs of UAV-borne lidar systems, we believe that the popularization and the development of new technologies will drastically reduce the costs associated to the use of these systems in the coming years.

We hope this thesis will assist and motivate new endeavors in the application lidar remote sensing to forest conservation and restoration. Lidar technology is revolutionizing forest measurement and has the potential to assist in decision making in the areas of restoration, conservation and forest management. Lidar allows to continuously evaluate canopy attributes at broad scales with accuracy and precision. In addition to the possibility of using lidar on ground and aerial platforms, there is also lidar data from satellite platforms. GLAS (Geoscience Laser Altimeter System) (https://attic.gsfc.nasa.gov/glas/) operated from 2003 to 2009 collecting full-waveform data lidar data with a footprint (resolution) of 70 m. Currently, NASA has another project, called GEDI (https://gedi.umd.edu/), which is expected to be launched to space still in 2018 (and operate for ~ 2 years) and will collect full-waveform lidar data with 25 m footprint. The objective of GEDI project is measure the biomass of tropical forests, also allowing studies such as dynamics, climate change and diversity. However, the estimation of vegetation height from satellite lidar data is limited in high-slope areas due to its low resolution when compared to high resolution air-borne discrete return systems.

Lidar has the potential to improve our understanding of forest structure and function in forest landscape restoration projects. We expected that the scientific results of this thesis may be key to the future monitoring of restoration programs implemented in the contexts of the Native Vegetation Protection Law (which replaced the Forest Code), the Brazilian commitments to the Paris Climate Agreement and

Bonn Challenge, and national coalitions as such the Atlantic Forest Restoration Pact, thus helping São Paulo state and Brazil in the accountability of their restoration programs.